

**THERMOTROPIC AND LYOTROPIC PHASE BEHAVIOURS
OF SPONTANEOUSLY SELF-ASSEMBLED
AMPHIPHILIC BRANCHED-CHAIN GLYCOSIDES
WITH VARIOUS CHAIN LENGTH**

HAIRUL AMANI BINTI ABDUL HAMID

**FACULTY OF SCIENCE
UNIVERSITI MALAYA
KUALA LUMPUR**

2020

**THERMOTROPIC AND LYOTROPIC PHASE
BEHAVIOURS OF SPONTANEOUSLY SELF-
ASSEMBLED AMPHIPHILIC BRANCHED-CHAIN
GLYCOSIDES WITH VARIOUS CHAIN LENGTH**

HAIRUL AMANI BINTI ABDUL HAMID

**THESIS SUBMITTED IN FULFILMENT OF THE
REQUIREMENTS FOR THE DEGREE OF
DOCTOR OF PHILOSOPHY**

**DEPARTMENT OF CHEMISTRY
FACULTY OF SCIENCE
UNIVERSITI MALAYA
KUALA LUMPUR**

2020

UNIVERSITI MALAYA

ORIGINAL LITERARY WORK DECLARATION

Name of Candidate: **HAIRUL AMANI BINTI ABDUL HAMID**

Matric No: **SHC110036**

Name of Degree: **DOCTOR OF PHILOSOPHY**

Title of Thesis ("this Work"):

**THERMOTROPIC AND LYOTROPIC PHASE BEHAVIOURS OF SPONTANEOUSLY
SELF-ASSEMBLED AMPHIPHILIC BRANCHED-CHAIN GLYCOSIDES WITH
VARIOUS CHAIN LENGTH**

Field of Study:

PHYSICAL CHEMISTRY

I do solemnly and sincerely declare that:

- 1) I am the sole author/writer of this Work;
- 2) This Work is original;
- 3) Any use of any work in which copyright exists was done by way of fair dealing and for permitted purposes and any excerpt or extract from, or reference to or reproduction of any copyright work has been disclosed expressly and sufficiently and the title of the Work and its authorship have been acknowledged in this Work;
- 4) I do not have any actual knowledge nor do I ought reasonably to know that the making of this work constitutes an infringement of any copyright work;
- 5) I hereby assign all and every rights in the copyright to this Work to the University of Malaya ("UM"), who henceforth shall be owner of the copyright in this Work and that any reproduction or use in any form or by any means whatsoever is prohibited without the written consent of UM having been first had and obtained;
- 6) I am fully aware that if in the course of making this Work I have infringed any copyright whether intentionally or otherwise, I may be subject to legal action or any other action as may be determined by UM.

Candidate's Signature

Date

Subscribed and solemnly declared before,

Witness's Signature

Date

Name:

Designation:

**THERMOTROPIC AND LYOTROPIC PHASE BEHAVIOURS OF
SPONTANEOUSLY SELF-ASSEMBLED AMPHIPHILIC BRANCHED-CHAIN
GLYCOSIDES WITH VARIOUS CHAIN LENGTH**

ABSTRACT

Lipid polymorphism is a process which illustrates the self-assembly of lipid aggregation depending on the environment. Lipids such as branched-chain glycolipids which are amphiphilic molecules also known as amphitropic tend to generate mesophases in thermotropic (dry) and lyotropic (solvation) conditions. These molecules are capable of self-aggregating into various types of glycolipid self-assemblies offering an interesting insight in relation to their functions in living cells. Hence, this study aims to investigate the mesophases of β -D-glycosides which are branched-chain synthetic glycolipids, namely, β -D-glucosides and β -D-maltosides. The study was carried out on the thermotropic phases of dry glycosides and the lyotropic phases of glycosides in excess water conditions, mesomorphic behaviours of β -D-maltosides and their lamellar hydration properties; and structural parameters at fixed hydration for β -Glc-C₁₂C₈ and β -Mal-C₁₂C₈ (the effect of different sugar head groups). These β -D-glycoside compounds are characterised using optical polarising microscopy (OPM), differential scanning calorimetry (DSC) and small-angle X-ray diffraction (SAXD). Optical textures of the β -D-glycosides were also observed via water contact penetration experiments. Results revealed that different types of phases were produced showing a variety of lipid self-assembly. Upon heating and cooling using OPM, the dry glucosides were observed to exhibit L₂, L_C and H_{II} phases. However, the glucosides in excess water condition produced L _{α} , Ia3d and H_{II}. On the other hand, the maltosides adopt L₂, L_C, V_{II} and H_{II}; L₁ and L _{α} in dry and excess water, respectively. Furthermore, the thermotropic transition temperatures and enthalpies of the β -D-glycosides were determined using a DSC. The β -D-glucosides series produce only a single transition peak T_C, however, the β -D-maltosides

series display the T_g and T_c . Moreover, X-ray beamline was used to determine the X-ray d -spacing values of β -D-glycosides subjected to certain temperatures in dry, excess water and limiting hydration conditions. X-ray results provide L_2 , L_α and H_{II} phases of dry β -D-glucosides and L_1 , L_α , $Ia3d$ and H_{II} phases of β -D-glucosides in excess water. From X-ray measurements, the β -D-maltosides give L_C phase in dry and L_α in excess water conditions. Only L_C phase appears for dry β -Mal-C₈C₄, β -Mal-C₁₀C₆, β -Mal-C₁₂C₈ and β -Mal-C₁₄C₁₀ characterised by SAXD. In overall, L_α phase dominates the lyotropic self-assembly in excess water of longer chain length maltosides as determined from the X-ray method. Consequently, an area per molecule and weight % of water can be estimated. The β -Mal-C₁₀C₆ shows the highest weight % of water (25%) and the lowest area per molecule (56.5 Å²). The β -Mal-C₁₄C₁₀ gives the highest value of area per molecule (59.7 Å²). Structural parameters of β -Mal-C₁₂C₈ and β -Glc-C₁₂C₈ were compared. Both compounds show the same trend in terms of water layer thickness, bilayer thickness, area per molecule as function of volume fraction of water and temperature. This work examined an in-depth study of glycolipid self-assembly mesophase in dry, excess water, and limiting hydration conditions, specifically looking at sugar head and branched-chain hydrocarbon with the effect of temperature. The liquid crystalline phases formed by these compounds makes them potential lipid candidates for variety applications such as drug delivery nanocarriers.

Keywords: Liquid crystals, Guerbet glycolipids, Limiting hydration conditions

**SIFAT FASA TERMOTROPIK DAN LIOTROPIK SWA PENYUSUNAN
SPONTAN GLIKOSIDA RANTAIAN BERCABANG AMFIFILIK DENGAN
KEPANJANGAN RANTAI PELBAGAI**

ABSTRAK

Polimorfisme lipid ialah suatu proses yang menggambarkan swa penyusunan pengagregatan lipid bergantung kepada persekitaran. Lipid seperti glikolipid rantai bercabang yang merupakan molekul amfifilik yang juga dikenali sebagai amfitropik, cenderung untuk menghasilkan mesofasa dalam keadaan termotropik (kering) dan liotropik (dalam larutan). Molekul ini boleh mengagregat sendiri kepada pelbagai jenis swa penyusunan glikolipid yang menawarkan perkembangan yang menarik berkaitan dengan fungsinya di dalam sel hidup. Oleh itu, kajian ini bertujuan untuk mengkaji mesofasa β -D-glikosida yang merupakan glikolipid sintetik rantai bercabang yang dikenali sebagai β -D-glukosida dan β -D-maltosida. Kajian ini telah dijalankan ke atas fasa termotropik glikosida kering dan fasa liotropik glikosida dalam keadaan air berlebihan, sifat mesomorfik β -D-maltosida dan ciri penghidratan lamela mereka; dan parameter struktur pada penghidratan tetap bagi β -Glc- $C_{12}C_8$ dan β -Mal- $C_{12}C_8$ (kesan perbezaan kumpulan kepala gula). Sebatian β -D-glikosida ini dicirikan dengan menggunakan kaedah mikroskopi pengutuban optik (OPM), kalorimetri pengimbasan pembezaan (DSC) dan pembelauan sinar-X bersudut kecil (SAXD). Tekstur optikal bagi β -D-glikosida telah diperhatikan juga melalui ujikaji penembusan sentuh air. Keputusan menunjukkan bahawa fasa berbeza telah dihasilkan yang mempamerkan kepelbagaian swa penyusunan lipid. Melalui pemanasan dan penyejukan menggunakan OPM, glukosida kering telah didapati mempamerkan fasa L_2 , L_C dan H_{II} . Walau bagaimanapun, glukosida dalam keadaan air berlebihan menghasilkan L_α , $Ia3d$ dan H_{II} . Sebaliknya, maltosida menghasilkan L_2 , L_C , V_{II} dan H_{II} ; L_1 dan L_α masing-masing dalam keadaan kering dan air berlebihan. Seterusnya, suhu dan entalpi peralihan termotropik bagi β -D-

glikosida telah ditentukan dengan menggunakan DSC. Siri β -D-glukosida menghasilkan hanya satu puncak peralihan tunggal T_C , sebaliknya, siri β -D-maltosida mempamerkan T_g dan T_C . Selanjutnya, alur pancaran sinar-X telah digunakan untuk menentukan nilai penjarakan- d sinar-X bagi β -D-glikosida di bawah pengaruh suhu tertentu dalam keadaan kering, air berlebihan dan penghidratan terhad. Keputusan sinar-X memberikan fasa L_2 , L_α dan H_{II} bagi β -D-glukosida kering dan fasa L_1 , L_α , $Ia3d$ dan H_{II} bagi β -D-glukosida dalam keadaan air berlebihan. Daripada pengukuran sinar-X, β -D-maltosida memberikan fasa L_C dalam keadaan kering dan L_α dalam keadaan air berlebihan. Hanya fasa L_C hadir bagi β -Mal-C₈C₄, β -Mal-C₁₀C₆, β -Mal-C₁₂C₈ dan β -Mal-C₁₄C₁₀ yang dicirikan oleh SAXD. Secara keseluruhannya, fasa L_α mendominasi swa penyusunan liotropik dalam air berlebihan maltosida berantai panjang yang ditentukan oleh kaedah sinar-X. Oleh yang demikian, luas per molekul dan peratus berat air boleh dijangkakan. β -Mal-C₁₀C₆ menunjukkan peratus berat air tertinggi (25%) dan luas per molekul terendah (56.5 Å²). β -Mal-C₁₄C₁₀ menunjukkan nilai paling tinggi bagi luas per molekul (59.7 Å²). Parameter struktur bagi β -Mal-C₁₂C₈ dan β -Glc-C₁₂C₈ juga telah dibandingkan. Kedua-dua sebatian ini menunjukkan tren yang sama dari segi ketebalan lapisan air, ketebalan dwilapisan, luas per molekul dengan fungsi pecahan isipadu air dan suhu. Kajian ini telah meneliti dengan mendalam mesofasa swa penyusunan glikolipid dalam keadaan kering, air berlebihan, dan penghidratan terhad, secara spesifiknya melibatkan kumpulan gula dan hidrokarbon rantai bercabang dengan kesan suhu. Fasa hablur cecair yang dibentuk oleh sebatian ini menjadikannya calon lipid berpotensi untuk pelbagai aplikasi seperti pengangkut nano penyampaian ubat.

Kata kunci: Hablur cecair, Glikolipid Guerbet, Keadaan penghidratan terhad

ACKNOWLEDGEMENTS

First of all, I am very grateful to Almighty ALLAH s.w.t for giving me the strength, peace of mind and good health in making this thesis to become a reality.

I would like to express my deepest heartfelt gratitude and appreciation to my supervisors, Dr. Noor Idayu Mat Zahid and Professor Dr. Rauzah Hashim for their guidance, belief, patience and encouragement throughout my journey in completing this challenging endeavour.

I would also like to extend my acknowledgement and sincere thanks to Professor Dr. John M. Seddon and Dr. Piers Gaffney from Imperial College London, United Kingdom for their supervision and guidance of the X-ray and chromatographic techniques, respectively.

Special thanks go to Dr. Nicholas J. Brooks, Dr. Gemma Shearman, Dr. Dora Tang, Dr. Arwen Tyler and Ms Beatrice Gauthé for their help, guidance and assistance for the laboratory works at Imperial College London.

I would also like to thank Associate Prof. Dr. Thorsten Heidelberg, Dr. Rusnah Syahila Duali Hussen, Dr. Noraini Ahmad, Dr. Seyed Mirzadeh Husseini, Dr. Vijayan Manickam Achari and Dr. Nguan Hock Seng for their help and assistance with regard to the equipment, techniques and fruitful discussions.

Finally, I am truly thankful and grateful to my husband, Professor Dr. Ayub Md. Som for his unwavering support and encouragement upon completion of this thesis. Last but not least, I would also like to express my utmost thankfulness to my children namely: Alzam Altof, Aina Syakirah and Arman Faris for giving me strength, support, so much love and being understandable throughout the long journey.

I would also like to acknowledge and thank Universiti Teknologi MARA for providing the scholarship for my Ph.D Study.

TABLE OF CONTENTS

ABSTRACT.....	iii
ABSTRAK.....	v
ACKNOWLEDGEMENTS.....	vii
TABLE OF CONTENTS.....	viii
LIST OF FIGURES.....	xi
LIST OF TABLES.....	xvii
LIST OF EQUATIONS.....	xix
LIST OF SYMBOLS AND ABBREVIATIONS.....	xx
LIST OF APPENDICES.....	xxii
CHAPTER 1: INTRODUCTION.....	1
1.1 Research Background.....	1
1.2 Problem Statement.....	5
1.3 Objectives of the Study.....	6
1.4 Scope of the Study.....	7
1.5 Significance of the Study.....	7
1.6 Thesis Outline.....	8
CHAPTER 2: LITERATURE REVIEW.....	10
2.1 Glycolipids Self-Assembly.....	10
2.2 Sugar Head Group.....	10
2.3 Hydrophobic Tail.....	11
2.4 Anomer.....	12
2.5 Fundamental of Liquid Crystals.....	13
2.5.1 Thermotropic Liquid Crystals.....	15
2.5.2 Lyotropic Liquid Crystals.....	17
	viii

2.6	Lyotropic Phase Behaviour.....	23
2.6.1	Micellar Solution.....	23
2.6.2	Lamellar Phase.....	26
2.6.3	Hexagonal Phase.....	27
2.6.4	Cubic Phase.....	29
CHAPTER 3: TECHNIQUES AND METHODS.....		31
3.1	Guerbet Glycosides Synthesis.....	31
3.1.1	General Glycosidation Procedure.....	33
3.1.2	General Deacetylation Procedure.....	34
3.2	Characterisation of Liquid Crystal Phase Behaviour.....	35
3.2.1	Optical Polarising Microscopy.....	36
3.2.2	Differential Scanning Calorimetry.....	45
3.2.3	Small-Angle X-ray Diffraction.....	46
CHAPTER 4: RESULTS AND DISCUSSION.....		57
4.1	Liquid Crystal Phases of Branched-Chain Glucosides: Thermotropic and Lyotropic.....	57
4.1.1	Optical Polarising Microscopy.....	61
4.1.2	Differential Scanning Calorimetry.....	65
4.1.3	Small-Angle X-ray Diffraction.....	68
4.1.4	Final Remarks.....	74
4.2	Mesophase Structures of Branched-chain Alkyl Maltosides in Dry and Excess Water Conditions.....	74
4.2.1	Optical Polarising Microscopy.....	77
4.2.2	Differential Scanning Calorimetry.....	83
4.2.3	Small-Angle X-ray Diffraction.....	87
4.2.4	Hydration of the Fluid Lamellar Phase.....	94

4.2.5	Final Remarks.....	98
4.3	Structural Parameters of Branched-chain β -Glc-C ₁₂ C ₈ and β -Mal-C ₁₂ C ₈ at Fixed Hydration of Water Conditions.....	99
4.3.1	Structural Parameters Determination.....	101
4.3.2	Small-Angle X-ray Diffraction.....	103
4.3.3	Final Remarks.....	116
CHAPTER 5: CONCLUSIONS AND RECOMMENDATIONS.....		117
REFERENCES.....		120
LIST OF PUBLICATIONS AND PAPER PRESENTED.....		137
APPENDIX.....		141

LIST OF FIGURES

Figure 1.1	Cell membrane structure. Redrawn from (Karp, 2010).	1
Figure 2.1	A diagram of the molecules alignment relative to the vector \hat{n} (director) and θ (angle of order parameter, S).	14
Figure 2.2	Micelles (Type I) self-assemblies showing (a) spherical micelle; (b) globular micelle; (c) rod-like micelle; and (d) spherical bilayer vesicle. Redrawn from (Hamley, 2000).	24
Figure 2.3	Micelles (Type II) self-assemblies showing (a) inverse spherical micelle; (b) inverse globular micelle; (c) inverse rod-like micelle; and (d) inverse spherical bilayer vesicle. Redrawn from (Lombardo <i>et al.</i> , 2015).	25
Figure 2.4	The different type lamellar phase i.e. (a) lamellar phase (L_α); and (b) lamellar crystalline (L_C). Redrawn from (Vill & Hashim, 2002).	26
Figure 2.5	Normal hexagonal phase (H_I). Redrawn from (Collings & Hird, 1997).	28
Figure 2.6	Inverse hexagonal phase (H_{II}). Redrawn from (Collings & Hird, 1997).	28
Figure 2.7	Discontinuous cubic phase showing (a) normal type (I_I); and (b) inverse type (I_{II}). Redrawn from (Efrat <i>et al.</i> , 2008).	30
Figure 3.1	The chemical structures of branched-chain β -D-glucosides. (a) β -Glc- C_6C_2 ; (b) β -Glc- C_8C_4 ; (c) β -Glc- $C_{10}C_6$; (d) β -Glc- $C_{12}C_8$; and (e) β -Glc- $C_{14}C_{10}$.	32
Figure 3.2	The chemical structures of branched-chain β -D-maltosides: (a) β -Mal- C_6C_2 ; (b) β -Mal- C_8C_4 ; (c) β -Mal- $C_{10}C_6$; (d) β -Mal- $C_{12}C_8$; and (e) β -Mal- $C_{14}C_{10}$.	33
Figure 3.3	Liquid crystal molecules upon heating and cooling. Redrawn from (An <i>et al.</i> , 2016).	35
Figure 3.4	Schematic diagram redrawn from (Dierking, 2003).	37
Figure 3.5	Schematic diagram of light polarisation process. Redrawn from (Feehan <i>et al.</i> , 2018; Radi, 2013).	38
Figure 3.6	Glycolipid liquid crystals optical textures of (a) glycolipid GalC ₁₁ smectic A showing maltese crosses in region A and pearl chains in region B. Adapted from (Garidel <i>et al.</i> , 2015). (b) Focal-conic of smectic layers of biomolecular-based thermotropic liquid crystal. Adapted from (Liu <i>et al.</i> , 2014). (c) Glycolipid columnar texture (MelC ₁₂ N ₃). Adapted from	

	(Garidel <i>et al.</i> , 2015). (d) CellC ₁₂₍₈₎ hexagonal columnar. [Reprinted (adapted) with permission from ref. (Takada <i>et al.</i> , 1992). Copyright 1992 Taylor & Francis].	40
Figure 3.7	Graft copolymers mesophase optical textures of (a) homeotropic region containing lamellar phase oily streaks; (b) oil streaks of lamellar phase connected by the nodes; (c) textures of lamellar quaternary system with polygonal arrays between oily streaks; (d) batonnets optical texture of polymeric systems; (e) inverse hexagonal angular texture; and (f) inverse hexagonal coarsely striated texture. [Reprinted (adapted) with permission from ref. (Candau <i>et al.</i> , 1982). Copyright 1982 Elsevier].	41
Figure 3.8	Glycolipid cubic phases observed under a polarised microscope. (a) Cel- β -glycero dioleoyl and Glu- β -glycero dioleoyl mixture (1:1); (b) a formation of rectangular isotropic cubic phase during transition from hexagonal to cubic phases of Glu- β -glycero didecanoyl; and (c) the phase sequence of MalOC ₃ OC ₁₂ mesophase structures. (A) water, (B) discontinuous cubic phase (I _I), (C) and (D) hexagonal phases (H _{II}), (E) bicontinuous cubic phase (V _I), (F) pure compound (water contact penetration). Adapted from (Garidel <i>et al.</i> , 2015).	42
Figure 3.9	Hydrated sample in excess water sandwiched between a cover slip and glass slide.	44
Figure 3.10	Formation of water gradient concentrations around the sample.	44
Figure 3.11	Typical DSC curve.	46
Figure 3.12	Bragg's Law. Redrawn from (Naik, 2010).	48
Figure 3.13	Schematic diagram of experimental setup of small-angle X-ray machine. Redrawn from (Changizi <i>et al.</i> , 2005).	50
Figure 3.14	Homogenised sample in excess water condition in an X-ray flame-sealed glass capillary tube.	52
Figure 3.15	An X-ray glass capillary tube containing dry homogenised sample.	52
Figure 3.16	Viscous sample in a disc-shaped teflon spacer.	53
Figure 3.17	A fixed hydration homogenised sample.	54
Figure 4.1	The chemical structures of the branched-chain β -D-glucosides.	61
Figure 4.2	OPM textures of β -Glc-C ₆ C ₂ for (a) thermotropic (dry) L _C phase at 31 °C before heating; (b) on cooling below 59 °C a birefringent texture consistent with an L _{α} (dry/thermotropic) phase is seen; and (c) a water contact penetration scan after 5 min gave L ₁ and L _{α} (lyo) phases in addition to the dry L _{α} state,	

	at room temperature. The sample transformed completely to an L_1 micellar solution in approximately half an hour.	62
Figure 4.3	OPM textures of β -Glc- C_8C_4 for (a) a dry /thermotropic sample at 31 °C, where the sample appears isotropic except at the edge (due to moisture adsorption from the atmosphere); (b) contact penetration with water caused myelins to form immediately.	63
Figure 4.4	OPM textures of β -Glc- $C_{10}C_6$ after the sample was extensively dried. (a) H_{II} phase at 40 °C (cooling at 5 °C min ⁻¹); (b) contact penetration with water showing a growing isotropic / cubic domain, with a strained H_{II} structure (optical evidence of strain is highlighted by a dotted circle).	63
Figure 4.5	(a) Thermotropic H_{II} texture at room temperature for β -Glc- $C_{12}C_8$; and (b) lyotropic H_{II} texture after 7 h of contact penetration with water.	64
Figure 4.6	(a) Thermotropic H_{II} texture on cooling from 50 °C to room temperature for dry β -Glc- $C_{14}C_{10}$; and (b) lyotropic H_{II} texture after 6 h of contact penetration with water.	64
Figure 4.7	DSC thermograms for dry β -D-glucosides at a heating scanning rate of 5 °C min ⁻¹ .	66
Figure 4.8	Synchrotron small-angle X-ray diffraction patterns from dry β -Glc- $C_{n+4}C_n$ samples at 25 °C unless otherwise stated. Patterns are offset along the y-axis for clarity. Diffraction patterns were collected at Diamond Light Source, with the exception of that from β -Glc- $C_{10}C_6$ which was collected at the Australian Synchrotron.	69
Figure 4.9	Small-angle X-ray diffraction patterns from dry β -Glc- C_6C_2 samples at 30 °C after cooling from 75 °C.	69
Figure 4.10	Synchrotron small-angle X-ray diffraction patterns from β -Glc- $C_{n+4}C_n$ samples in excess water at 25 °C unless otherwise stated. Patterns are offset along the y-axis for clarity. Diffraction patterns were collected at Diamond Light Source.	71
Figure 4.11	Two-dimensional small-angle X-ray diffraction pattern from β -Glc- $C_{10}C_6$ in excess water, characteristic of a cubic phase of space group $Ia3d$.	73
Figure 4.12	OPM textures of β -Mal- C_6C_2 for (a) thermotropic L_C phase; and (b) when it dissolves in water producing L_1 solution. 10× magnification at room temperature.	77
Figure 4.13	OPM textures of β -Mal- C_8C_4 for (a) thermotropic L_C phase; and (b) lyotropic texture by water gradient experiment giving myelin figures of L_α phase. 10× magnification at room temperature.	78

Figure 4.14	OPM textures of β -Mal-C ₁₀ C ₆ for (a) thermotropic L _C phase; and (b) contact penetration with water giving L _{α} birefringence textures. 10 \times magnification at room temperature.	79
Figure 4.15	Polymorphism of anhydrous β -Mal-C ₁₂ C ₈ observed upon heating under an optical polarising microscope shows (a) L _C phase at 85 °C; (b) isotropic V _{II} phase slowly form at 123 °C; (c) V _{II} phase at 162 °C; and (d) H _{II} texture at 209 °C. (e) An L _{α} phase appears during water penetration experiment at 27 °C with 20 \times magnification.	80
Figure 4.16	OPM textures of β -Mal-C ₁₄ C ₁₀ for (a) thermotropic L _C phase at 25 °C; (b) V _{II} phase at 71 °C; (c) H _{II} phase at 128 °C; (d) L ₂ phase at 217 °C; and (e) contact penetration with water giving L _{α} birefringence textures. 10 \times magnification at room temperature.	81
Figure 4.17	DSC thermograms for dry β -D-maltosides at a heating scanning rate of 5 °C min ⁻¹ .	84
Figure 4.18	A representative L _C phase (a) Bragg's diffraction pattern image of dry β -Mal-C ₈ C ₄ upon heating and cooling at temperatures ranging from 0–80–0 °C which corresponds to the (b) image integrated intensity plots.	87
Figure 4.19	A representative L _C phase (a) Bragg's diffraction pattern image of dry β -Mal-C ₁₀ C ₆ upon heating and cooling at temperatures ranging from 0–80–0 °C which corresponds to the (b) image integrated intensity plots.	88
Figure 4.20	A representative L _C phase Bragg's diffraction patterns image of dry β -Mal-C ₁₂ C ₈ at different temperatures (top) which correspond to image integrated intensity plot (bottom).	89
Figure 4.21	A representative L _C phase (a) Bragg's diffraction pattern image of dry β -Mal-C ₁₄ C ₁₀ upon heating and cooling at temperatures ranging from 0–80–0 °C which corresponds to the (b) image integrated intensity plots.	90
Figure 4.22	No appearance of (a) Bragg's diffraction peak for an excess water sample of β -Mal-C ₈ C ₄ which corresponds to (b) a parasitic scatter.	91
Figure 4.23	A representative L _{α} phase (a) Bragg's diffraction pattern image of β -Mal-C ₁₀ C ₆ in excess water upon heating and cooling at temperatures ranging from 0–80–0 °C which corresponds to the (b) image integrated intensity plots.	92

Figure 4.24	A representative L_{α} phase (a) Bragg's diffraction pattern synchrotron image of β -Mal- $C_{10}C_6$ in excess water sample with pressure which corresponds to the (b) stackplot image analysis.	92
Figure 4.25	A representative L_{α} phase Bragg's diffraction patterns of β -Mal- $C_{12}C_8$ in excess water at different temperatures (top) which correspond to image integrated intensity plot (bottom).	93
Figure 4.26	A representative L_{α} phase (a) Bragg's diffraction pattern image of β -Mal- $C_{14}C_{10}$ in excess water upon heating and cooling at temperatures ranging from 0–80–0°C which corresponds to the (b) image integrated intensity plots.	94
Figure 4.27	A graph of d -spacing versus temperature of β -Mal- $C_{10}C_6$ in dry and excess water conditions upon heating and cooling processes.	95
Figure 4.28	A graph of d -spacing versus temperature of β -Mal- $C_{12}C_8$ in dry and excess water conditions upon heating and cooling processes.	96
Figure 4.29	A graph of d -spacing versus temperature of β -Mal- $C_{14}C_{10}$ in dry and excess water conditions upon heating and cooling processes.	96
Figure 4.30	(a) The bilayer lamellar; and (b) the thickness of water layer of hexagonal phase dimension schematic diagram. Redrawn from (Costigan <i>et al.</i> , 2000).	101
Figure 4.31	X-ray diffraction patterns (L_{α} phase) of 10 water molecules of β -Mal- $C_{12}C_8$ at (a) 25 °C; (b) 40 °C; (c) 60 °C; and (d) 80 °C.	103
Figure 4.32	X-ray diffraction patterns (H_{II} phase) of 10 water molecules of β -Glc- $C_{12}C_8$ at (a) 25 °C; (b) 40 °C; (c) 60 °C; and (d) 80 °C.	104
Figure 4.33	Water layer thickness against fraction of water at different temperatures for L_{α} phase of the β -Mal- $C_{12}C_8$.	107
Figure 4.34	Bilayer thickness against fraction of water at different temperatures for L_{α} phase of the β -Mal- $C_{12}C_8$.	107
Figure 4.35	Area per molecule against fraction of water at different temperatures for L_{α} phase of the β -Mal- $C_{12}C_8$.	108
Figure 4.36	Water layer thickness against fraction of water at different temperatures for H_{II} phase of the β -Glc- $C_{12}C_8$.	108
Figure 4.37	Bilayer thickness against fraction of water at different temperatures for H_{II} phase of the β -Glc- $C_{12}C_8$.	109
Figure 4.38	Area per molecule against fraction of water at different temperatures for H_{II} phase of the β -Glc- $C_{12}C_8$.	109
Figure 4.39	Water layer thickness against different temperatures for L_{α} phase of the β -Mal- $C_{12}C_8$.	111

Figure 4.40	Bilayer thickness against different temperatures for L_α phase of the β -Mal- $C_{12}C_8$.	111
Figure 4.41	Area per molecule against different temperatures for L_α phase of the β -Mal- $C_{12}C_8$.	112
Figure 4.42	Water layer thickness against different temperatures for H_{II} phase of the β -Glc- $C_{12}C_8$.	112
Figure 4.43	Bilayer thickness against different temperatures for H_{II} phase of the β -Glc- $C_{12}C_8$.	113
Figure 4.44	Area per molecule against different temperatures for H_{II} phase of the β -Glc- $C_{12}C_8$.	113
Figure 4.45	Schematic diagram of frustration. Redrawn from (Sadoc & Charvolin, 1986).	115

LIST OF TABLES

Table 2.1	Molecular structures and their related thermotropic phases.	16
Table 2.2	Mesomorphic lyotropic phase structures and X-ray diffraction/scattering patterns. Compiled from (Sun & Zhang, 2004; Zahid <i>et al.</i> , 2013; Liew <i>et al.</i> , 2015; Hashim <i>et al.</i> , 2018).	18
Table 2.3	Formation of lipid molecules geometries packing properties and self-assembly structures. Redrawn from (Israelachvili <i>et al.</i> , 1980).	22
Table 3.1	Typical values peak position of crystal symmetry. Compiled from (Schnablegger & Singh, 2011).	49
Table 4.1	Comparison between the conventional notation for thermotropic phases used for mesogenic liquid crystals, and that used here for amphitropic liquid crystals, based on the lyotropic convention. Adopted from (Seddon & Templer, 1995).	59
Table 4.2	Thermotropic phase transition temperatures above 25 °C for the dry β -D-glucosides determined by optical polarising microscopy. Note: these transition temperatures are measured after initial heating and cooling during sample preparation.	65
Table 4.3	For comparison, dry Guerbet glucosides and xylosides data obtained using DSC are provided.	66
Table 4.4	Phase assignments and d -spacings or lattice parameter for the dry and excess water β -D-glucosides at 25 °C. Error in d -spacings or lattice parameter is ± 0.1 °C.	73
Table 4.5	Thermotropic phase transition temperatures above 25 °C for the dry β -D-maltosides determined by optical polarising microscopy. Note: these transition temperatures are measured after initial heating and cooling during sample preparation.	82
Table 4.6	Phase transition temperatures for anhydrous Guerbet and monoalkylated β -D-maltoside determined by DSC.	86
Table 4.7	Phase assignments and d -spacings for the dry and excess water β -D-maltosides at temperatures ranging from 0–80–0 °C.	91
Table 4.8	The structural parameters of the fluid lamellar L_α phase of Guerbet maltosides at full hydrations varying at temperatures 0–80 °C except for β -Mal-C ₁₂ C ₈ (25–85 °C) (heating and cooling). X-ray data were taken from SOL (β -Mal-C ₁₀ C ₆ , β -Mal-C ₁₄ C ₁₀) and Bede (β -Mal-C ₁₂ C ₈).	97

Table 4.9	Structural parameters of β -Mal-C ₁₂ C ₈ at different temperatures. d is the d -spacing, ϕ_w is the volume fraction of water, d_w water layer thickness, d_l monolayer thickness, S area per molecule at the maltoside/water interface.	105
-----------	--	-----

Table 4.10	Structural parameters of β -Glc-C ₁₂ C ₈ at different temperatures. d is the d -spacing, ϕ_w is the volume fraction of water, d_w water layer thickness, d_l monolayer thickness, S area per molecule at the glucoside/water interface.	106
------------	--	-----

University of Malaya

LIST OF EQUATIONS

Equation 2.1	Order parameter, S	13
Equation 2.2	Critical packing parameter, CPP	21
Equation 3.1	Retardation, r	39
Equation 3.2	Scattering vector, q	47
Equation 3.3	Bragg's Law	48
Equation 4.1	Area per molecule and volume fraction of water of L_α phase	95
Equation 4.2	Volume fraction of the maltoside, Φ_l	102
Equation 4.3	Lipid layer thickness, d_l	102
Equation 4.4	Cross-sectional area per maltoside, S	102
Equation 4.5	Diameter of the water cylinders, d_w	102
Equation 4.6	Glycoside layer thickness (along the line connecting the cylinder axes), d_l	103
Equation 4.7	Area per molecule at the glycoside/water interface, S	103

LIST OF SYMBOLS AND ABBREVIATIONS

α	:	Alpha
β	:	Beta
Col _h	:	Columnar hexagonal
Cr	:	Crystalline
Cub	:	Cubic
DSC	:	Differential Scanning Calorimetry
GL	:	Glycolipid
Glc	:	Glucose
ΔH	:	Enthalpy change
H _I	:	Normal hexagonal phase
H _{II}	:	Inverse hexagonal phase
I	:	Isotropic phase
I _I	:	Normal discontinuous cubic phase
I _{II}	:	Inverse discontinuous cubic phase
L ₁	:	Normal micellar solution
L ₂	:	Inverse micellar solution
L _a	:	Lamellar liquid crystal phase
L _C	:	Lamellar crystal
LC	:	Liquid crystal
Mal	:	Maltose
\hat{n}	:	Director axis
NMR	:	Nuclear Magnetic Resonance
OH	:	Hydroxyl group
OPM	:	Optical Polarising Microscopy

S	:	Order parameter
SAXD	:	Small-Angle X-ray Diffraction
SmA	:	Smectic A phase
SmC	:	Smectic C phase
T_C	:	Clearing temperature
T_g	:	Glass transition temperature
T_m	:	Melting temperature
V_I	:	Normal bicontinuous cubic phase
V_{II}	:	Inverse bicontinuous cubic phase

LIST OF APPENDICES

Appendix A	^1H -NMR Data	141
Appendix B	^1H -NMR Spectra	146
Appendix C	DSC Data	156
Appendix D	DSC Thermograms	238
Appendix E	Reprint Permission	243

University of Malaya

CHAPTER 1: INTRODUCTION

1.1 Research Background

Plasma membrane is a very thin fragile structure that is only five to ten nanometres wide. Hence, all interior cells are separated from the extracellular environment via this so called thin sheet (Fragneto *et al.*, 2018; Karp, 2010). Apart from this function, others are involved as compartmentalisation, selective permeable barrier, solute transportation, external signal responses, intercellular interaction and energy transduction. Consequently, an astonishing structural variability made up by a wide variety of lipid compositions in the plasma or cellular membrane as depicted in Figure 1.1 has currently become a subject of interest due to their important functions and roles.

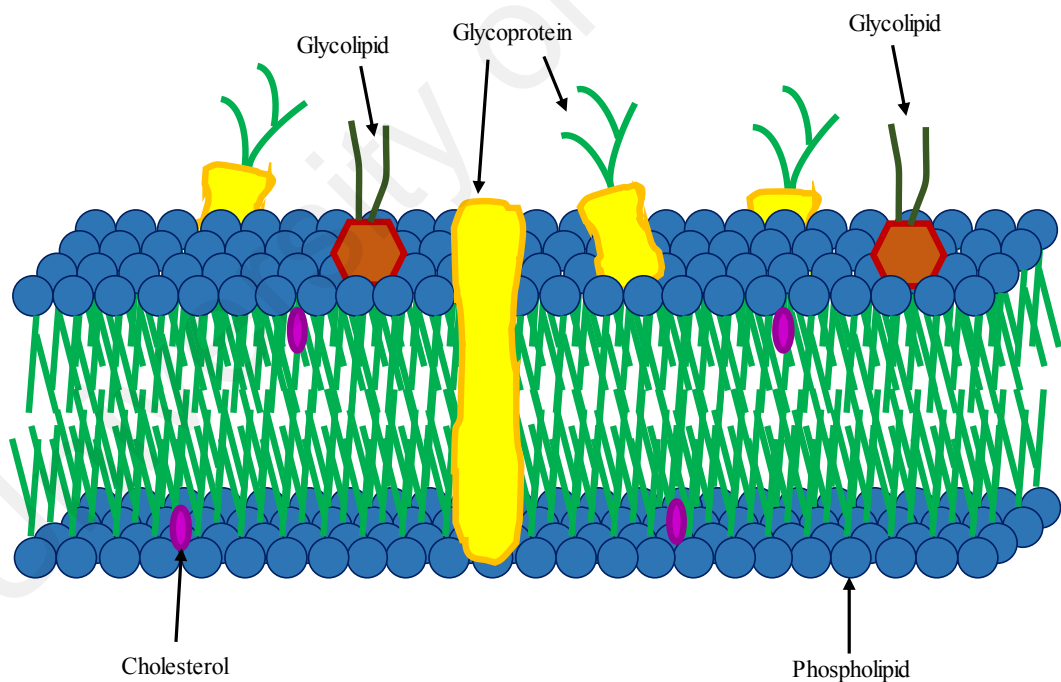


Figure 1.1: Cell membrane structure. Redrawn from (Karp, 2010).

The membrane lipids are all amphipathic in which they have two different affinities, as a hydrophilic that contains a polar head group water-loving and a hydrophobic that

comprises a non-polar fat-loving (Fragneto *et al.*, 2018). Cell membrane structure is largely made up from the amphiphilic molecules called phospholipids. The membrane constituents also consists of glycolipids (GLs) (Chester, 1997).

GLs are carbohydrate that link with lipids (Yu *et al.*, 2011). These compounds are plasma membrane essential components and can be found in eukaryotes and prokaryotes, including plants (Malhotra, 2012). Therefore, they play many important roles associated with plasma membrane functions. Figure 1.1 also illustrates GLs and glycoproteins which are normally discovered on the exterior surface of the cell membranes. This happens due to the head group of carbohydrates are hydrophilic, hence, they favour the aqueous cytoplasmic membrane located outside of its surface over the hydrocarbon lipid rich-based. This orientation helps in controlling the biological membrane asymmetric nature, and also permits carbohydrate moieties of both macromolecules to participate as cell attachment-recognition parts (Yamakawa & Nagai, 1978).

Sphingolipids are sphingosine derivatives that consist of a long hydrocarbon chain of amino alcohol. Phosphorylcholine and carbohydrate substituted sphingosine-based lipids are some examples of such derivatives (Karp, 2010). The former is widely known as sphingomyelin and the latter is recognised as one of GLs' groups known as glycosphingolipids. These sphingolipids normally present in animal and plant tissues (Kubota *et al.*, 2016; Lynch & Dunn, 2004). Cerebrosides which are galactocerebrosides occur in mammalian brain tissues, specifically myelin; whereas gangliosides, which can be obtained in abundance particularly in the brain (Kracun *et al.*, 1984) and nervous system (Yu *et al.*, 2011), are glycosphingolipids whose structures constitute simple and cluster of sugars, respectively.

Specific diseases are related to glycolipid abnormal quantities in tissues which are believed to be a key to various pathological disorders (Ruocco *et al.*, 1981). In the central

nervous system, these diseases are classified into two namely, demyelinating diseases and lysosomal storage disorders. Demyelination is defined as myelin loss with axon preservation. In the demyelinating diseases or disorders, there are several categories which are based on their pathogenesis. One of them is inflammatory processes demyelination. The disease is classified into three namely; multiple sclerosis, acute haemorrhagic leucoencephalitis (AHL), and acute-disseminated encephalomyelitis (ADEM). For instance, neuromyelitis optica is a specific multiple sclerosis disease which is also called Devic's disease. The patients with this disease have to endure sensory and vision loss; which, in turn, may develop paraplegia. It usually occurs due to an extensive demyelination at the optic nerve and spinal cord. Headache, pyrexia and vomiting are some of the clinical features of AHL. There is an extensive build-up of serious fluid which is oedema and fibrinoid necrosis of parenchymal blood vessels in the affected zones of the demyelinated brain tissues. Patients with ADEM may undergo some clinical features such as speech impairment, agitation and vomiting due to certain parts of the brain which are oedematous and demyelinated (Love, 2006). According to (Schulze & Sandhoff, 2011), the occurrence of lysosomal storage disorders is mainly attributed to the cells and tissues that comprise of huge amount of complex lipids abundancy and catabolic disorders inheritance. Some of these diseases are also known as Gaucher diseases (Enquist *et al.*, 2006), Metachronic Leokudystriphy (Biffi *et al.*, 2006) and Tay-Sachs diseases (Cachon-Gonzalez *et al.*, 2006). Therefore, the therapeutic approaches in handling GLs related diseases would still remain sparse and need to be established urgently.

Owing to the lipids chemical complexity found in cellular membranes, substantial research and attentions will continue to progress on synthetic GLs which mimic the natural ones in order to have deep understanding on the dynamic roles of biomembranes (Aripin *et al.*, 2013; Yang *et al.*, 2017; Zahid *et al.*, 2012). The wide spread and various

industrial applications of novel alkyl polyglycosides (APGs) act as a candidate for the synthetic GLs which can emerge in the form of detergents (Ehsan *et al.*, 2016), emulsions (Ji *et al.*, 2019), drug delivery (Vaskan *et al.*, 2018), food processing (Zhou *et al.*, 2017) and pharmaceuticals (Sekhon, 2013). These APGs show amphiphilic properties which, in turn, tend to display self-assembled thermotropic and lyotropic liquid crystalline mesophases over a very wide range of conditions; for examples, with a change in temperature and hydration. Therefore, the mesophases produced exhibit a phase transition from lamellar to non-lamellar phases, such as hexagonal and cubic. These phases are presently gaining attention and interest among researchers due to their importance in biological phenomena and technological applications. The APGs, which are GLs, are also called as surfactants (surface-active agents) associated with their amphiphilic structures (Knepper & Berna, 2003).

A literature review reveals that the phase behaviour of a surfactant-solvent system is affected by changing either component. For instance, usually in the pure state, single straight-chain and branched-chain glycosides exhibit only one mesophase and a variety of liquid crystal phases, respectively. Similarly, different types of phases may be adopted ranging from micellar to cubic phases, in a lyotropic system for both single straight-chain and branched-chain alkyl glycosides (Hashim *et al.*, 2006). These liquid crystalline phases have been characterised extensively via optical polarising microscopy, differential scanning calorimetry and small-angle X-ray diffraction (Brooks *et al.*, 2011; Liew *et al.*, 2015; Patrick *et al.*, 2018). Liao *et al.* (2006) studied the branched-chain GLs thermotropic mesomorphism. The results showed that a smectic phase is obtained for a single chain, dodecyl- β -D-glucopyranoside ($C_{12}G_1$) and the shortest branched-chain which are butyl-octyl- β -D-glucopyranoside ($C_{8-4}G_1$) and ethyl-hexyl- β -D-maltopyranoside ($C_{6-2}G_2$), as compared to the GLs with a longer branched-chain which

produces phases between columnar and smectic. However, these results are not in agreement with (Nilsson *et al.*, 1998) in which they observed that lyotropic alkyl glucosides of the branched hydrocarbon chain (2-ethyl-hexyl β/α -D-glucosides) exhibit only a lamellar phase; whereas the straight hydrocarbon chain (*n*-octyl β/α -D-glucosides) adopt several different types of liquid crystalline phase.

Moreover, hydrations of lipid surfactants are entropically driven that links with a phase transition (Kocherbitov & Soderman, 2006; Kocherbitov *et al.*, 2002). Therefore, an investigation on the structural parameters of its hydrated phases is significantly important. These give several advantages in relation to, for example, the uptake number of water molecules, interfacial area per molecule and limiting water content. Similar studies have been done using small-angle X-ray diffraction methods (Kocherbitov & Söderman, 2003; Markova *et al.*, 2000; Seddon *et al.*, 1997). Therefore, the purpose of this study is to analyse the effect of branched-chains and sugar head groups on mesophase behaviours in thermotropic and lyotropic systems of glucosides and maltosides.

1.2 Problem Statement

Numerous research studies have presently been carried out in regards to sugar lipids due to its breadth of carbohydrate chemistry since 1908 (Freudenberg, 1967). This is understandable because of the emergence of many complex sugar lipids structures; for example, GLs. Most of these GLs are amphitropic liquid crystals and can be found naturally and synthetically. The former is linked to the plasma membrane and its functions, hence natural GLs are undeniably an important biologically constituent (Cameotra & Makkar, 2004). Moreover, the latter is related to industrial sciences (Han *et al.*, 2016). The GLs are amphiphilic molecules capable of organising themselves leading into various phases such as lamellar, hexagonal and cubic. Therefore, identification and

characterisation of these different phases have been the subject of interest at the present moment (Yang *et al.*, 2017).

Alkyl glycosides are one of the GLs which also display liquid-crystalline structures. The glycosides tend to undergo a phase transition under the influence of temperature and hydration; which in turn forms thermotropic and lyotropic liquid-crystalline phases, respectively. In addition, lipid chemical structures; namely sugar head group and hydrocarbon chain length are among the factors that may affect their phase transition as well (Hashim *et al.*, 2012; Vill & Hashim, 2002).

Since the alkyl glycosides may exhibit various mesophase transitions governed by its thermodynamic parameters, thus, in-depth studies should be conducted on alkyl glycosides under the pretext of temperature and hydration variables. The resultant mesophases adopted ranging from lamellar to cubic phases may lead to different potential applications in life-sciences and technology.

1.3 Objectives of the Study

The overall goal is to study the liquid crystalline phase behaviour formed by branched-chain Guerbet β -D-glucosides and β -D-maltosides. To achieve the research main purpose, here are the following objectives:

- 1) To investigate the phase behaviour of five homologous series of branched-chain Guerbet β -D-glucosides in dry and excess water conditions.
- 2) To investigate the phase behaviour of five homologous series of branched-chain Guerbet β -D-maltosides and hydration properties of their lamellar phases.
- 3) To study the effect of sugar head group size having identical hydrocarbon chain ($C_{12}C_8$) on structural parameters of their mesophases at fixed hydration of water conditions.

1.4 Scope of the Study

The scope of this study focuses on the synthetic GLs namely branched-chain Guerbet glucosides and maltosides. These glycosides are amphiphiles; and hence, exhibit liquid- crystalline phases. Therefore, the scope of the study refers to the investigation on the effects of the hydrocarbon chain lengths and sugar head groups; and the influence of temperatures and hydrations on the thermotropic and lyotropic liquid crystals mesophases. The physical testing methods employed for characterisation of the glycosides are differential scanning calorimetry, optical polarising microscopy and small-angle X-ray diffraction.

Synthetic glycolipids are preferred to be used in most biophysical experiments because the natural ones are difficult to extract in large quantities and purity although the latter is plentiful in nature. In this project, the branched-chain Guerbet glycolipids have been chosen to closely mimic the double chain glycosides such as monogalactosyl diacylglycerol (MGDG) and digalactosyl diacylglycerol (DGDG).

1.5 Significance of the Study

The study of mesophase behaviours of liquid crystal synthetic branched-chain glycosides could provide new knowledge on the biological applications such as drug carrier (Salim *et. al.*, 2015), membrane protein crystallisation (Arachea *et. al.*, 2012) and skin penetration (Aripin *et. al.*, 2013). This is because the branched-chain glycosides, one of the synthetic GLs mimicking the natural GLs, are desirable alternatives that may consequently unravel certain cellular membrane function which is not yet fully understood until now.

Even though, numerous research works on liquid crystal GLs have been conducted in the field of lipids, the study pertaining to the thermotropic and lyotropic

phases produced from liquid crystal synthetic branched-chain glycosides may contribute to the basic understanding of the knowledge on the various technological potential applications in the fields of pharmaceuticals, drug delivery systems, detergency, and cosmetics.

1.6 Thesis Outline

This thesis comprises of five chapters. **Chapter 1** identifies the research background. This part describes GLs as one of the important constituent cellular membranes and are involved in cell wall functions. Therefore, some research relating to natural and synthetic GLs have been addressed. The current research topic, research gap and research needed to be done are highlighted in the problem statement. There are three main objectives for this study. The research scope, significance of the work and thesis outline are also briefly described.

Chapter 2 reviews the GLs self-assembly that exhibits liquid crystal mesophases in both thermotropic and lyotropic systems. The structure-property relationship of GLs is discussed at greater length.

Chapter 3 consists of the techniques and methods utilised for the current study. This encompasses the instrument common in principles of differential scanning calorimetry, optical polarising microscopy, and small-angle X-ray diffraction. An AXcess software programme is used to analyse the X-ray data.

Chapter 4 focuses on results and discussion of the work which have been conducted throughout the study. The first part reports on the phase behaviour of five homologous series of branched-chain Guerbet β -D-glucosides, both in dry state and in excess water using a combination of techniques. The second part of the project focuses

on the phase behaviour of five homologous series of branched-chain Guerbet β -D-maltosides and hydration properties of their lamellar phases.

Finally, the structural parameters of 2-octyl-dodecyl β -D-glucoside (β -Glc-C₁₂C₈) and 2-octyl-dodecyl β -D-maltoside (β -Mal-C₁₂C₈) at fixed water contents are also discussed to study the effect of sugar head group size on their phase behaviour.

Chapter 5 concludes the work performed and presents some suggestions for future works in this study.

University of Malaya

CHAPTER 2: LITERATURE REVIEW

2.1 Glycolipids Self-Assembly

Glycolipids are compounds which have a hydrophilic sugar head (polar) and a lipophilic tail (non-polar) (Thiesen *et al.*, 2006). These compounds are amphiphilic molecules. “Like dissolves like” is a rule of thumb which explains the interaction between the hydrophilic head group and water, and the lipophilic non-polar chain and non-polar solvents. This interaction allows the amphiphilic molecules to spontaneously assemble when in contact with water or solvents. These molecules are further aggregated into a variety of shapes in different forms of phases (Collings & Hird, 1997). Because of these characteristics, glycolipids are used in laundry detergents, and as hard surface cleaners in agriculture industries (Thiesen *et al.*, 2006). There are two types of glycolipids, namely synthetic (Vill & Hashim, 2002) and biosurfactant glycolipids (Kitamoto *et al.*, 2009). The former is made from a chemical substance, whereas the latter is made from renewable resources. Property-structure relationships such as functional groups and anomeric centres, big structures, biodegradable and toxicity, critical micelle concentration and surface active, and self-assembly are of the important parameters which can be employed to distinguish between these surfactants (Kitamoto *et al.*, 2009).

2.2 Sugar Head Group

Hexoses are an aldose sugar with six carbon atoms. Other types of aldoses are glyceraldehydes, tetrose and pentoses. These differ from the hexoses based on the number of carbon atoms in the structure of aldose sugar. A glucose is one of the hexoses (Karp, 2010). Sugar compounds may contain one or more glucose unit, called monosaccharide

(e.g. alkyl glucosides (AG)) or polysaccharide (e.g. alkyl polyglucosides (APGs), respectively (Vill & Hashim, 2002). An extensive research associated with sugar head groups were carried out in relation to the number of glucose molecules. The effects of glucose-based surfactants on structure-property relationships were investigated by Boyd *et al.* (2000). One of them was the effect of glucose head group polymerisation on thermotropic and lyotropic phases. The thermotropic transition temperatures and a surfactant solubilisation were significantly higher and increased, respectively from glucose (one sugar molecule) to maltose (two sugar molecules) head groups. The increase in the transition temperature was proposed due to more interactions between maltose head group and sites of hydrogen bonding (Sasaki, 2008). Similarly, the research on mono- and disaccharide head groups were addressed by Howe and co-workers (Collings & Hird, 1997) with respect to aggregation structures. The effect of adding the sugar head from one to two yielded the existence of inverse hexagonal (H_{II}) phase in the monosaccharide compounds and multilamellar phases in the disaccharide compounds.

2.3 Hydrophobic Tail

A hydrophobic tail, which is a lipophilic tail, is a non-polar part of the amphiphilic molecules (Karp, 2010). A branched hydrocarbon chain (surfactant-based) was identified as the major cause of the phase behaviour patterns (Jeffrey, 1986). The findings of this study suggest that hydrophobicity is higher in the branched hydrocarbon as compared to straight hydrocarbon chains. However, the most important limitation lies in the fact that hydrophobicity depends on amount and type of branching group in the surfactant. Hashim *et al.* (2012) reported that the surfactant hydrophobicity increases by increasing the alkyl hydrocarbon chain. At lower surfactant concentrations, the rise in hydrophobicity mainly affects the behaviour of lyotropic liquid crystalline phases due to a phase separation.

However, at higher surfactant concentrations, the lamellar phases with small composition are formed. Moreover, the transition temperatures increase in thermotropic and lyotropic conditions owing to the molecule dispersion interactions in relation to the alkyl hydrocarbon increment. No formation of hexagonal or cubic phases is observed as a result of increasing branched hydrocarbons. On the contrary, the formation of hexagonal or cubic phases is observed for the case of straight hydrocarbon chains. These are probably as a result from packing difficulties on branched hydrocarbon chains (Nilsson *et al.*, 1997). Another important finding is that the alkyl length has a significant impact on the mesophase obtained (Funari & Rapp, 1999).

2.4 Anomer

An anomer, which is a cyclic form of sugar molecule, is an epimer with two chiral centres. This epimer differs in its configuration at carbon chiral centres, which are anomeric carbons i.e. C1 atom of an aldose or C2 atom of ketose. There are two types of anomers, namely α -anomer and β -anomer. If the anomeric carbon configuration is similar to a Fischer projection asymmetric carbon, it is identified as α (axial configuration) (Garrett & Grisham, 2017). On the other hand, the anomer is designated as β (equatorial configuration) if it is different. The α - and β -forms of glucose are the examples of such configurations. As for sugar molecules configurations, the differing phenomenon can be identified in glucose molecule (Balzer & Luders, 2000). An anomeric effect is a phenomenon at which an electronegative substituent is in favour of an axial arrangement (Karp, 2010). As such, based on the observation made by Hashim *et al.* (2012), phases and transition temperatures of lyotropic structures are mainly affected by the anomeric orientation for the case of shorter hydrocarbon chain. These are however not the case for longer hydrocarbon chain. Moreover, surface tensions or calculated head group areas are

not essentially affected by the anomeric configuration. A rotation of a molecule which occupies space volume is able to influence its clearing temperature in relation to different types of anomers (Zhang *et al.*, 2004). The α - and β -anomeric maltosides are self-assembled into quasi-spherical aggregates and an oblate ellipsoid shape, respectively. These are caused by their anomer orientations.

2.5 Fundamental of Liquid Crystals

Liquid crystals exhibit an intermediate phase between the ordered solid and the ordinary liquid states of matter (Dierking, 2003). The solid state comprises of molecules with two different types of orders, namely positional and orientational. Therefore, in solid, these molecules are closely packed in the specific lattice position and preferred orientation. On the contrary, these molecules do not exhibit both orders when they are in liquid form. In other words, in liquid, the molecules are not in the preferred direction and randomly distributed. Hence, the liquid crystal molecules do possess some of the order of crystalline solids. Moreover, the molecular axes of these molecules favour to a point along a certain direction that is termed as a director with the unit vector \hat{n} as provided in Figure 2.1. Another parameter which is called an order parameter (S) represents the degree of the molecular long axes' alignment with the director on average as shown in Equation 2.1. (Collings & Hird, 1997):

$$S = \langle \frac{3\cos^2\theta - 1}{2} \rangle \quad \text{(Equation 2.1)}$$

where S is the order parameter and θ is the angle between the long axes and director of molecules. Figure 2.1 illustrates the angle (θ) of order parameter, S and vector director, \hat{n} .

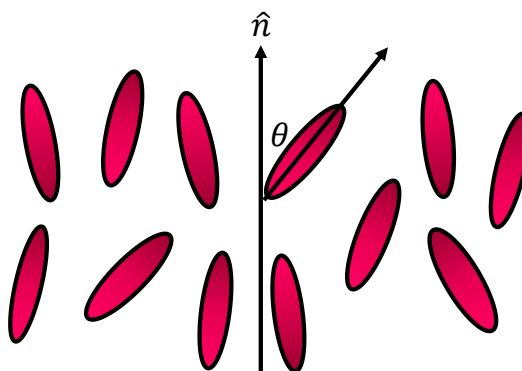


Figure 2.1: A diagram of the molecules alignment relative to the vector \hat{n} (director) and θ (angle of order parameter, S).

An order with non-zero degree can be used to differentiate between the liquid crystals and liquid phase. Therefore, when this preferred order or direction is destroyed, the compound turns to isotropic liquid with uniformity in all orientations. Furthermore, according to Collings & Hird (1997), isotropy or anisotropy of the compounds adopted is dependent on the molecular shape that occupies the solid lattices. For instance, the spherical or spherical-like molecules display an isotropic liquid crystal phase (e.g. cubic liquid crystals) and non-spherical molecules exhibit the anisotropic liquid crystal lattice e.g. graphite (Guo *et al.*, 2006a; Guo *et al.*, 2006b).


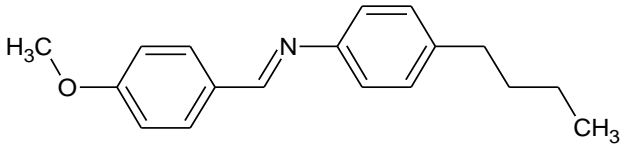
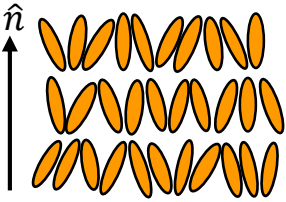
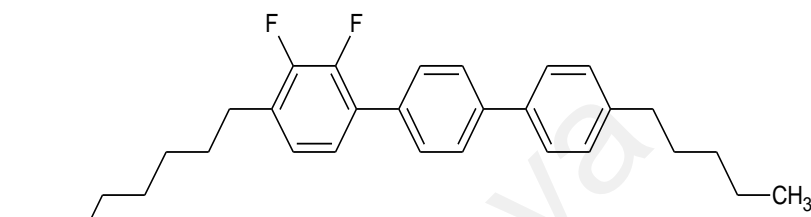
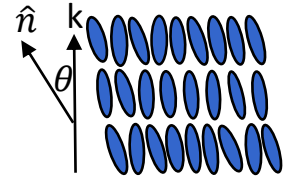
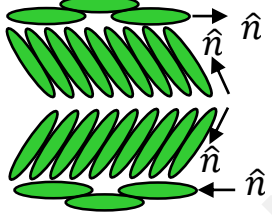
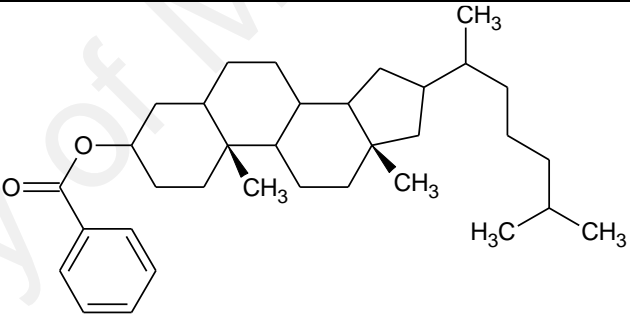
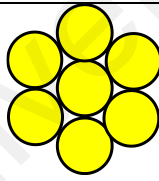
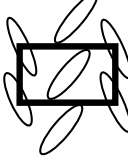
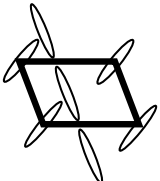
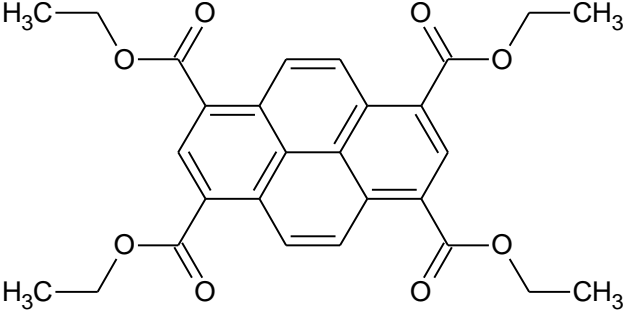
There are two categories of liquid crystals, namely thermotropic and lyotropic (Brooks *et al.*, 2011). The occurrence of thermotropic liquid crystals is due to the effect of the temperature variations. However, the lyotropic liquid crystal phase formed is due to the effects of both temperature and concentration of solvent (Dierking, 2003; Tschierske, 2007). Moreover, according to Dierking (2003) and Vill and Hashim (2002), amphitropic mesogens display both the thermotropic and lyotropic phase behaviours. Brief description of liquid crystal classifications will be explained in the subsequent section.

2.5.1 Thermotropic Liquid Crystals

According to Dierking (2003), the basic molecular shapes; for instance, the calamitic (rod-like shape), discotic (disc-like shape) and sanidic (brick-like shape) determine the various types of thermotropic liquid crystals (Dierking, 2003). Usually, the calamitic is the most common type of shape molecules adopted in forming the liquid crystal phase, hence producing different liquid crystal structures. The long molecular axis alignment interaction will be favoured due to the elongated shape of these molecules. In contrast, the short molecular axis alignment interaction will be favoured involved due to the discotic nature of the molecule. Therefore, thermotropic liquid crystals exhibited are stable at certain temperature range for both calamitic and discotic liquid crystal molecules (Collings & Hird, 1997).

Referring to Table 2.1, the calamitic mesogen e.g. 4-butyl-N-(methoxybenzylidene)-aniline (MBBA) exhibits the nematic phase with the presence of orientational order but no positional order (Dierking, 2003). Compound such as 2,3-difluoro-4-heptyl-4''-pentyl-1,1':4',1''-terphenyl shows phase changes from the nematic to the Smectic A (SmA) and Smectic C (SmC) (see Table 2.1) as the temperature decreases. Moreover, the molecular arrangement of this compound adopts the positional order due to its molecule centers of mass are arranged in layers (SmA) and with the SmC, the long molecular axes are tilted. In addition, both the SmA and SmC possess the orientational order where in the former, the director axis \hat{n} is perpendicular to their normal layer planes, while in the latter \hat{n} is at some other angle to the planes.

Table 2.1: Molecular structures and their related thermotropic phases.

Phase	Phase Behaviour	Structure of the Molecule
Nematic (<i>N</i>)		 (a) 4-butyl-N-[methoxy-benzylidene]-aniline (MBBA)
Smectic (<i>SmA</i>)		
Smectic (<i>SmC</i>)		(b) 2,3-difluoro-4-heptyl-4''-pentyl-1,1':4',1''-terphenyl
Cholesteric (<i>N*</i>)		 (c) Cholesteryl benzoate
Columnar	 Hexagonal  Rectangular  Oblique	 (d) Tetraethyl pyrene-1,3,6,8-tetracarboxylate

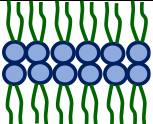
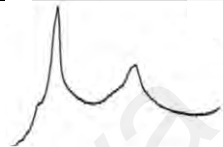
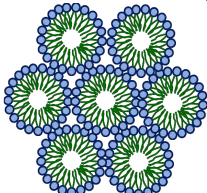
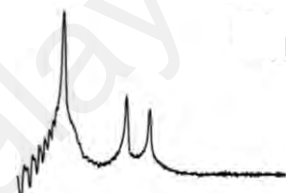
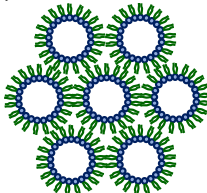
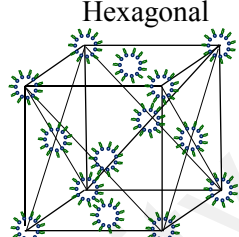
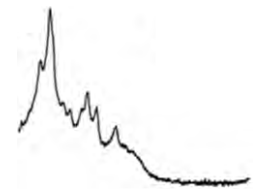

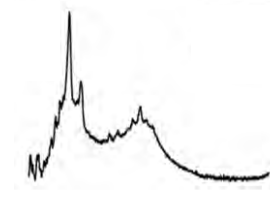

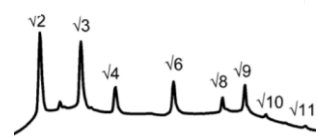

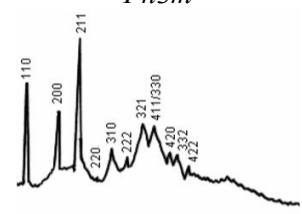
Moreover, a chiral nematic phase is exhibited by chiral molecules such as cholesteryl benzoate. In this phase, which is also known as the cholesteric (N^*), the layered structure is rotated in a helical twist with an axis perpendicular to the \hat{n} (director) and tilted with an angle θ (see Table 2.1). Both nematic and columnar phases can be formed by discotic liquid crystal molecules e.g. tetraethyl pyrene-1,3,6,8-tetracarboxylate (see Table 2.1) whereby in the columnar phases, the molecules can have an order or disorder. The top view of the columnar discotic liquid crystal compound (hexagonal, rectangular and oblique) is also shown in the table.

2.5.2 Lyotropic Liquid Crystals

A special mesophase of liquid crystal called lyotropic, is formed upon mixing in a suitable solvent such as water. This type of liquid crystal phase is achieved due to the role of solvent concentration and temperature factors. A daily example of a lyotropic liquid crystal is a soap and water mixture. In other words, lyotropic liquid crystal is used to describe the common material behaviours which consist of amphiphilic molecules when they dissolve in a solvent. Such molecules possess both hydrophilic head group and hydrophobic tail group, where one part has high-affinity binding towards polar solvents, and another part shows a strong-affinity towards a non-polar. Hence, these molecules are also called as amphiphile with dual tendency for water-hating and water-loving. According to Collings and Hird (1997), in both polar and non-polar solvents, these molecules produce normal phase and inverse phase ordered structures, respectively. Phase behaviours of lyotropic liquid crystals are extensively studied over the entire concentration range. Varying concentration of solvents provides a wide variety of well-defined lyotropic liquid crystal phases depending on the volume among hydrophilic head groups and hydrophilic tail chain length. Table 2.2 shows different structures of common

lyotropic liquid crystals such as lamellar, hexagonal and cubic phases which have been characterised by X-ray technique (Collings & Hird, 1997; Guo *et al.*, 2010).

Table 2.2: Mesomorphic lyotropic phase structures and X-ray diffraction/scattering patterns. Compiled from (Sun & Zhang, 2004; Zahid *et al.*, 2013; Liew *et al.*, 2015; Hashim *et al.*, 2018).

Possible Mesophases	Typical Bragg Reflections (Scattering Pattern)
 (a) Lamellar, L_a	 L_a
 (b) (i) Normal H_I	 H_{II}
 (ii) Inverse H_{II}	
 (c) Discontinuous Cubic, $Fd3m$	 $Fd3m$
 (i) $Ia3d$	 $Ia3d$
 (ii) $Pn3m$	 $Pn3m$
 (iii) $Im3m$	 $Im3m$
(d) Bicontinuous Cubic	

Hyde (2001) states that a lamellar (L_a) phase is obtained from double chained and a longer chain amphiphilic molecule. The lamellar structures are arranged in the form of bilayer amphiphile of planar and parallel stacks (see Table 2.2). Solvent layer separates the polar head group. A lamellar mesomorph state displays a smectic diffraction pattern and has an optically anisotropic character (Hyde, 2001). Furthermore, the viscosity of the lamellar phase, which contains less water due to its parallel layers, is less compared to a hexagonal phase (Collings & Hird, 1997; Hyde, 2001).

Molecular aggregates with the hexagonal arrangement pattern correspond to the hexagonal phase. In comparison with the bicontinuous cubic phase and micellar, the hexagonal phase possesses an intermediate viscosity strength. Polarised light optical texture of this phase exhibits the similar birefringent texture as columnar thermotropic phase which is often recognised as a fan texture. This texture is associated with focal conic domains of columns (Hyde, 2001). As shown in Table 2.2, hexagonal phase of lyotropic liquid crystal can be found in two types namely, the normal hexagonal phase (H_I) and inverse hexagonal phase (H_{II}). The hexagonal phase contains densely packed cylinder micelles that are arranged in a hexagonal pattern. Typically, the inverse hexagonal phase possesses a small cylinder diameter and is acquired at a relatively high temperature when compared with the closer-packed cylinders of the normal hexagonal phase (Amar-Yuli *et al.*, 2007; Collings & Hird, 1997) with the first three X-ray characteristic diffraction/scattering pattern appeared at 1, $\sqrt{3}$ and $\sqrt{4}$.

The cubic phase formation is not as ordinary as the lamellar and hexagonal phases. Phase diagram gives valuable information about their occurrence in different areas and position. These may rely on their molecular structures. They can be formed whether in the normal phase or the inverse phase. The cubic phase is known for its highly viscous ordered self-assembling structures; however, it shows isotropic properties similar to

micelles. For example, when the lipid monolayer surface curves move towards the chain region, it indicates a positive mean curvature (i.e. micelle that is elliptic); nevertheless, when these curves move towards the polar part, it displays a negative mean curvature (i.e. saddle surface which is hyperbolic) (Shearman *et al.*, 2006). Consequently, the planar surface (i.e. lamellar) or parallel stack (i.e. hexagonal) demonstrates zero mean curvature with the parabolic surface (Liew *et al.*, 2015; Shearman *et al.*, 2006).

A discontinuous cubic phase, which is an intermediate lyotropic liquid crystal phase structure, is a mesophase made up of discrete discontinuous micellar phase with different sizes packed in a specific space group cubic array. $Fd3m$, for instance, self-organises as a discontinuous cubic phase (see Table 2.2). This cubic phase is made up of densely packed ordered micellar in a face centered cubic lattice (Pouzot *et al.*, 2007; Seddon *et al.*, 2000; Yaghmur & Rappolt, 2013). Guerbet xyloside produces the $Fd3m$ in excess water with the Bragg reflections of $\sqrt{8}$, $\sqrt{11}$, $\sqrt{16}$, $\sqrt{19}$, $\sqrt{24}$, $\sqrt{27}$, $\sqrt{32}$ and $\sqrt{43}$ (Liew *et al.*, 2015; Pouzot *et al.*, 2007).

A bicontinuous cubic phase which is observed as black polarised microscopic texture is very viscous, rigid and isotropic (Hyde, 2001). A triply periodic hyperbolic surface folds the bicontinuous cubic phase bilayer which resembles homogeneous sponges associated with zero mean curvature (Hyde, 2001; Seddon *et al.*, 2000). According to Vill and Hashim (2002), a mesophase between the lamellar and the hexagonal phases is called the bicontinuous cubic phase. As listed in Table 2.2, there are three different types of space groups of inverse bicontinuous cubic phase; namely D surface ($Pn3m$), G surface ($Ia3d$) and P surface ($Im3m$) (Hyde, 2001; Seddon *et al.*, 2000; Seddon *et al.*, 2006). The X-ray diffraction pattern for $Ia3d$ usually have the peak positions of $\sqrt{6}$, $\sqrt{8}$, $\sqrt{14}$, $\sqrt{16}$, $\sqrt{20}$, $\sqrt{22}$, $\sqrt{24}$ and $\sqrt{26}$; while, the typical diffraction pattern of $Pn3m$ appeared at $\sqrt{2}$, $\sqrt{3}$, $\sqrt{4}$, $\sqrt{6}$, $\sqrt{8}$, $\sqrt{9}$, $\sqrt{10}$ and $\sqrt{11}$. The $Im3m$ produces

the Bragg reflections with typical values of $\sqrt{2}$, $\sqrt{4}$, $\sqrt{6}$, $\sqrt{8}$, $\sqrt{10}$, $\sqrt{12}$, $\sqrt{14}$ and $\sqrt{16}$ (Sun & Zhang, 2004). In comparison with the other two cubic phases, the simplicity of $Im3m$ makes it less common (Seddon *et al.*, 2000).

Rheology study is conducted to gain insight into the flow behaviour of the different liquid crystalline phases formed. A few rheological studies on lyotropic liquid crystalline phases exhibit various materials including the glycolipid of interest i.e. Guerbet glucosides and maltosides have been studied. These glycolipids possess the same number of carbons in their alkyl chain but differ in head group size. It was reported that all their lamellar, inverse hexagonal and inverse bicontinuous cubic phases exhibited shear thinning behaviour. The subsequent frequency sweep experiments showed that these mesophases followed the typical viscoelastic G' , G'' response for non-Newtonian fluid (Mislán *et al.*, 2019).

Theory of Amphiphile Molecules

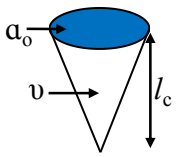
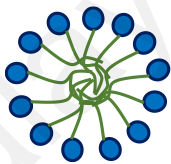
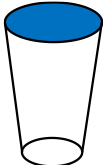
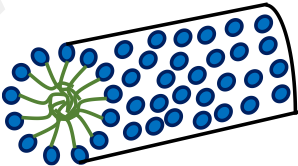

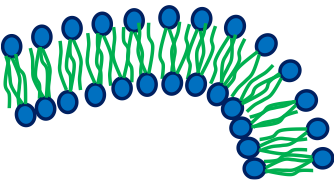
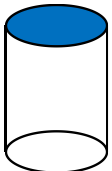
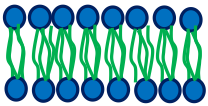
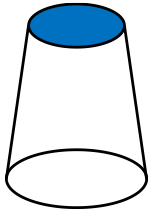
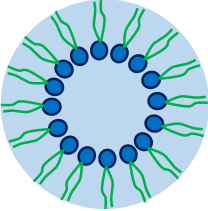
Spherical and non-spherical micelles are formed by the amphiphiles in aqueous medium. The shape of these micelles is determined by a critical packing parameter (CPP). A theory proposed by Israelachvili and co-workers (1994, 1980, 1976) states that the CPP is calculated based on the dimensionless packing parameter and is defined as follows (Equation 2.2):

$$CPP = \frac{v}{a_o l_c} \quad \text{(Equation 2.2)}$$

where v is the molecular volume of the molecule, a_o is the optimum head group surface area and l_c is the maximum or chain length of the hydrophilic tail molecule. Therefore, the CPP value is related with the shape of the amphiphilic molecule which, in turn, determines the type of self-assembly. The CPP will identify whether the glycolipid

compounds produce spherical micelles ($CPP < 1/3$), non-spherical micelles ($1/3 < CPP < 1/2$), rod-like micelles ($CPP \cong 1/2$), flexible bilayer vesicles ($1/2 < CPP < 1$), planar bilayer ($CPP \cong 1$) and inverse structures ($CPP > 1$) (Israelachvili, 2011; Israelachvili *et al.*, 1980). Table 2.3 depicts the adopted lipid possible structures with different CPP values.

Table 2.3: Formation of lipid molecules geometries packing properties and self-assembly structures. Redrawn from (Israelachvili *et al.*, 1980).

Lipid	Shape of Lipid	CPP	Type of Self-Assembly
Lipids with large head group and single-chained tail	 Cone	$< 1/3$	 Spherical micelles
Lipids with small head group and single-chained tail	 Truncated cone	$1/3 - 1/2$	 Cylindrical micelles
Lipids with large head group and double-chained tails	 Truncated cone	$1/2 - 1$	 Flexible bilayers
Lipids with small head group and double-chained tails	 Cylinder	~ 1	 Planar bilayers
Lipids with small head group and double-chained tails	 Inverse truncated cone	> 1	 Inversed micelles

2.6 Lyotropic Phase Behaviour

The types of phases produced are determined by the thermodynamic properties of amphiphatic compounds in solutions, which are controlled by the hydrophobic effect (Hamley, 2000). Apart from producing a micellar phase, these compounds can generate a number of other phases. A lamellar, for instance, is characterised by a stack of amphiphilic molecules arranged in bilayers, whereas hexagonal and cubic phases are packed in geometrically distinctive molecular pattern-assemblies. The sequence of phases formed by varying the concentration (Seddon *et al.*, 2000). Detailed description on the micellar solution and lyotropic phases are described in the following section.

2.6.1 Micellar Solution

Spherical aggregations of the amphiphilic molecules are known as micelles. They are stable in water as long as their concentration is above the critical micelle concentration. Micelles can be divided into normal (type I) and inverse (type II) micelles as shown in Figures 2.2 and 2.3, respectively. The normal micelles occur in oil-water mixtures where water surrounds the micelles. In this case, the hydrophilic head groups point outwards into water and the lipophilic non-polar chains point inwards into oil. On the other hand, inverse micelles occur in water-oil mixtures where water fills the void in the micelle centre in which the lipophilic non-polar chain points outwards into oil, whereas the hydrophilic head group points inwards into water (Collings & Hird, 1997). In relation to this matter, Nagarajan (2002) points out that not only should the hydrophilic head group be considered, but the hydrophobic tail also another important factor should be addressed in determining the aggregation of shape and size molecules. However, Cecutti *et al.* (1991) suggest that the steric factors, namely the conformation and

orientation of hydrophilic head group; and chain-hydrophilic head group interface affect the aggregation of micelles (Seddon *et al.*, 2000).

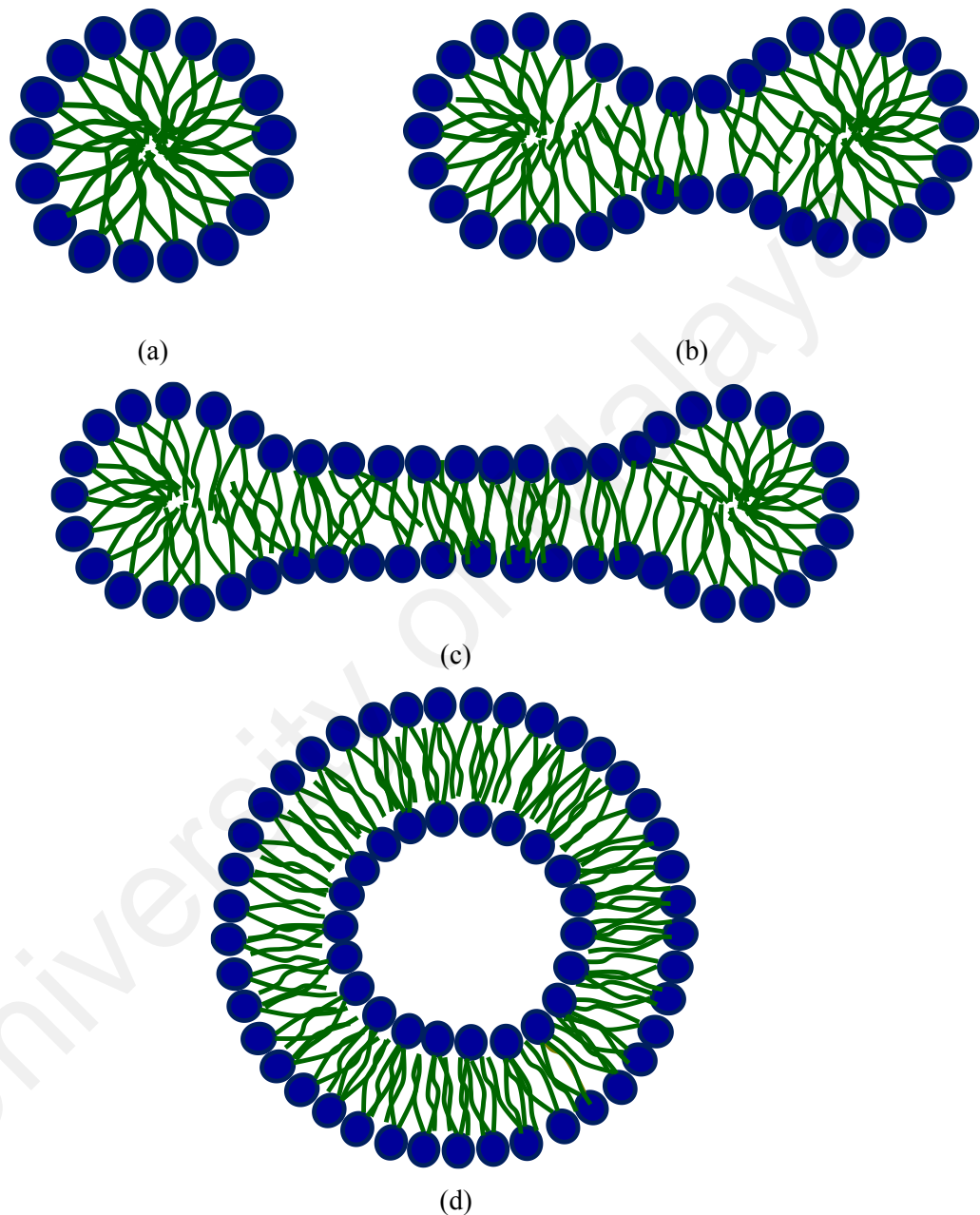


Figure 2.2: Micelles (Type I) self-assemblies showing (a) spherical micelle; (b) globular micelle; (c) rod-like micelle; and (d) spherical bilayer vesicle. Redrawn from (Hamley, 2000).

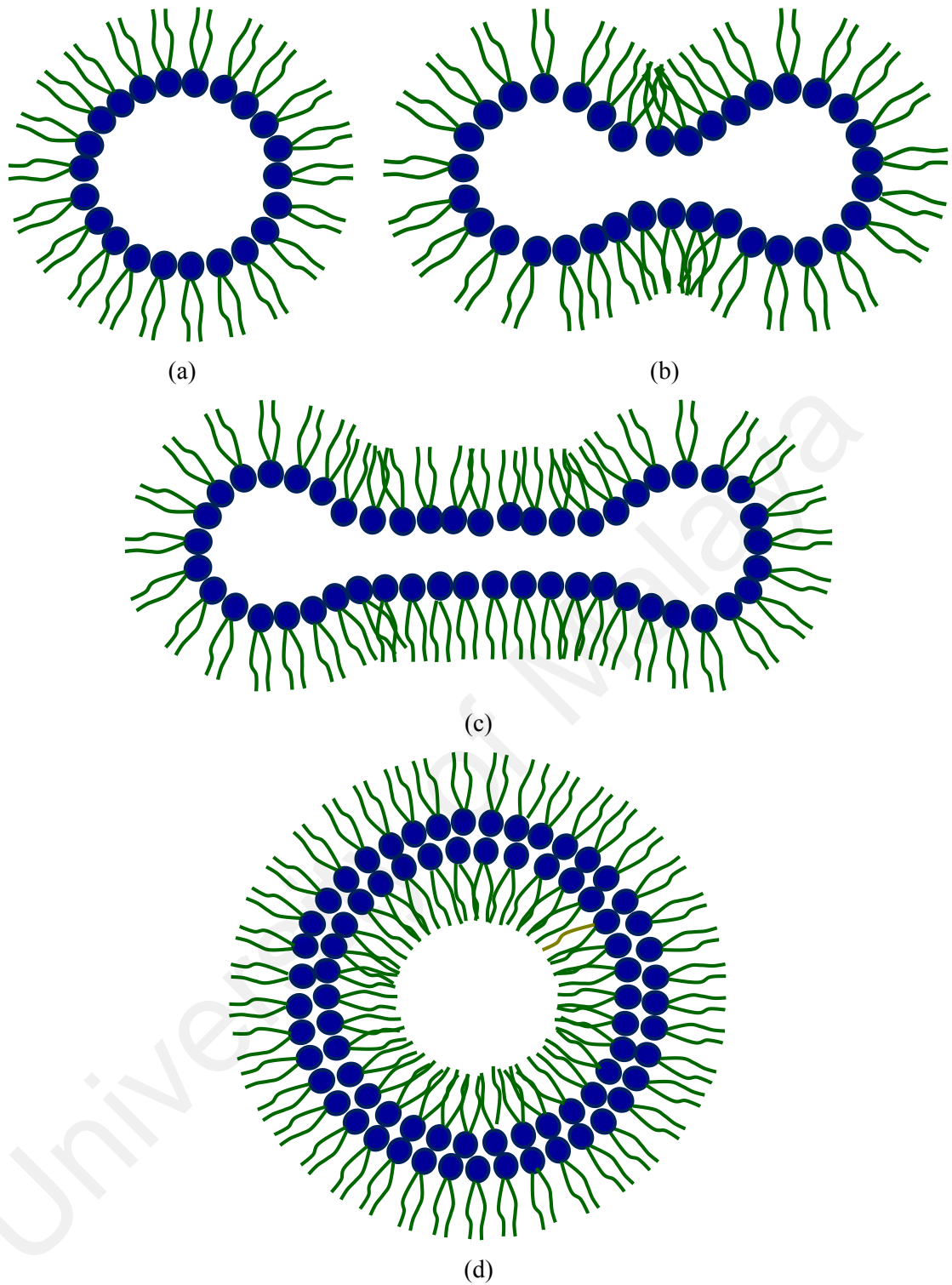


Figure 2.3: Micelles (Type II) self-assemblies showing (a) inverse spherical micelle; (b) inverse globular micelle; (c) inverse rod-like micelle; and (d) inverse spherical bilayer vesicle. Redrawn from (Lombardo *et al.*, 2015).

2.6.2 Lamellar Phase

The lamellar phase is made up of one-dimensional stacks of amphiphilic bilayers by water layers. Each bilayer comprises two monolayers which are stacked with the lipophilic non-polar chain in order to avoid contact with water. While the hydrophilic head group of the molecules is in contact with the aqueous solvent. The lamellar phase can be divided into three types, namely a L_C 'crystalline phase', which consists of bilayers with all rigid chains; a L_α 'fluid lamellar', which comprises randomly ordered and fluid-like hydrocarbon chains (Figure 2.4); and a L_β 'gel phase', which consists of hydrocarbon in *trans* conformation (Collings & Hird, 1997). In relation to one-dimensional structure, Howe and co-workers (2007) identify only multilamellar phases occurring in a disaccharide compound. Moreover, Garidel *et al.* (2008) state that the type of linkage in sugar head groups affect the structural characteristics of observed phases, such as an 'orthorhombic symmetry' and interdigitated structure which are found in gel phase.

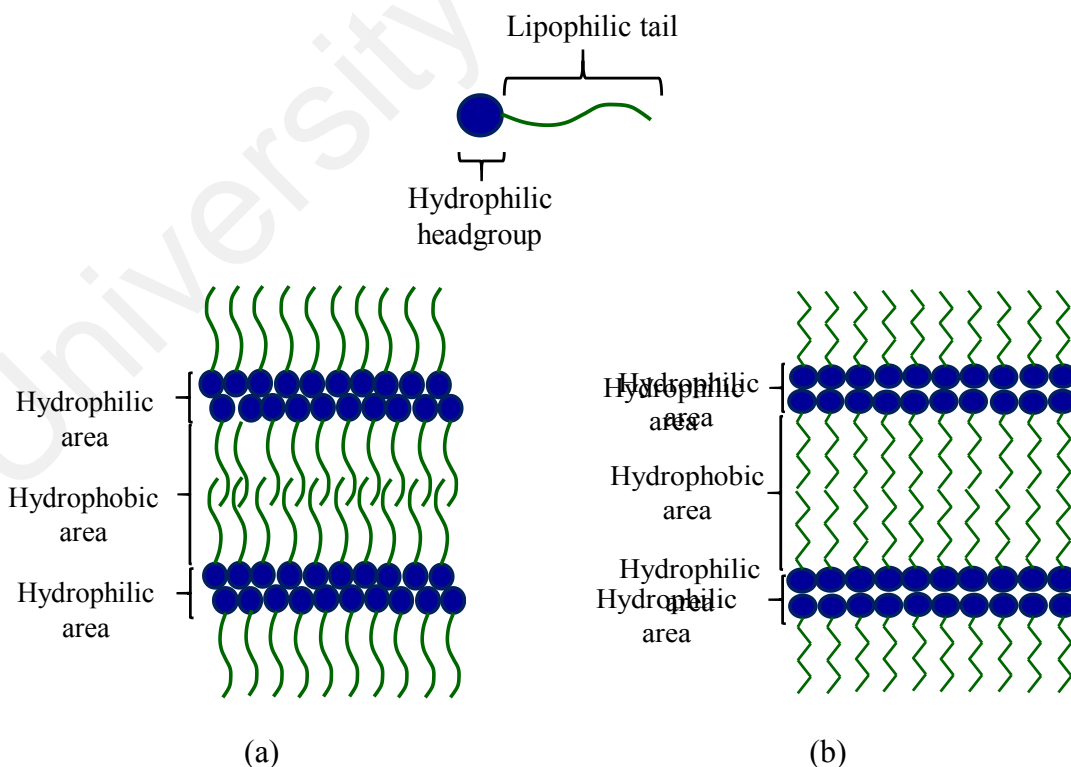


Figure 2.4: The different type lamellar phase i.e. (a) lamellar phase (L_α); and (b) lamellar crystalline (L_C). Redrawn from (Vill & Hashim, 2002).

2.6.3 Hexagonal Phase

The hexagonal phase contains aggregated amphiphilic molecules packed in an hexagonal arrangement of an indefinite length, which are also known as cylinders of micelles. There are two types of hexagonal phases, namely the hexagonal phase (H_I phase) as depicted in Figure 2.5 and the inverse hexagonal phase (H_{II} phase) as shown in Figure 2.6. The most viscous hexagonal phases embody 30 to 60% of water by weight whereby the hydrophilic head group chains point outwards from the cylinders (normal hexagonal phase). In contrast, the inverse hexagonal phase comprises micellar cylinders with the lipophilic non-polar chains pointing outwards from the cylinders (Collings & Hird, 1997). ‘Leaf-type fan-shaped’, which is the phase of columnar, is an example of hexagonal phase. Furthermore, the cubic and hexagonal phases were surprisingly found to exist in diluted *n*-decyl β -D-glucopyranoside ($C_{10}G_1$)/water system (Hantzel *et al.*, 1999). In contrast to the earlier finding by Loewenstein and Igner (1993) in Hantzel *et al.* (1999), no evidence was discovered for the existence of the hexagonal phase.

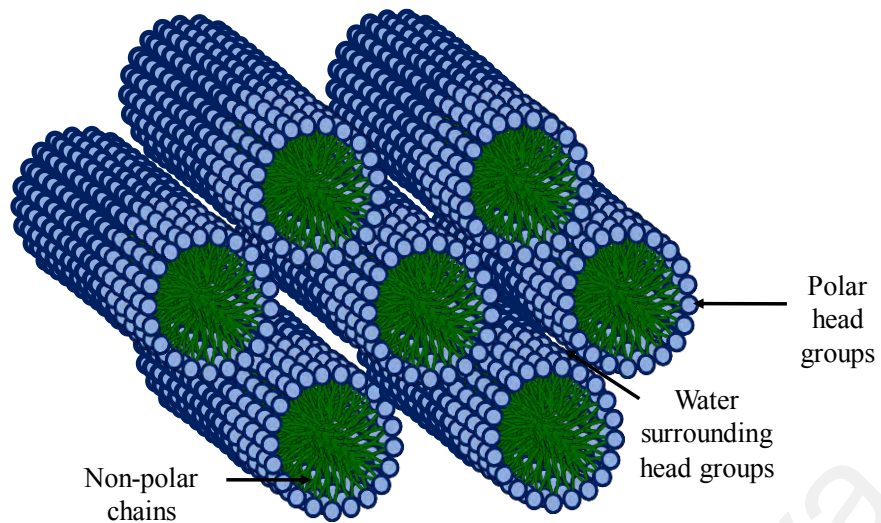


Figure 2.5: Normal hexagonal phase (H_1). Redrawn from (Collings & Hird, 1997).

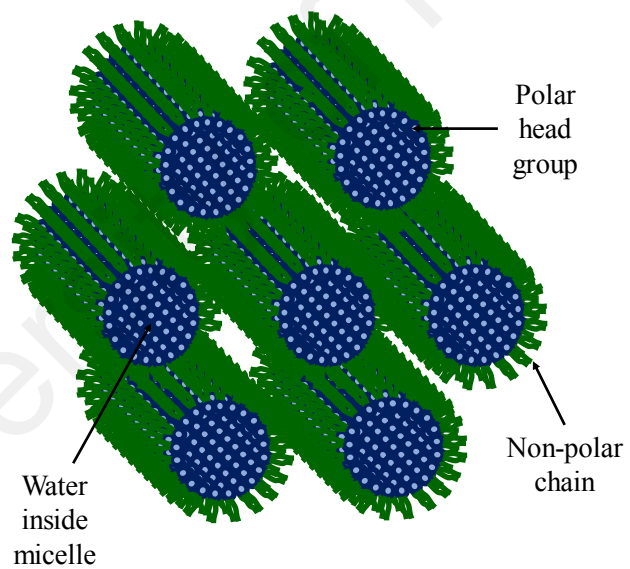
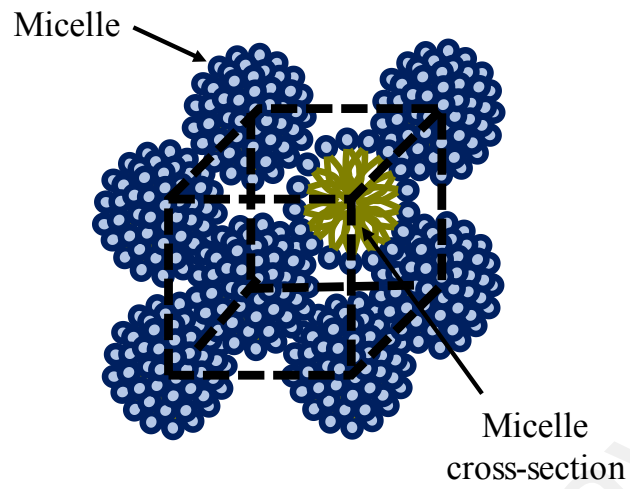


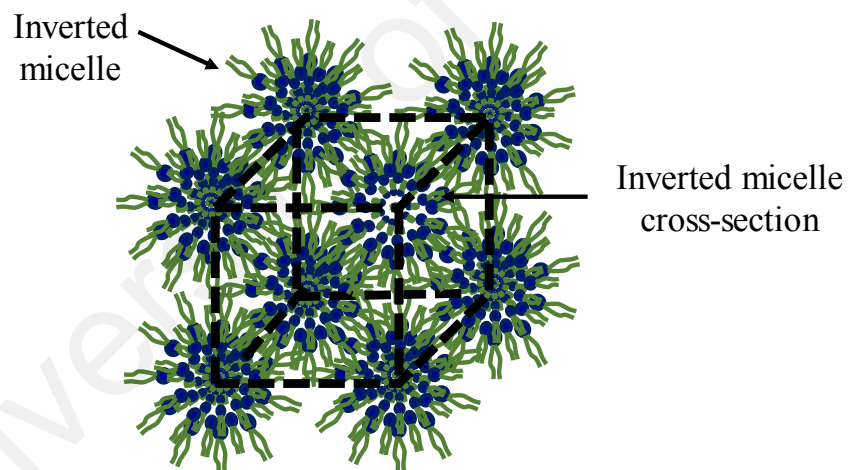
Figure 2.6: Inverse hexagonal phase (H_{II}). Redrawn from (Collings & Hird, 1997).

2.6.4 Cubic Phase

There are four different types of cubic phases. The most common cubic phase is in the form of a cubic molecular-pattern assembly. The molecular structure of the assembly tends to appear as normal discontinuous cubic phase (I_I phase) having normal micelles arrangement or inverse discontinuous cubic phase (I_{II} phase) with inverse micelles arrangement as can be found in Figure 2.7. Moreover, the cubic phases are able to aggregate between the hexagonal and lamellar phases. The aggregated molecules can be divided into normal (V_I phase) and inverse (V_{II} phase) bicontinuous phases. Such phases comprise either continuous water (V_I phase) or non-polar chain (V_{II} phase) (von Rybinski & Hill, 1998). An example of inverse micelles (L_2 phase) is an inverse micellar $Fd3m$ cubic phase. Complex cubic arrangement is a pattern assembly on which the inverse micellar can be packed. This type of packing is also known as discontinuous cubic phases. Huang *et al.* (1996) carried out an experiment which involves a mixture of phosphatidylcholine/fatty alcohol (PC/FAlc). The most striking result which emerges from the data is that the inverse micellar $Fd3m$ cubic phase exists in the mixtures of (PC/FAlc). C_{14} , C_{16} , C_{18} and C_{20} are the number of hydrophobic chain length investigated. Another important finding was found by Conn *et al.* (2006) which revealed the first ever kinetic reproducibility of a bicontinuous cubic lipid phase.



(a)



(b)

Figure 2.7: Discontinuous cubic phase showing (a) normal type (I₁); and (b) inverse type (I₁₁). Redrawn from (Efrat *et al.*, 2008).

CHAPTER 3 TECHNIQUES AND METHODS

3.1 Guerbet Glycosides Synthesis

The starting sugar, β -D-glucose pentaacetate (98%) and β -D-maltose octaacetate (98%), five Guerbet alcohols (97%) 2-ethyl-hexyl, 2-butyl-octyl, 2-hexyl-decyl, 2-octyl-dodecyl, and 2-decyl-tetradecyl, and boron trifluoride diethyl etherate ($\text{BF}_3 \cdot \text{OEt}_2$) were obtained from Sigma-Aldrich. Common reagents and solvents of AR or GR grade were supplied by Fisher Scientific including dichloromethane, acetonitrile, ethyl acetate, *n*-hexane and methanol. These were used as supplied without further purification. Ion exchange resin (Amberlite IR-120) and all the deuterated solvents used for the NMR study were purchased from Merck. The Guerbet glycosides shown in Figures 3.1 and 3.2 were synthesised following a previously reported procedure (Hashim *et al.*, 2006), and their anomeric purity was estimated to be $\geq 97\%$ according to analytical limitations based on instrumentation, i.e. ^1H -NMR and thin layer chromatography. All lipids were extensively dried before further characterisation by placing the sample in a vacuum oven over diphosphorus pentoxide for at least 24 h.

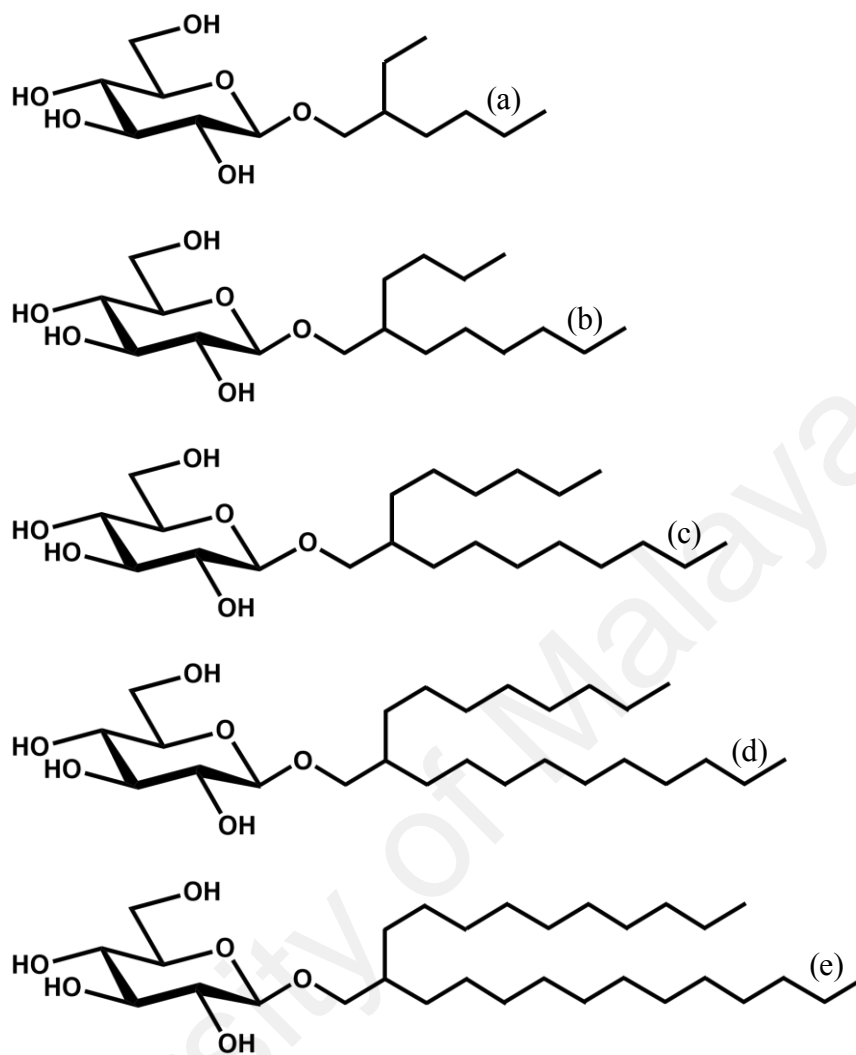


Figure 3.1: The chemical structures of branched-chain β -D-glucosides. (a) β -Glc-C₆C₂; (b) β -Glc-C₈C₄; (c) β -Glc-C₁₀C₆; (d) β -Glc-C₁₂C₈; and (e) β -Glc-C₁₄C₁₀.

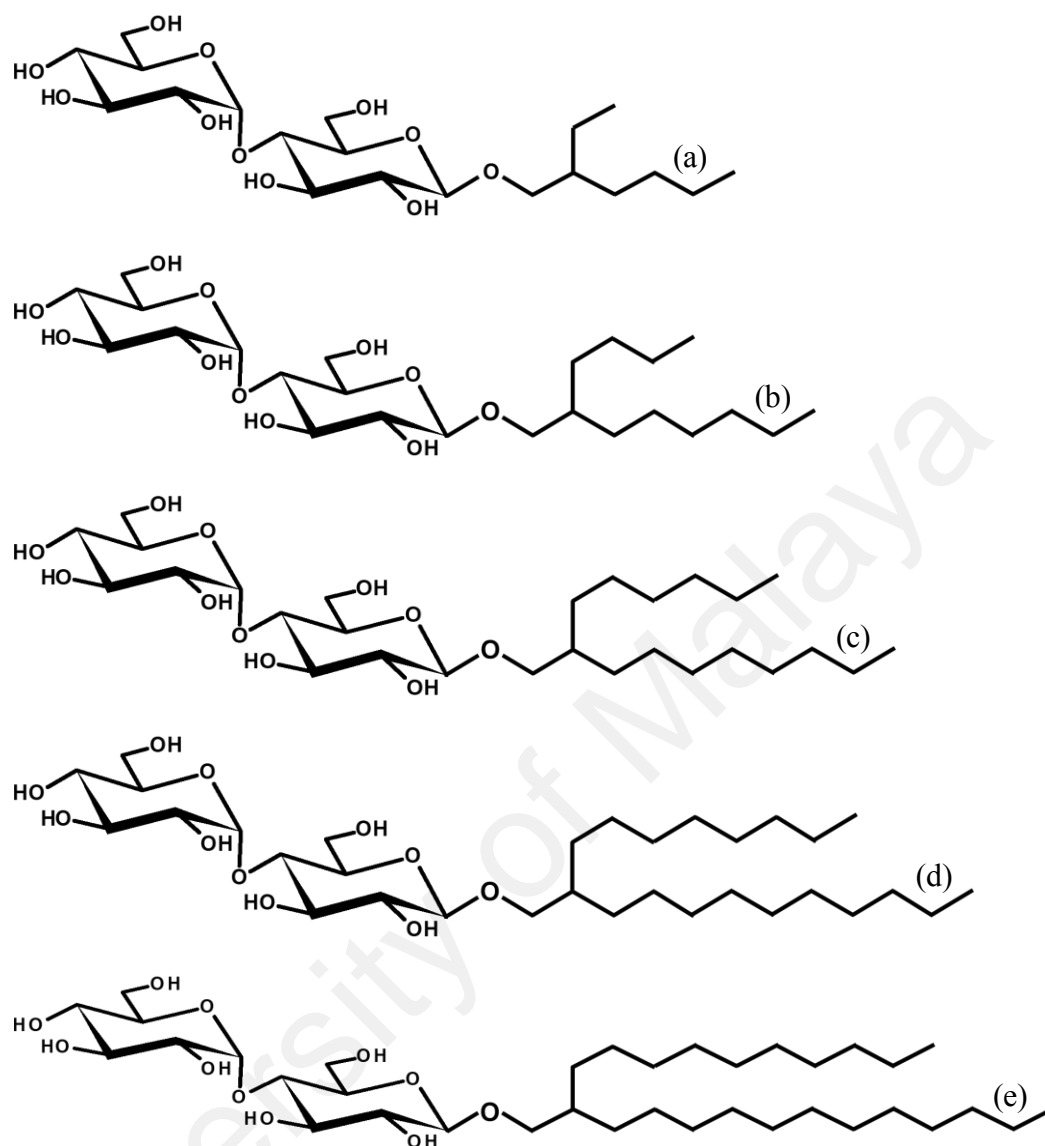


Figure 3.2: The chemical structures of branched-chain β -D-maltosides. (a) β -Mal-C₆C₂; (b) β -Mal-C₈C₄; (c) β -Mal-C₁₀C₆; (d) β -Mal-C₁₂C₈; and (e) β -Mal-C₁₄C₁₀ .

3.1.1 General Glycosidation Procedure

Approximately 5 g (12.8 mmol, 1.0 equiv.) of glucose pentaacetate was treated with 3 g (16.1–8.5 mmol, 1.3–0.7 equiv.) Guerbet alcohol in the presence of Lewis-acid (catalyst). In this reaction, an acetoxy group at the first carbon was replaced with the branched chain hydrocarbon tail of the Guerbet alcohol. The process involved was a mixing of the peracetylated glucose sugar and Guerbet alcohols in a dry 50 mL

dichloromethane. Boron trifluoride diethyl etherate (2.5 mL, 20.3 mmol, 1.6 equiv.), a Lewis acid catalyst (Ferrier & Furneaux, 1976), was then added using a plastic syringe. The solution was stirred for five hours at room temperature, and it was then followed by quenching the reaction solution with a saturated hydrogen carbonate solution to form an aqueous phase. The aqueous phase was then extracted twice. The phase was first extracted with dichloromethane and water (when necessary), and the product was dried with magnesium sulphate. It was then filtered and evaporated in order to obtain a crude product. The desired product was finally obtained from the purification of the crude extract using a column chromatography.

The column chromatography technique was applied after the glycosidation stage to separate α - and β -anomeric products and to remove the unwanted products such as excess alcohols, unreacted sugars and other unknown by products. The column chromatography was performed on a silica gel of 230–400 mesh sizes using a mixture of dichloromethane, hexane and diethyl ether with varying ratios. Their chromatographic purities were checked by a thin layer chromatography on silica-gel glass plates (60 Merck F₂₅₄). Detection of the desired product (β -anomer) was made by immersing these glass plates into a potassium permanganate solution or 2% sulphuric acid in ethanol followed by heating them with a heat gun. The same glycosidation process was repeated for Guerbet maltoside series.

3.1.2 General Deacetylation Procedure

Deacetylation is a process of removing an acetyl group from the sugar head group (Agoston *et al.*, 2001). The purified compound was dissolved in an anhydrous methanol (~1 g in 30 mL). A small amount of sodium methoxide was added to the solution until the solution turned basic and the solution was stirred overnight. After the reaction was

completed, the solution was neutralised with H^+ resin (Amberlite IRC-50) ion and filtered with a filter paper. The filtered solution was then evaporated and the remaining product was dried for 48 h in a vacuum drier at 40 °C. The same procedures were applied for Guerbet maltoside series.

3.2 Characterisation of Liquid Crystal Phase Behaviour

After over a century, liquid crystal (LC) still remains as a popular candidate for their application in this modern technology; for instance, liquid crystal displays (Schadt, 1997), LC thermometers (Scholefield *et al.*, 1982), LC photovoltaic devices and light-harvesting systems (Bushby & Kawata, 2011), LC drug and laser (Kasch, 2013). Liquid crystal is a mesophase (Andrienko, 2018) with which thermotropic and lyotropic liquid crystal phase behaviours can be determined. The mesophase is an intermediate state of matter which forms between the crystalline solid and liquid as provided in Figure 3.3 (An *et al.*, 2016).

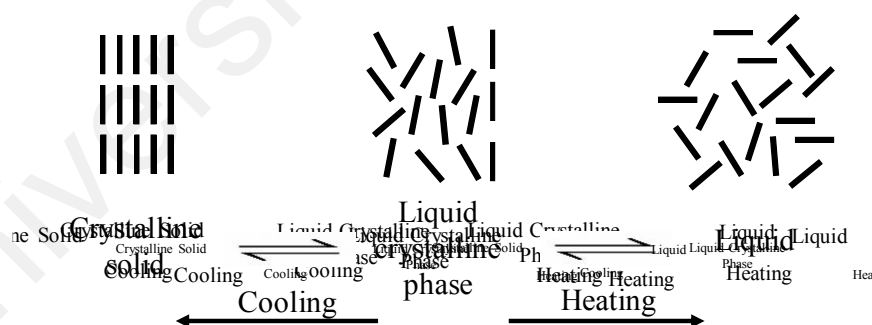


Figure 3.3: Liquid crystal molecules upon heating and cooling. Redrawn from (An *et al.*, 2016).

The LC molecules possess anisotropy property that has a long-range orientational order in the molecule arrangement. Consequently, the LC molecules exhibit different type of phases. These phases can be distinguished from each other based on their structures and physical properties (An *et al.*, 2016). Therefore, many techniques have been employed to characterise the liquid crystals such as optical polarising microscopy, differential scanning calorimetry, small- and wide-angle X-ray scattering/diffraction, transmission electron microscopy and circular dichroism. In this chapter, the techniques, basic principles, measurements and procedures involved in the research are outlined.

3.2.1 Optical Polarising Microscopy

Polarising microscopy is utilised to determine various liquid crystal mesophases (Garidel *et al.*, 2015). Even though this instrument is unable to identify all liquid crystal phases it is very useful as a complementary analysis tool used with another technique (Candau *et al.*, 1982).

Figure 3.4 represents a common set up of an optical polarising microscope. An ordinary white light source, which is emitted by a halogen microscope light bulb, is reflected by a mirror upwardly. The light which is also known as a non-polarised light, travels randomly in all directions. Therefore, a polarising plate (polariser), which can be rotated by 360° , is utilised to convert the non-polarised light into a polarised light as shown in Figure 3.5 (Feehan *et al.*, 2018). A linearly polarised light has vibrational direction. The function of a condenser is to concentrate the light to enable it to focus onto the sample which is essential in producing a clear and sharper image. This microscope is an instrument designed with a heating rotatable stage that holds the mounted sample on a glass slide in place and controls the movement of the glass slide in a certain direction. The most important part in an optical microscope is called the objective lens which

collects the transmitted light generated from the sample. This determines the function and basic performance of the microscope. Hence, there are four objective lenses magnifications which are namely 5 \times , 10 \times , 20 \times and 40 \times . A removable and 360 $^\circ$ rotating analyser is a device that acts as a second polarising filter in which the light passes through it after transmitted from the objective lens. The eyepiece or ocular is one of two systems of lenses that can be used in producing a greater magnification of image. The image can also be captured by a camera mounted on the microscope (Dierking, 2003).

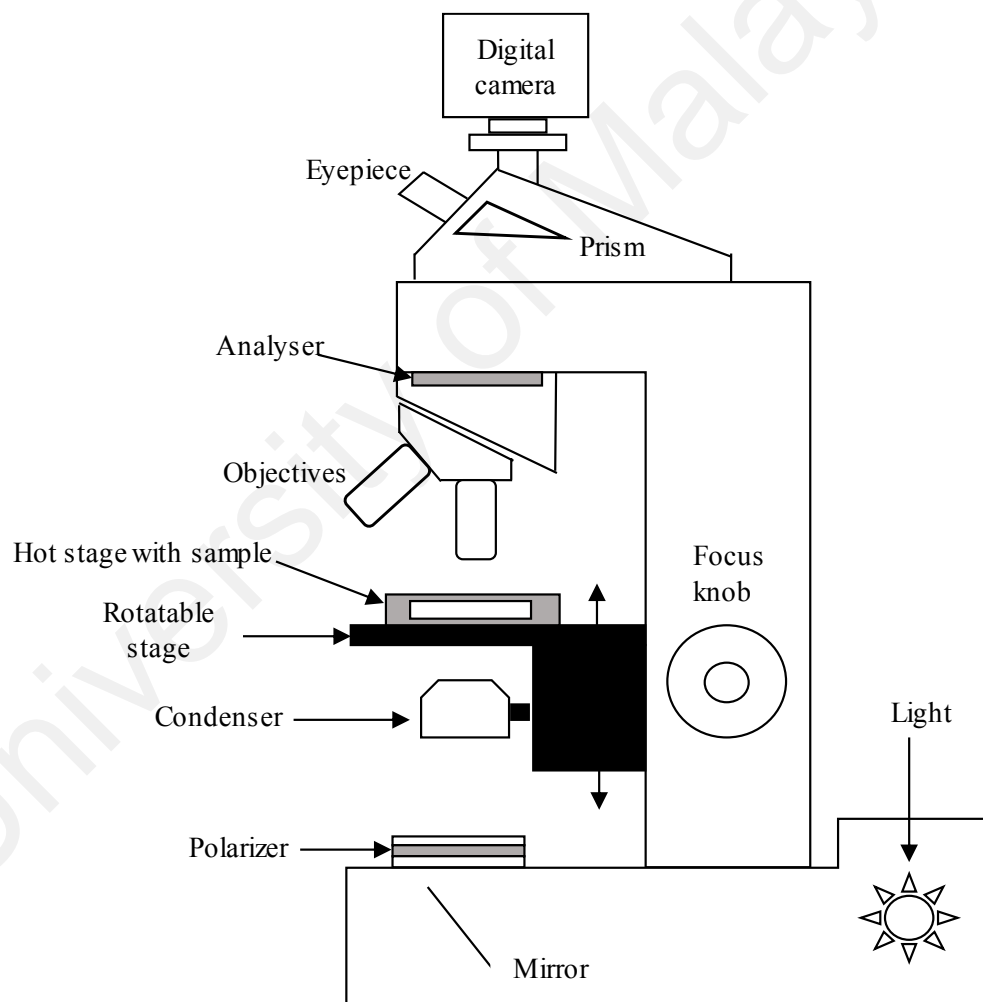


Figure 3.4: Schematic diagram redrawn from (Dierking, 2003).

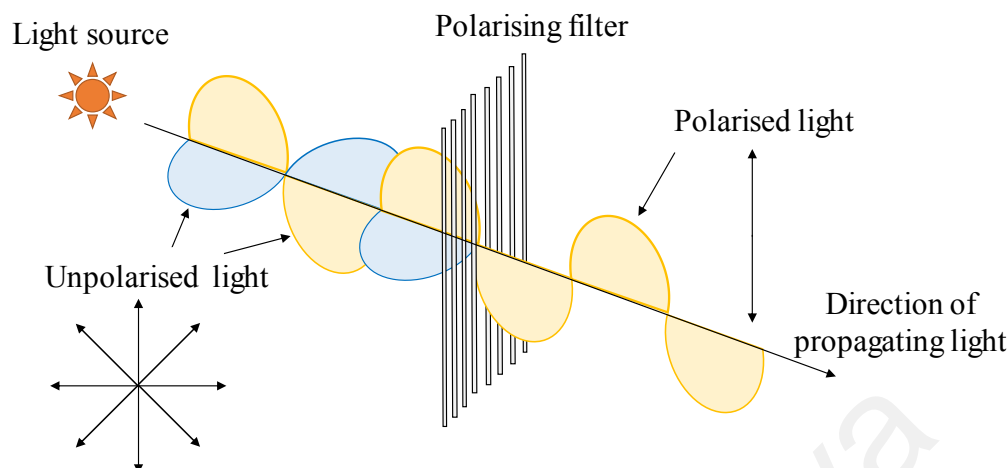


Figure 3.5: Schematic diagram of light polarisation process. Redrawn from (Feehan *et al.*, 2018; Radi & Rasmusen, 2013).

Optical Textures of Liquid Crystal Mesomorphic Structures

LC exhibit their mesomorphic or mesophase structures due to the molecular self-organisation. Therefore, an optical polarising microscope enables the existence of the LC's structure of phases and unique textures to be detected upon heating and cooling processes. Glycolipid liquid crystal (glycosides) may give birefringent texture with certain order parameter (Fan & Haase, 1991; Andrienko, 2018).

Birefringence or birefractive is an optical property of material. In polarisation microscopy, the polarised light is doubly refracted by the optically anisotropic glycolipid materials into two light components namely, ordinary and extraordinary waves with different directions. While entering the glycolipid liquid crystals that are locally self-organised into many domains with the same orientation, the light waves will be scattered. The ordinary light wave passes through the glycolipids following the refraction law

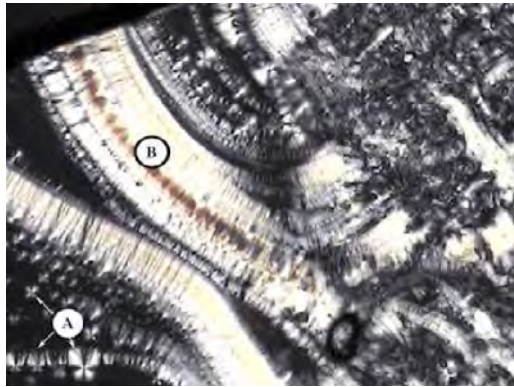
(Cevc, 1993). In contrast, many domains in the LC phase have made the extraordinary light wave bents because of the change in the refractive index of the LC.

Interference between the ordinary and extraordinary waves that are related with light intensity produces a polarisation colour of the LC. This has the order of polarisation either low or high order. The one that possesses low order exhibits darker colour. On the contrary, another one with higher order shows brighter colour. Therefore, the polarisation colour and order of the LC can be compared with the Michel-Lévy Colour Chart. The birefringence value of the LC can be estimated by using its thickness and Michel-Lévy Chart. Moreover, the retardation is expressed in Equation 3.1 as follows:

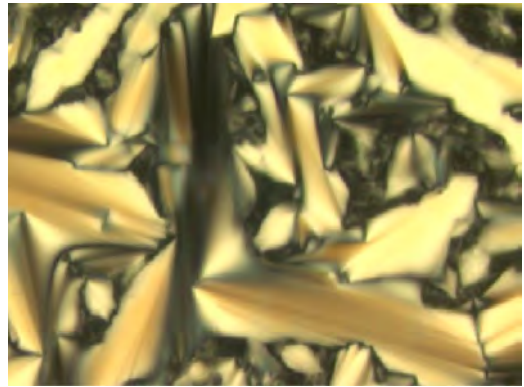
$$r = 1000t \times B \quad \text{(Equation 3.1)}$$

where r is the retardation in nm, t is the thickness in μm (t in μm is multiplied by 1000 (1000 nm/ μm) for the conversion to nm in an Equation 3.1, $1000t$) and B is the birefringence (Carlton, 2011).

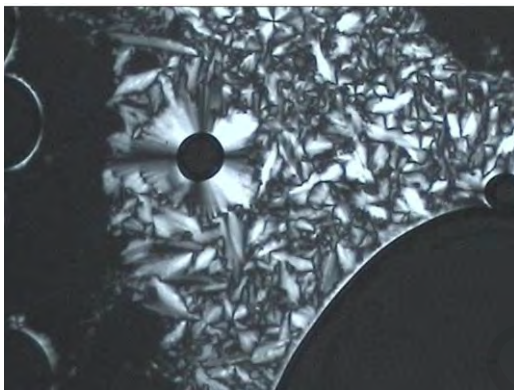
The complexity of the glycolipid mesophases depends on their molecular structure. According to Liao *et al.* (2006), the glycolipids have weak birefringence with the value of smaller than 0.05. This is due to its longer hydrophobic chain of the molecule which shows higher disorder of apolar part compared to polar part. Consequently, the textures of the glycolipids examined by the optical polarising microscope appear dull in colour. Some of the glycolipid and graft copolymers optical textures are illustrated in Figures 3.6 and 3.7, respectively.



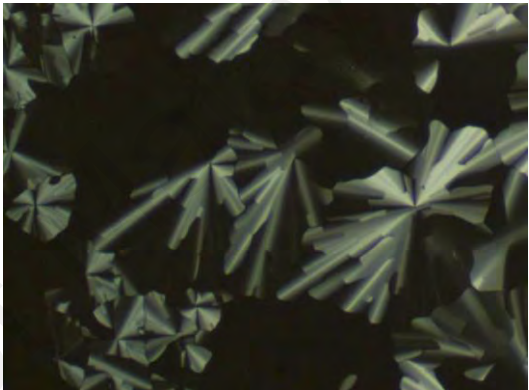
(a)



(b)

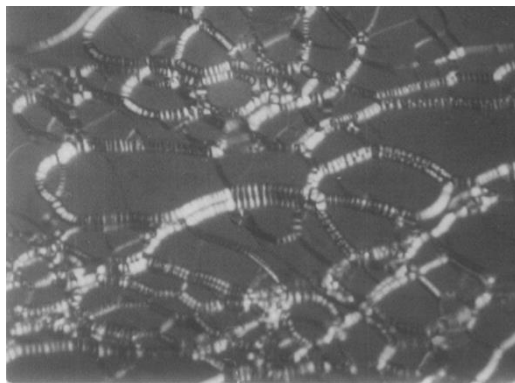


(c)



(d)

Figure 3.6: Glycolipid liquid crystals optical textures of (a) glycolipid GalC₁₁ smectic A showing maltese crosses in region A and pearl chains in region B. Adapted from (Garidel *et al.*, 2015). (b) Focal-conic of smectic layers of biomolecular-based thermotropic liquid crystal. Adapted from (Liu *et al.*, 2014). (c) Glycolipid columnar texture (MelC₁₂N₃). Adapted from (Garidel *et al.*, 2015). (d) CellC₁₂₍₈₎ hexagonal columnar. [Reprinted (adapted) with permission from ref. (Takada *et al.*, 1992). Copyright 1992 Taylor & Francis].



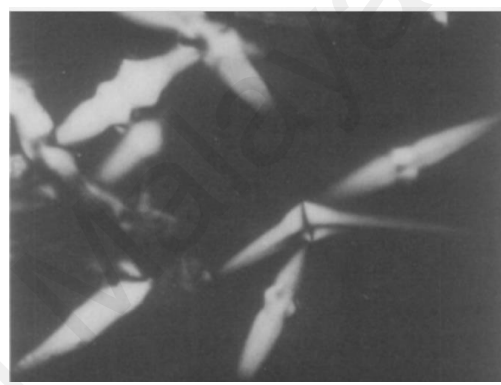
(a)



(b)



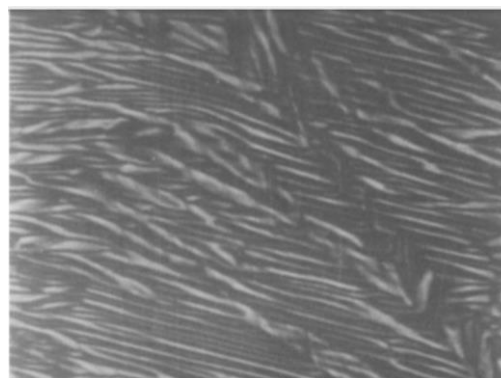
(c)



(d)



(e)



(f)

Figure 3.7: Graft copolymers mesophase optical textures of (a) homeotropic region containing lamellar phase oily streaks; (b) oil streaks of lamellar phase connected by the nodes; (c) textures of lamellar quaternary system with polygonal arrays between oily streaks; (d) batonnets optical texture of polymeric systems; (e) inverse hexagonal angular texture; and (f) inverse hexagonal coarsely striated texture. [Reprinted (adapted) with permission from ref. (Candau *et al.*, 1982). Copyright 1982 Elsevier].

Figure 3.8 presents cubic phases which are optically very viscous isotropic cubic symmetry of 3-dimensional lyotropic phases and differ from the solution of isotropic or micellar. Garidel *et al.* (2015) reported that the optical polarising microscope detected a cubic phase with no texture and was appeared as isotropic due to the light rays passing through the glycolipid sample refracted in all directions.

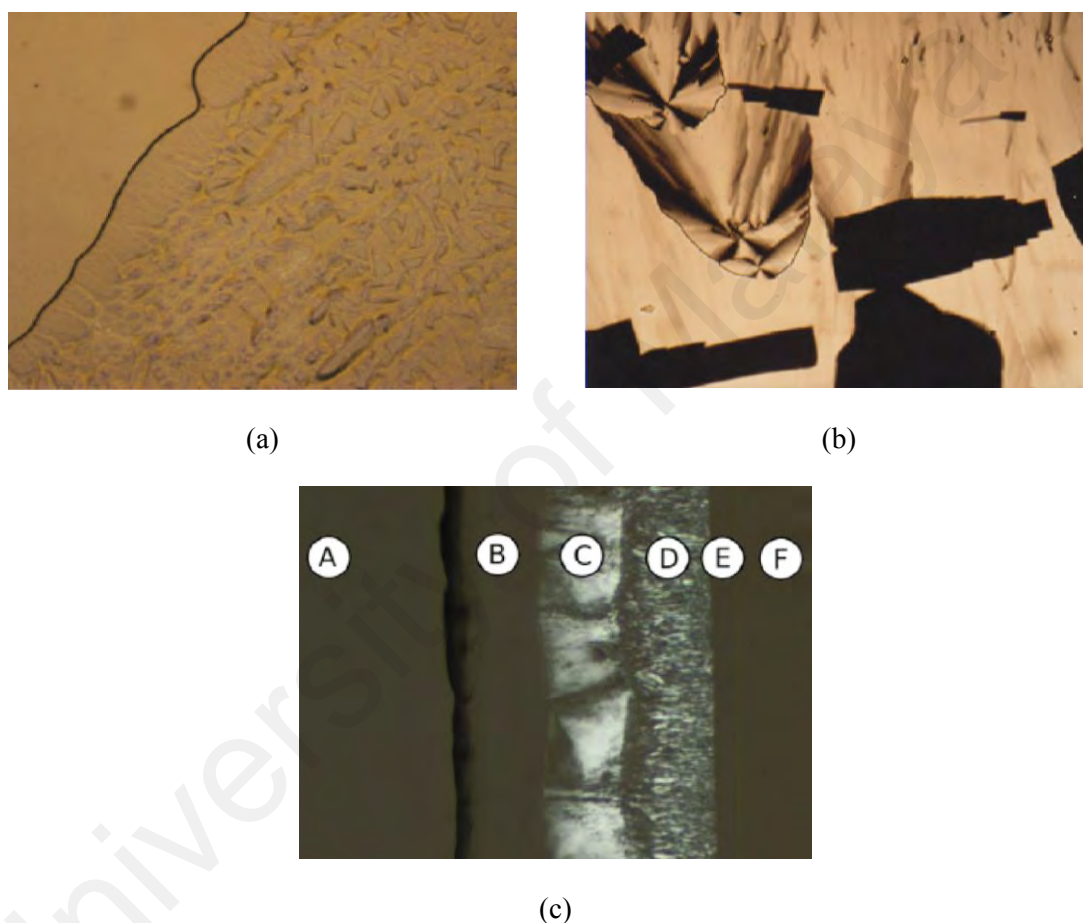


Figure 3.8: Glycolipid cubic phases observed under a polarised microscope. (a) Cel- β -glycero dioleoyl and Glu- β -glycero dioleoyl mixture (1:1); (b) a formation of rectangular isotropic cubic phase during transition from hexagonal to cubic phases of Glu- β -glycero didecanoyl; and (c) the phase sequence of MalOC₃OC₁₂ mesophase structures. (A) water, (B) discontinuous cubic phase (I₁), (C) and (D) hexagonal phases (H_{II}), (E) bicontinuous cubic phase (V_I), (F) pure compound (water contact penetration). Adapted from (Garidel *et al.*, 2015).

Thermotropic Phase Behaviour

Formation of various self-assembly phases of thermotropic liquid crystals are driven by the induced temperature in dry conditions. Hence, a dry glycolipid sample was carefully transferred to a glass microscope slide and sandwiched with a glass cover slip. The sample was placed on the rotatable hot stage and further investigated its thermotropic behaviour by controlling the temperature during the heating and cooling conditions. Identification of different thermotropic mesophases was determined by their unique textures for both conditions.

Lyotropic Phase Behaviour

Lyotropic liquid crystal study was determined using the optical polarising microscope equipped with a rotatable hot stage. Variation in solution concentrations produces different types of lyotropic liquid crystal mesophases. Two methods were employed, namely hydrated and contact penetration.

For the hydrated sample, a sample was placed on the glass microscope slide and certain amount of water was added. The mixture was then covered with a glass cover slip and sealed with a silicone sealant to avoid leaking of water during excess water conditions as shown in Figure 3.9. Heating and cooling were employed on the sample under investigation.

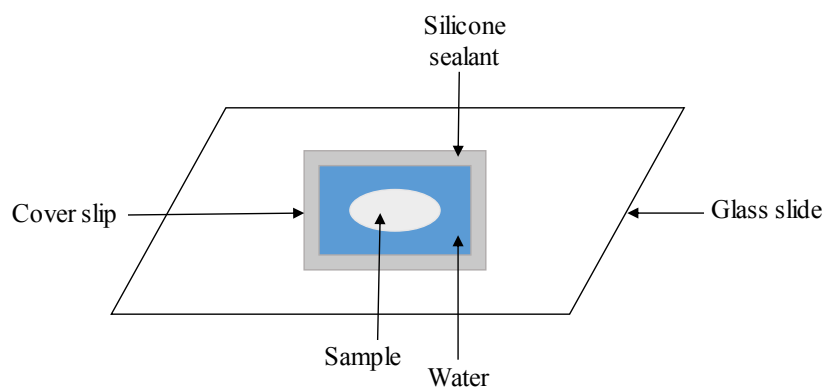


Figure 3.9: Hydrated sample in excess water sandwiched between a cover slip and glass slide.

Contact penetration scan was utilised to examine the sequence of mesomorph states. The contact penetration method is illustrated in Figure 3.10, a sample was compressed between the glass microscope and the glass cover slip in order to have a uniform thin layer sample. Subsequently drops of water were added on the edge of the glass cover slip which was in contact with the sample. The water will enter the sample via capillary force creating a concentration gradient of excess water at the cover slip edge to neat surfactant under the glass cover slip. The penetration scan was carried out on the sample at room temperature based on different concentration gradients.

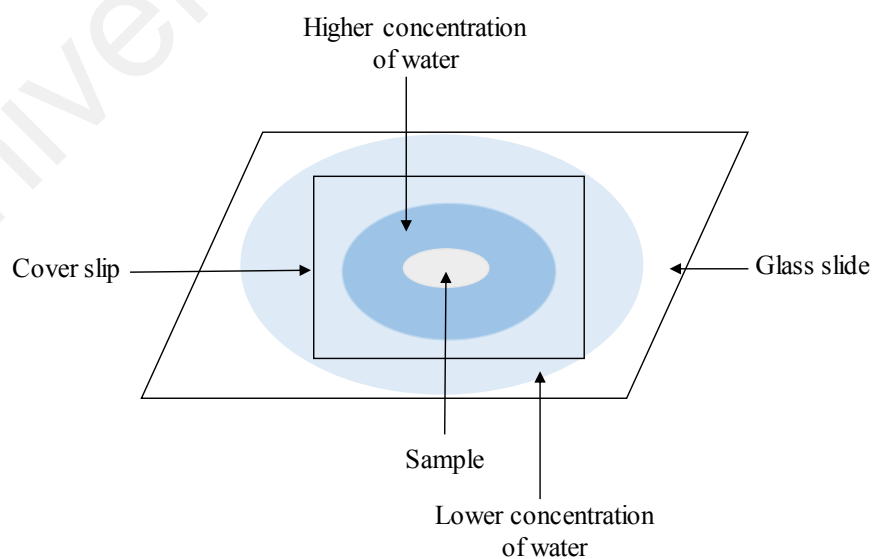


Figure 3.10: Formation of water gradient concentrations around the sample.

Measurement

In this study, there are two microscope systems used for taking sample images: (i) an Olympus BH polarising microscope equipped with a Mettler FP82 heating stage, linked to a Soft Imaging System Color View XS camera; and (ii) a Nikon Eclipse E600 polarising microscope combined with a Nikon DXM1200F digital camera. As Nikon Act-1 (version 2.70) recorded the actual images, Linkam heating stage controlled by Linkam Controller software was utilised to heat and cool the sample.

3.2.2 Differential Scanning Calorimetry

A differential scanning calorimeter is an instrument that is capable of identifying the enthalpy change associated with a phase transition between a sample and a reference in relation to its temperature (Hynie, 2008; Haines *et al.*, 1998). The sample and reference are both heated and cooled at a certain rate. On heating and cooling, the phase transitions observed are endothermic and exothermic peaks, respectively. Area under the peak corresponds to the enthalpy of the transition. In addition, the transition temperature is obtained by constructing a line which is tangential to the curve. When the tangent line intersects the baseline, it is called a peak onset (Cooper, 2004; Cooper, 2000; Cooper *et al.*, 2001). A diagram of the identification of the transition enthalpy and temperature are given in Figure 3.11.

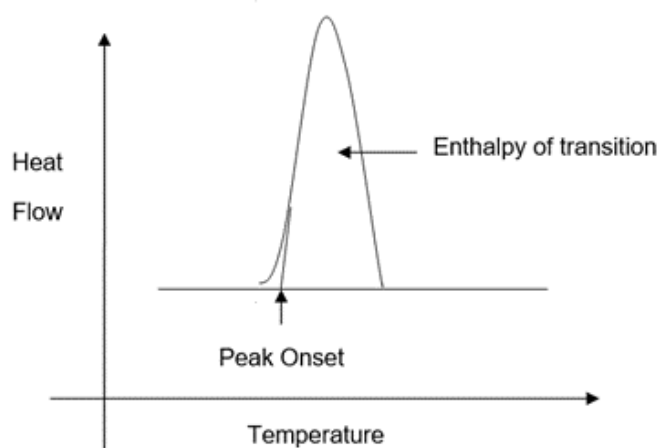


Figure 3.11: Typical DSC curve.

Measurement

DSC experiments were conducted by using a DSC 822^e (Mettler Toledo) equipped with Haake EK90/MT intercooler. STAR^e Thermal Analysis System software was employed in determining the measurement data analysis. An inert environment is maintained during calibration and sample measurement by nitrogen purging to minimise potential oxidation. The instrument is calibrated with Indium standard for heat flow calibration, temperature calibration and furnace calibration. An approximately 4–8 mg samples were weighed in the 40 μ L aluminium crucible. The samples were subjected to two cycles of heating and cooling at the rate of 5 $^{\circ}\text{C min}^{-1}$ from a temperature of 0 $^{\circ}\text{C}$.

3.2.3 Small-Angle X-ray Diffraction

More than 300 years ago an observation of visible light diffraction effects was noted which, in turn, resulted in diffraction grating invented by Fraunhofer in 1820. Furthermore, early stages of the related research in X-ray diffraction had been developed by Wilhelm Rontgen, Max von Laue, William Henry Bragg and William Lawrence Bragg (Sands, 1969). Occurrence of the diffraction is due to the scattered wave interference by an object (Glatter & Kratky, 1982), and X-rays are a short wavelength electromagnetic

radiation generated by decelerated moving electrons. Small-angle X-ray diffraction (SAXD) or small-angle X-ray scattering (SAXS) is often used interchangeably. It is a technique which is capable to characterise the samples ranging from 1 to 100 nm. SAXD is an important, powerful analytical and non-destructive method (Li *et al.*, 2017) for samples such as biological macromolecules and archaeological bone (Wess *et al.*, 2001). Furthermore, complexity of liquid crystals identification requires SAXD analysis complements with those from OPM.

SAXD is a technique that measures the X-ray diffraction/scattering intensity from the SAXD pattern as a function of the scattering vector, q , which corresponds to the scattering angle, 2θ , represented by Equation 3.2 as follows:

$$q = \frac{4\pi}{\lambda} \sin\theta \quad \text{(Equation 3.2)}$$

where λ is the incident radiation wavelength (Allec *et al.*, 2015). The SAXD patterns which are represented by the position, intensity and angular distribution of diffraction/scattering peaks provide information of the sample internal structures. These diffraction/scattering patterns can be divided into two, namely isotropic and anisotropic (Gille, 2014). The occurrence of the isotropic scattering is due to the light which is scattered in all directions. However, the anisotropic scattering is obtained due to some lights which are allowed to pass through the sample and affect the light polarisation. Furthermore, the diffraction/scattering peaks are created by the constructive interference of scattered light. As it was first introduced by William Henry and his son William Lawrence Bragg in 1913, hence, it was commonly known as Bragg's Law of X-ray diffraction (Bragg & Bragg, 1913).

The X-ray diffraction is an important technique which characterises, for instance, lipid phase structures (Arsov *et al.*, 2018; Akabori & Nagle, 2015; Lalitha *et al.*, 2018). This technique is based on Bragg's Law as shown in Figure 3.12. The equation involved is represented in Equation 3.3 as follows:

$$n\lambda = 2d \sin\theta \quad \text{(Equation 3.3)}$$

where: n is a reflection order, λ is an incident X-ray beam wavelength, d is a lattice parameter spacing, and θ is an incidence X-ray beam angle.

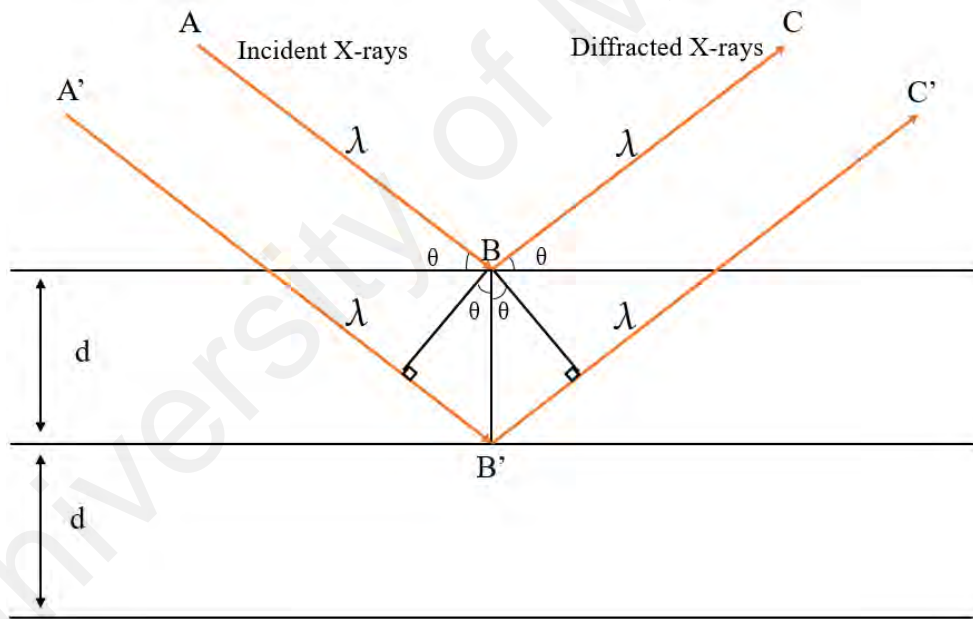


Figure 3.12: Bragg's Law. Redrawn from (Naik, 2010).

Particles with the unit of \AA are known to possess a structure in real space. However, the interference diffraction/scattering pattern with the unit of \AA^{-1} , which is Bragg reflection intensity, is usually termed as a structure in reciprocal space. The pattern oscillates representing the form factor ($P(q)$) of the scattering of one particle from which

the resultants of summation all the wave amplitudes of atoms have been squared. On the other hand, the term structure factor ($S(q)$) is used for a concentrated sample whereby the single particle form factor has been multiplied with the extra interference of neighbouring particles. The Bragg peak, therefore, is defined as a pronounced peak of highly ordered and periodic arrangement aligned particles (Schnablegger & Singh, 2011). The reciprocal distances, s is related to d -spacing and scattering vector, q by $s = 1/d$ and $q = 2\pi s$, respectively.

More pronounced peaks in the structure factor are obtained for the increasing order particle position. Hence, for a crystalline substance the structure factor is usually called lattice factor. It shows a crystal symmetry that contains a set of narrow and intensive peaks at well-defined angles. The crystal symmetry produces the typical values peak position ratios on the q -scale (Table 3.1); for instance,

Table 3.1: Typical values peak position of crystal symmetry. Compiled from (Schnablegger & Singh, 2011).

Type of Phase	Crystal Symmetry Values Peak Position
Lamellar	1, 2, 3, 4, ...
Hexagonal	1, $\sqrt{3}$, $\sqrt{4}$, $\sqrt{7}$, ...
Cubic ($Ia3d$)	$\sqrt{6}$, $\sqrt{8}$, $\sqrt{14}$, $\sqrt{16}$, ...
Cubic ($Pn3m$)	$\sqrt{2}$, $\sqrt{3}$, $\sqrt{4}$, $\sqrt{6}$, ...
Cubic ($Im3m$)	$\sqrt{2}$, $\sqrt{4}$, $\sqrt{6}$, $\sqrt{8}$, ...
Cubic ($Fd3m$)	$\sqrt{3}$, $\sqrt{8}$, $\sqrt{11}$, $\sqrt{12}$, ...

Phase identification involves the small-angle and wide-angle regions of X-ray diffraction. The former determines the symmetry and long range ordered structures; and the latter determines the packing of molecules and short range ordered structures (Seddon

& Templer, 1995). These structures are classified based on one, two or three lattices dimensions, such as lamellar (phase in one dimension), hexagonal (phase in two dimensions) and cubic (phase in three dimensions) (Chen *et al.*, 2014; Klacsova, *et al.*, 2016; Reese *et al.*, 2015; Tenchov & Koynova, 2017).

Figure 3.13 illustrates small-angle X-ray parts namely; X-ray tube, collimator, sample and X-ray detector. The X-ray tube source emits a bundle of X-rays. The tube is sealed which comprises of wire filament and targeted rotating anode. Emission of electrons are produced from the electrically heated filament and the electrons are accelerated towards the rotating anode which is usually made of copper or molybdenum materials. Emission of X-ray radiations are due to decelerated electrons after which the accelerated electrons bombard the targeted anode. Hence, the emission radiations are known as Bremsstrahlung or white radiation (Ladd & Palmer, 2013).

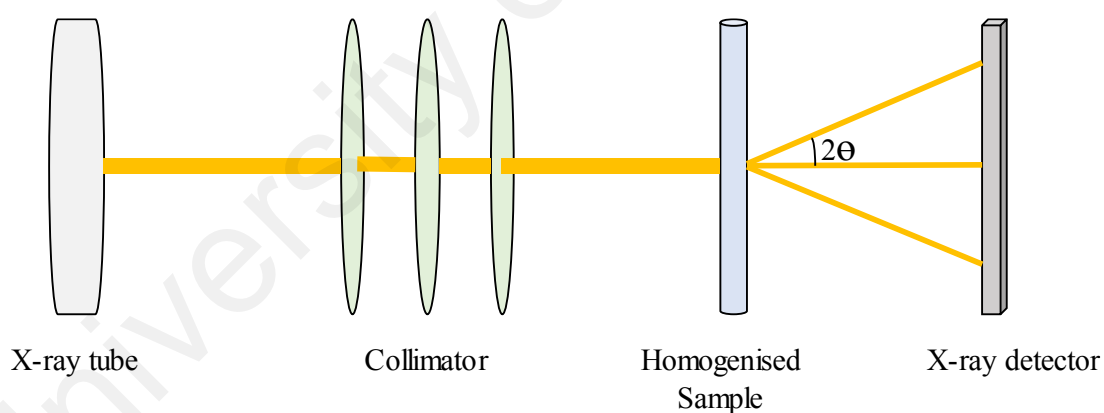


Figure 3.13: Schematic diagram of experimental setup of small-angle X-ray machine. Redrawn from (Changizi *et al.*, 2005).

A collimator system is the second part of the X-ray instrument which cuts the bundle of X-ray into small incoming beam divergence. There are classified in two systems, namely point and line collimations. The former comprises of pinholes which are

capable of shaping the X-ray beam which is in the form of small circular or elliptical spot. Hence, the sample illumination of small spot is involved. The latter consists of slits that provide a long, narrow beam. Therefore, the X-ray beam irradiates a larger sample volume as compared to the point-collimation (Schnablegger & Singh, 2011). The specific X-ray detector which is protected by the beamstop, is able to capture the diffraction/scattering intensity resulting in a small-angle X-ray diffraction/scattering pattern. The pattern reveals the sample structural information from crystalline to non-crystalline.

Dry Condition and Excess Water Sample Preparations

Two types of sample holders were used in X-ray diffraction techniques, namely glass capillary tube and teflon spacer. These types of sample holders were chosen depending on the nature of the samples.

For the excess water sample preparation using an X-ray glass capillary tube, a mixture of approximately 5–10 mg solid sample and 30 μ l water was inserted into a 1.5 mm diameter glass capillary tube. The sample tube was then flame sealed and partly submerged in a silicon sealant to maintain the hydration as shown in Figure 3.14. Homogeneous dispersion was achieved by heating the sample gently until 100 °C followed by repeatedly centrifuging it under the sealed tube. The homogenised sample was left equilibrated for at least 24 h. It was then placed into a sample holder in the X-ray machine.

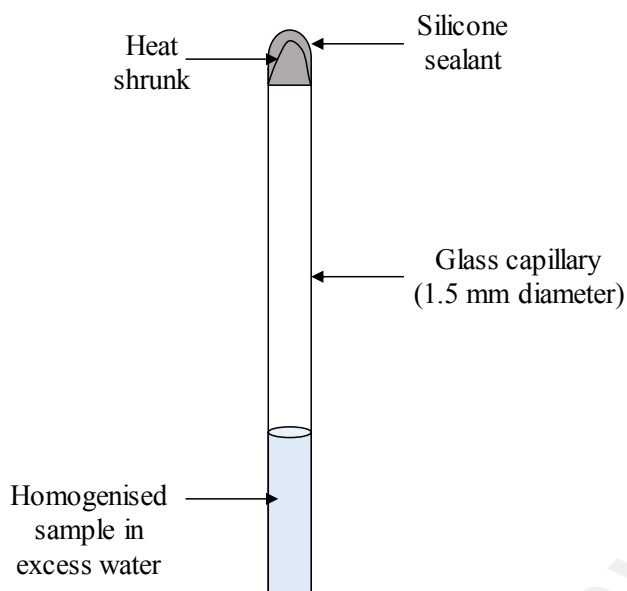


Figure 3.14: Homogenised sample in excess water condition in an X-ray flame-sealed glass capillary tube.

However, for the dry sample conditions, an approximately 5–10 mg solid sample was added into a 1.5 mm diameter glass capillary tube as illustrated in Figure 3.15. The sample-glass capillary tube was centrifuged in order to allow the sample to settle at the bottom of the tube. The sample tube was flame sealed and was then inserted into the sample holder in the X-ray machine.

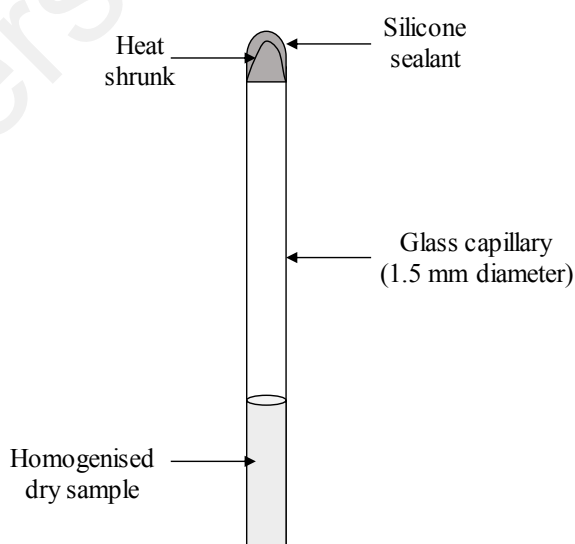


Figure 3.15: An X-ray glass capillary tube containing dry homogenised sample.

A disc-shaped teflon spacer was used as a sample holder for a viscous sample. For the excess water sample, a mixture of approximately 10 mg of viscous sample and 30 μ l water was added into a small vial. It then underwent five freeze-thaw-vortex cycles to homogenise the dispersion of the sample. The homogenised sample was left equilibrated for at least 24 h. A small amount of sample was transferred to a circular hole in the middle of the teflon spacer and sealed with mylar films on both sides as shown in Figure 3.16. It was then placed in the sample holder in the X-ray machine.

For the dry sample, on the other hand, a small amount of the viscous sample was added into a circular hole in the middle of teflon spacer and sealed with mylar films on both sides. It was then placed in the sample holder in the X-ray machine.

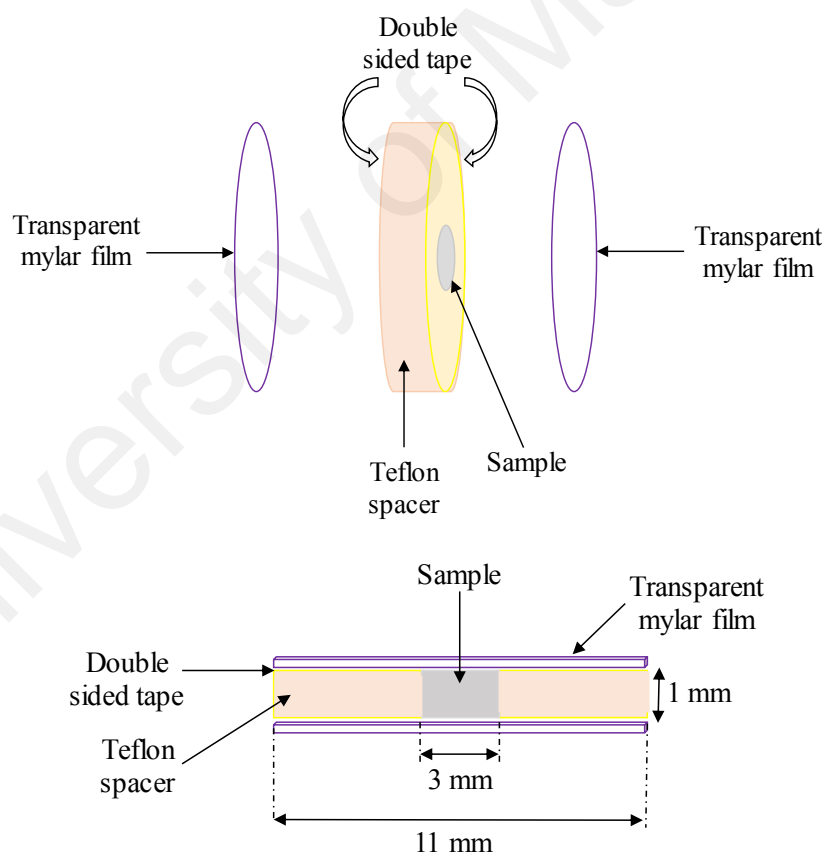


Figure 3.16: Viscous sample in a disc-shaped teflon spacer.

Preparation of Limiting Hydration Sample

An overnight dried lyophilised lipid sample (approximately 2 mg) was loaded into a 1.5-mm X-ray glass capillary tube. It was then made up to the required water content using a micro-syringe. The mixture of lipids and water was spun down in a bench centrifuge. Figure 3.17 shows the flame-sealed sample tube, coated with silicon sealant to prevent possible water loss, and it was then left to equilibrate for 24 h at room temperature.

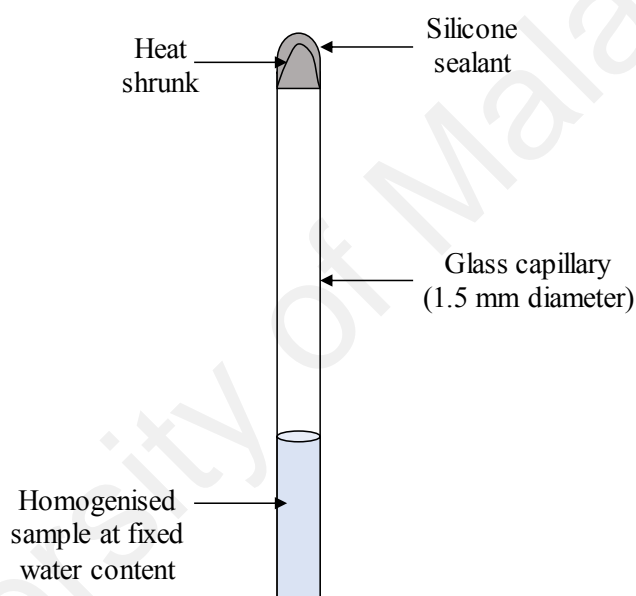


Figure 3.17: A fixed hydration homogenised sample.

In this work, there are three X-ray diffraction machine systems used for measuring the structural information of the mesophases namely:

(i) BEDE X-ray Beamline

X-ray diffraction experiments were conducted at 25 °C using a Bede Microsource (Durham, UK) generator operated at 40 kV and 2 mA, generating Cu-K α ($\lambda = 1.542 \text{ \AA}$)

X-rays. A Gemstar intensified CCD X-ray detector (Photonic Science Ltd, Battle, UK) was used to record 2-D small angle diffraction patterns, with a typical exposure time of 30 s for a single image. The programme AXcess (software developed in-house by Seddon *et al.*, (2006) was used to analyse the diffraction data. 1.5-mm diameter X-ray glass capillary tubes (Capillary Tube Supplies, UK) were used to load lipid mixture samples and then placed in a copper sample holder with Peltier heaters (Melcor, NJ, USA), which controlled the temperature in the chamber within ± 0.1 °C (Hamid *et al.*, 2014).

(ii) Diamond Synchrotron X-ray Source

Time-resolved X-ray experiments were conducted by using a synchrotron at 122 beamline Diamond Light Source located in Oxford, United Kingdom. The synchrotron is a cyclic particle accelerator that generates very intense beams of X-rays with an energy ranging from 3.7 to 20 keV which is able to detect *d*-spacing range between 1–5000 Å. A schematic diagram and detailed design specifications can be found on the Diamond Light Source website (<https://www.diamond.ac.uk/Instruments/Soft-Condensed-Matter/small-angle/122.html>).

(iii) SOL X-ray Beamline

A SOL camera is a custom-built instrument, which is a film Guinier camera based upon a line X-ray source. For X-ray measurements, Philips generator was operated at 40 kV and 30 mA, which was capable of generating X-rays. Line X-ray beam was focused due to the isolation of Cu radiation by quartz crystals monochromator. Copper block, which consisted of X-ray capillary or teflon spacer for holding the sample, was heated and cooled at temperatures in the range of 0–80 °C. The heating or cooling rate was at 10 °C h⁻¹. The diffraction pattern was recorded on a Kodak Biomax MS autoradiography

film. The film was inserted into a film holder which was able to move at the rate of 0.06 mm min⁻¹ (Hamid *et al.*, 2015). It was developed using standard procedures and analysed using AXcess software.

Image Analysis AXcess

AXcess is a software programme which was developed in-house by Andrew Heron (Seddon *et al.*, 2006). This programme was used to analyse SOL X-ray, BEDE X-ray and synchrotron data.

Pre-calibration of the software was required for each image analysis. This step was undertaken by using a silver behenate with well-defined peak at $d = 58.38 \text{ \AA}$ (Li *et al.*, 2017). A one-dimensional plot of intensity (1-D plot) versus pixel number was produced, as a result of centering and integrating of an image over a horizontal line or a butterfly-shaped area by the programme. By selecting and indexing each peak within pre-specified constraints, namely a Gaussian or maximum value fitting, a lattice parameter (d -spacing) was calculated. Further analysis was carried out by converting 1-D plot into a 'stackplot' plot. This plot shows Bragg peaks characterisations which are fitted to the intensities in order to determine the d -spacing of each image, intensity of a particular peak, and phases involved.

CHAPTER 4: RESULTS AND DISCUSSION

4.1 Liquid Crystal Phases of Branched-Chain Glucosides: Thermotropic and Lyotropic

A series of reviews by Dembitsky shows the astonishing structural diversity of natural glycolipids and, despite being only a minor component in biological membranes of animal cells, the presence of glycolipids in nature is pervasive (Dembitsky, 2004a; Dembitsky, 2004b; Dembitsky, 2005a; Dembitsky, 2005b; Dembitsky, 2005c; Dembitsky, 2005d; Dembitsky, 2005e). This strongly suggests that their importance is no less than that of the major membrane lipid components such as phospholipids. Moreover, they play functional roles in many cell processes, including cell-surface molecular-recognition and membrane structure stabilisation (Ernst *et al.*, 2000; Kren & Martinkova, 2001). Natural lipids are difficult to extract in sufficient quantities and purity for biophysical experiments, and a total synthesis of these lipids is often challenging (van Boeckel & van Boom, 1980; van Boeckel *et al.*, 1981). Thus, synthetic substitutes, which closely mimic natural lipids (Garidel *et al.*, 2008; Mannock *et al.*, 1988; Minamikawa & Hato, 1997) are highly sought after, and are especially attractive when produced from renewable resources (plants and/or animals). Alkyl polyglucosides (APG), which meet these stringent green industrial and economic criteria are one example with many successful commercial applications (Balzer & Luders, 2000); however, APG is a monoalkylated mixture, with clear drawbacks, since most natural lipids are double-chained and highly pure materials are necessary for detailed studies to understand how the chemical structures of these glycolipids govern their phase behaviour. The stereochemistry of the sugar headgroup is highly complex, and influences the liquid crystalline phase behaviour even for the simple straight-chain glycolipids (Vill & Hashim,

2002); chain branching adds to this complexity, and hence requires systematic evaluation. When considering the large variety of possible starting materials, both in the sugar (mono-, di- and oligo, etc.) and lipid components (monoalkylated and branched), the potential structural diversity of glycolipids is enormous. The sugar head group may be a mono- or oligosaccharide and the complex sugar stereochemistry contributes further to the diversity due to the combinations and permutations of anomers, epimers, and the inter-sugar linkage orientation.

Glycolipid self-assembly has been studied extensively over the past few decades to clarify the structures of the various ordered lyotropic liquid crystalline phases and their locations in phase diagrams (Corti *et al.*, 2007; Costantino *et al.*, 1999; Sasaki, 2008; Duesing *et al.*, 1997). Both natural and synthetic glycolipids have been widely studied within the biological sphere and in surfactant science (Tyman, 1992; Holmberg, 2001; Kates, 1990). Through the extensive work of Vill *et al.* (1989), Jeffrey and Wingert (1992), Jeffrey (1986) and others, their importance as thermotropic liquid crystals has been established and this has led to a new interest in their thermotropic properties and potential applications, even though Emil Fischer, who prepared the first synthetic glycosides (Fischer & Beensch, 1894), had already recognised their thermotropic behaviour at that time (Fischer & Helferich, 1911). The thermotropic phase behaviour of these systems (without solvent) is closely related to that of lyotropic systems and can be tuned by varying the molecular structure. In the present work, the phases are described using the standard lyotropic nomenclature, both in the dry and hydrated states as the molecules involved are amphiphilic rather than mesogenic. Thus, for the dry (thermotropic) systems, the notation L_α is used rather than SmA, and H_{II} is used rather than Col_h. Table 4.1 shows the comparison between the conventional thermotropic nomenclature and the more general one based on lyotropic systems adopted here.

Table 4.1: Comparison between the conventional notation for thermotropic phases used for mesogenic liquid crystals, and that used here for amphitropic liquid crystals, based on the lyotropic convention. Adopted from (Seddon & Templer, 1995).

Thermotropic Liquid Crystals		Amphitropic Liquid Crystals	
Phase Name	Symbol	Phase Name	Symbol
Crystal	Cr	Lamellar crystal	L _C
Smectic A	SmA	Lamellar (fluid)	L _α
Columnar hexagonal	Col _h	Hexagonal	H _I (normal)/H _{II} (inverse)
Isotropic	I	Micellar (aggregate)	L ₁ (normal)/L ₂ (inverse)
Cubic	Cub	Cubic (discontinuous)	I _I (normal)/I _{II} (inverse)
		Cubic (bicontinuous)	V _I (normal)/V _{II} (inverse)

Recently, a new class of branched-chain Guerbet glycosides (Hashim *et al.*, 2006) has been synthesised by Lewis acid catalysed glycosidation (Vill *et al.*, 1989) using a variety of mono (glucose and galactose) and disaccharide sugars (maltose, lactose and cellobiose) and Guerbet alcohols (O'Lenick, 2001), whose total number of carbon atoms in the branched chain ranges from 8–24 (Figure 4.1). The emphasis of previous work (Hashim *et al.*, 2006) was to explore the effect of sugar stereochemical diversity on the thermotropic phase behaviour. Based on OPM and DSC, the stereochemistry of these Guerbet glycolipids was found to affect the phase behaviour in a similar way to that of the monoalkylated glycosides (Vill & Hashim, 2002). However, due to the chain branching, the former tends to adopt liquid crystalline phases at room temperature (apart from the lactoside series; the anomalous behaviour of lactosides and galactosides has been discussed elsewhere (Rodzi, 2006; Hussen, 2006; Hashim *et al.*, 2012). Moreover, it was observed that the shorter Guerbet glycolipids stabilise a fluid lamellar phase, while the longer branched chains promote inverse non-lamellar phases. The preferred curvature in these systems is set by a balance between hydrogen bonding within the head group region and the splay of the hydrocarbon chains. For certain Guerbet glycolipids, (e.g. maltoside

with C₂₀ and C₂₄), a more complex polymorphism was observed, with an L_α–V_{II}–H_{II} phase sequence (Hashim *et al.*, 2006; Nguan *et al.*, 2010). Thermotropic polymorphism in amphitropic compounds such as glycolipids is rather uncommon, but has been previously observed in certain systems (Mannock *et al.*, 2007) and there are other branched chain glycolipids whose behaviour has been extensively studied (Mannock *et al.*, 2007; Mannock *et al.*, 2000; Milkereit *et al.*, 2004; Minamikawa & Hato, 1998; Minamikawa *et al.*, 1994; von Minden *et al.*, 2002). Some common trends have been found, such as the formation of inverse non-lamellar phases for the monosaccharide (glucose and galactose) lipids (Mannock *et al.*, 2007; Hato *et al.*, 1999). On the other hand, disaccharide and oligosaccharide branched-chain glycolipids mainly adopt the lamellar L_α phase (Minamikawa & Hato, 1997; Hato & Minamikawa, 1996). The phase boundaries exhibited by these systems tend to be relatively insensitive to temperature. The monosaccharides show a variety of inverse bi-continuous cubic phases of space groups *Pn3m*, *Im3m* and *Ia3d*, which may be important in biological function, especially when stable in excess water (Mannock *et al.*, 2007; Minamikawa & Haro, 1998; Hato *et al.*, 2004; Mannock *et al.*, 2001).

In the present work the phase behaviour of five branched-chain Guerbet β-D-glucosides, both in dry state (thermotropic) and in excess water (lyotropic), using a combination of OPM, DSC and small-angle X-ray diffraction has been reported.

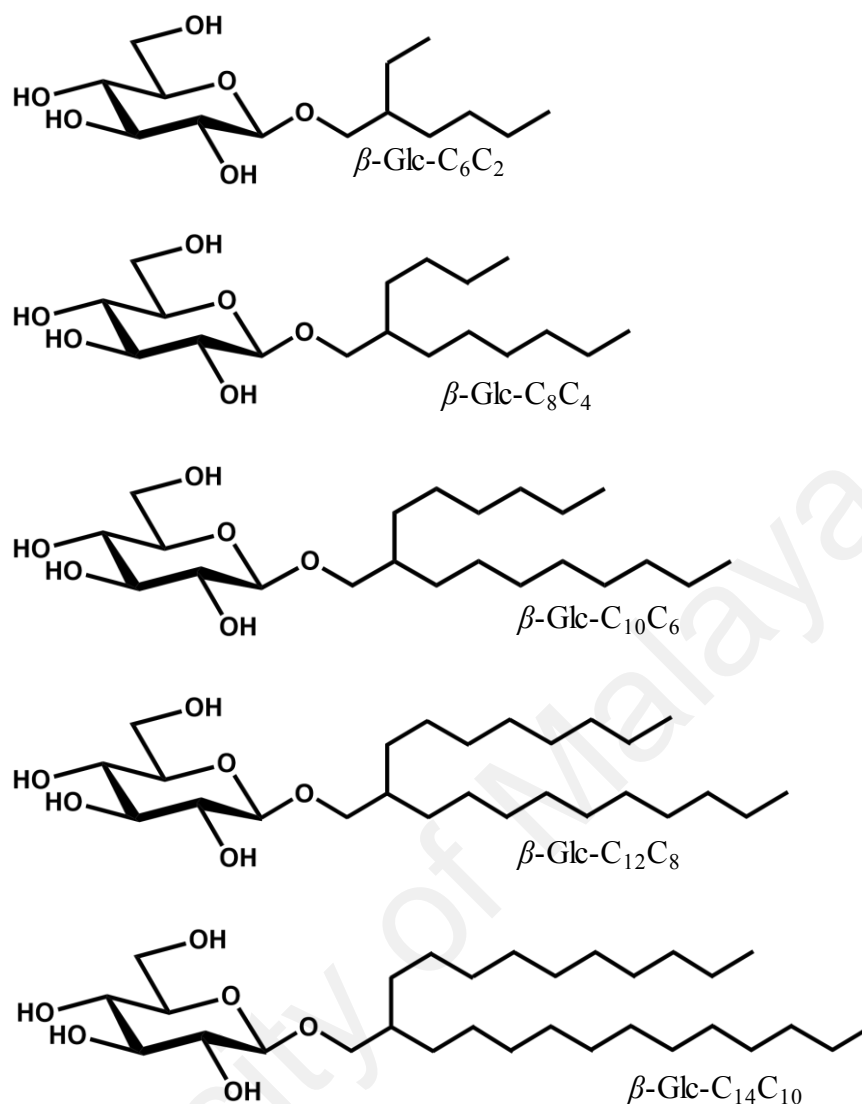


Figure 4.1: The chemical structures of the branched-chain β -D-glucosides.

4.1.1 Optical Polarising Microscopy

On heating, the dry β -Glc-C₆C₂ gave an OPM texture typical of an L_C (lamellar crystal) phase (Figure 4.2a), which started to melt at 55.4 °C and became completely clear at 62 °C. In the cleared state, the sample was fluid, suggesting the phase to be an inverse micellar L₂ phase. Upon cooling, birefringence appeared in the OPM image (Figure 4.2b) at 59 °C, which was consistent with a fluid lamellar (L _{α}) phase. Thus, the shortest chain β -Glc-C₆C₂ gave a monotropic transition in the absence of water. Upon addition of water to the monotropic phase, an L _{α} (lyotropic) phase formed quickly as water penetrated the

bulk sample, replacing the L_α (thermotropic) phase (Figure 4.2c). After half an hour, the sample was completely dissolved into the L_1 micellar solution phase. The dry β -Glc- C_8C_4 compound was found to be an optically isotropic viscoelastic fluid, presumably an L_2 inverse micellar solution. A trace of birefringence could be observed in the air/sample interface (Figure 4.3a) probably due to moisture absorption. During water contact penetration experiments, the sample formed myelin figures, indicating an L_α phase (Figure 4.3b).

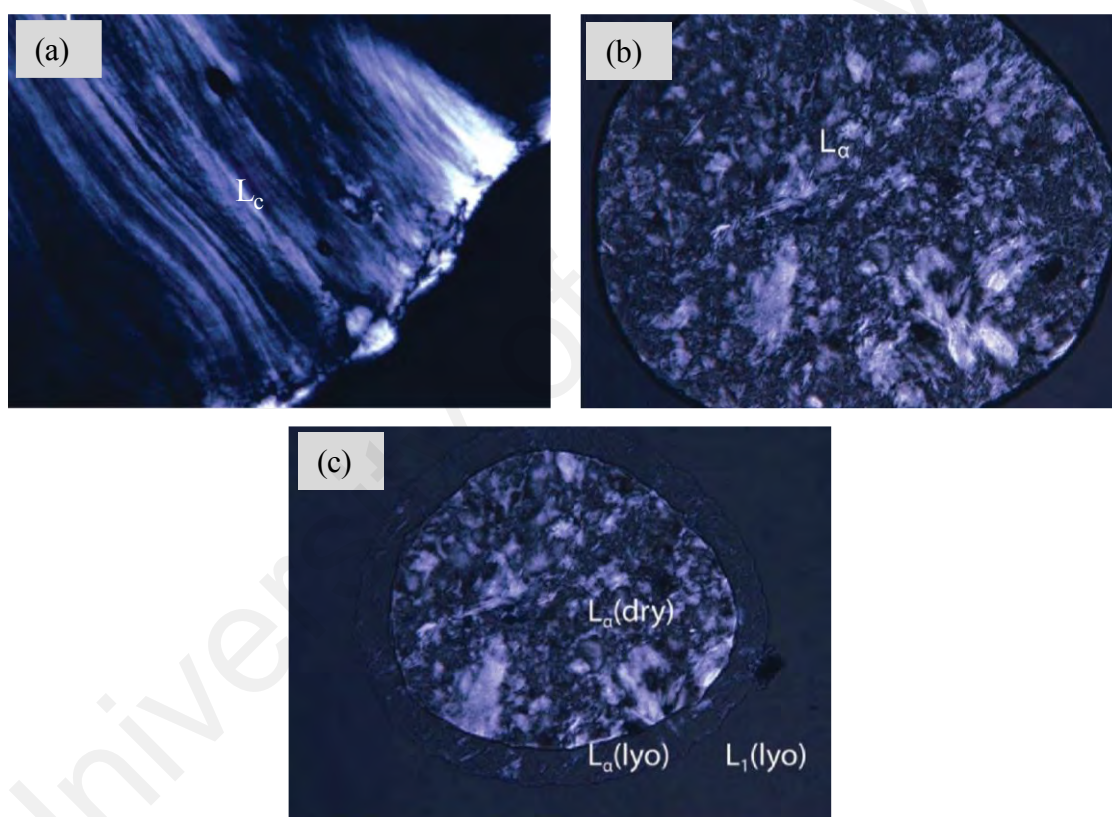


Figure 4.2: OPM textures of β -Glc- C_6C_2 for (a) thermotropic (dry) L_c phase at 31 °C before heating; (b) on cooling below 59 °C a birefringent texture consistent with an L_α (dry/thermotropic) phase is seen; and (c) a water contact penetration scan after 5 min gave L_1 and L_α (lyo) phases in addition to the dry L_α state, at room temperature. The sample transformed completely to an L_1 micellar solution in approximately half an hour.

The dry C_{16} β -Glc- $C_{10}C_6$ compound initially gave strong birefringence with an undefined texture under OPM at room temperature. Upon heating (at 5 °C min⁻¹) the

sample cleared at 55–56 °C and on cooling, an inverse hexagonal (H_{II}) texture started to appear below 49 °C (Figure 4.4a). Upon re-heating at 2 °C min⁻¹, the H_{II} texture disappeared between 54–55 °C. Water contact penetration experiments for this compound gave a single viscous isotropic (cubic) phase at the water-rich side of the H_{II} phase (Figure 4.4b).

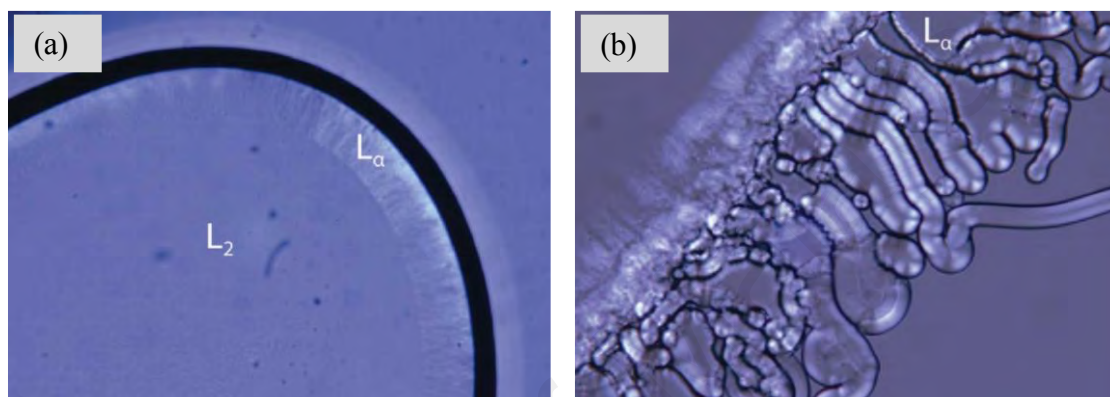


Figure 4.3: OPM textures of β -Glc- C_8C_4 for (a) a dry /thermotropic sample at 31 °C, where the sample appears isotropic except at the edge (due to moisture adsorption from the atmosphere); (b) contact penetration with water caused myelins to form immediately.

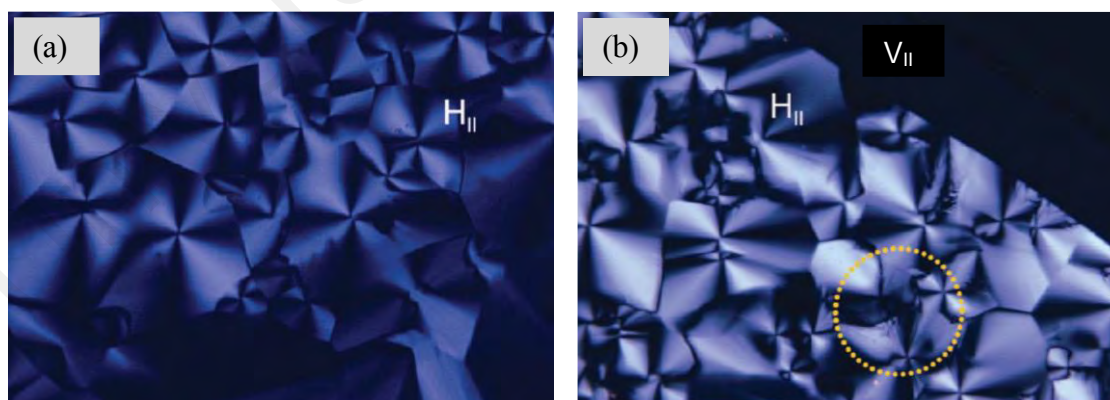


Figure 4.4: OPM textures of β -Glc- $C_{10}C_6$ after the sample was extensively dried. (a) H_{II} phase at 40 °C (cooling at 5 °C min⁻¹); (b) contact penetration with water showing a growing isotropic / cubic domain, with a strained H_{II} structure (optical evidence of strain is highlighted by a dotted circle).

The longer chain compounds (β -Glc-C₁₂C₈ and β -Glc-C₁₄C₁₀) form hexagonal H_{II} phases both when dry and in excess water, with typical optical textures as shown in Figures 4.5 and 4.6. The thermotropic phase transition temperatures measured by OPM are summarised in Table 4.2.

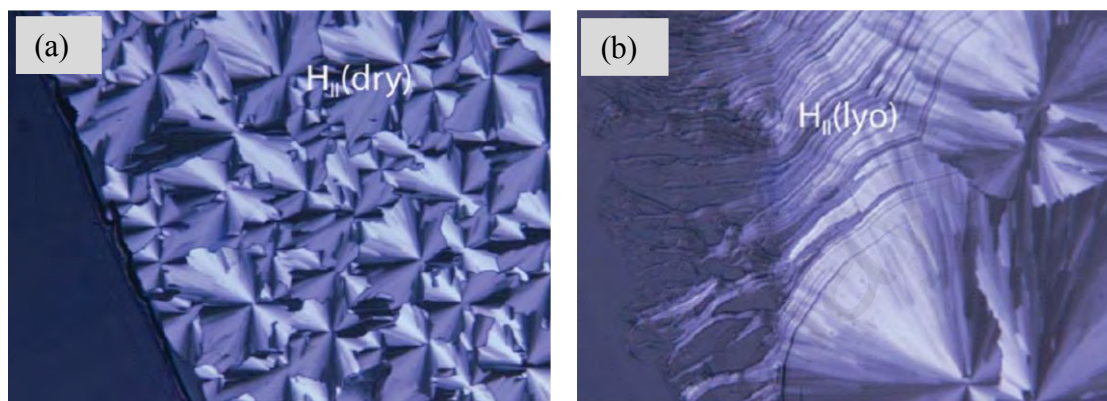


Figure 4.5: (a) Thermotropic H_{II} texture at room temperature for β -Glc-C₁₂C₈; and (b) lyotropic H_{II} texture after 7 h of contact penetration with water.

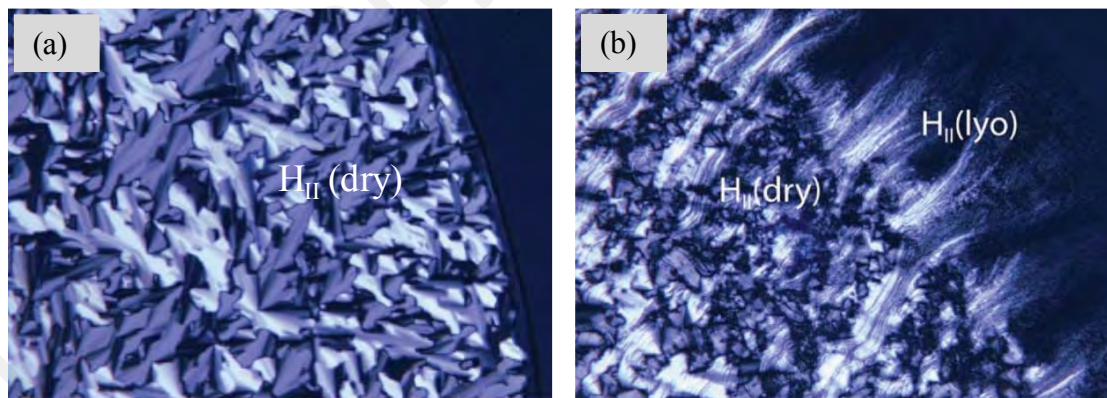


Figure 4.6: (a) Thermotropic H_{II} texture on cooling from 50 °C to room temperature for dry β -Glc-C₁₄C₁₀; and (b) lyotropic H_{II} texture after 6 h of contact penetration with water.

Table 4.2: Thermotropic phase transition temperatures above 25 °C for the dry β -D-glucosides determined by optical polarising microscopy. Note: these transition temperatures are measured after initial heating and cooling during sample preparation.

Glycolipid	Phase Transitions and Transition Temperatures
β -Glc-C ₆ C ₂	L _C –L ₂ : 62 °C (heating) L ₂ –L _{α} : 59 °C (cooling)
β -Glc-C ₈ C ₄	L ₂ at all temperatures studied
β -Glc-C ₁₀ C ₆	H _{II} –L ₂ : 55 °C
β -Glc-C ₁₂ C ₈	H _{II} –L ₂ : 113 °C
β -Glc-C ₁₄ C ₁₀	H _{II} –L ₂ : 139 °C

4.1.2 Differential Scanning Calorimetry

Thermal properties of β -D-glucoside homologous series are determined via a DSC. The β -D-glucosides heating DSC thermograms are provided in Figure 4.7. In addition, Table 4.3 gives the phase transitions and their corresponding enthalpy changes (ΔH). Generally, the OPM and DSC results obtained are complementary to each other. Both experimental methods produce similar results within the accepted value range of 1–9 °C. This discrepancy in temperature is due to the transfer of heat between the sample on an OPM glass slide and a DSC pan. The DSC thermograms illustrated in Figure 4.7 shows the compound's endothermic clearing temperature before it is changed into the isotropic phase. As observed, for every compound there is only a single transition temperature peak. In contrast, it is not the case for the β -D-maltosides homologous series that has, in addition, a glass transition peak.

During heating, β -Glc-C₆C₂ in the liquid crystalline phase turns into an isotropic phase at 60 °C with ΔH value of 1.2 kJ mol⁻¹. No other phase transitions were observed as confirmed by the OPM measurement.

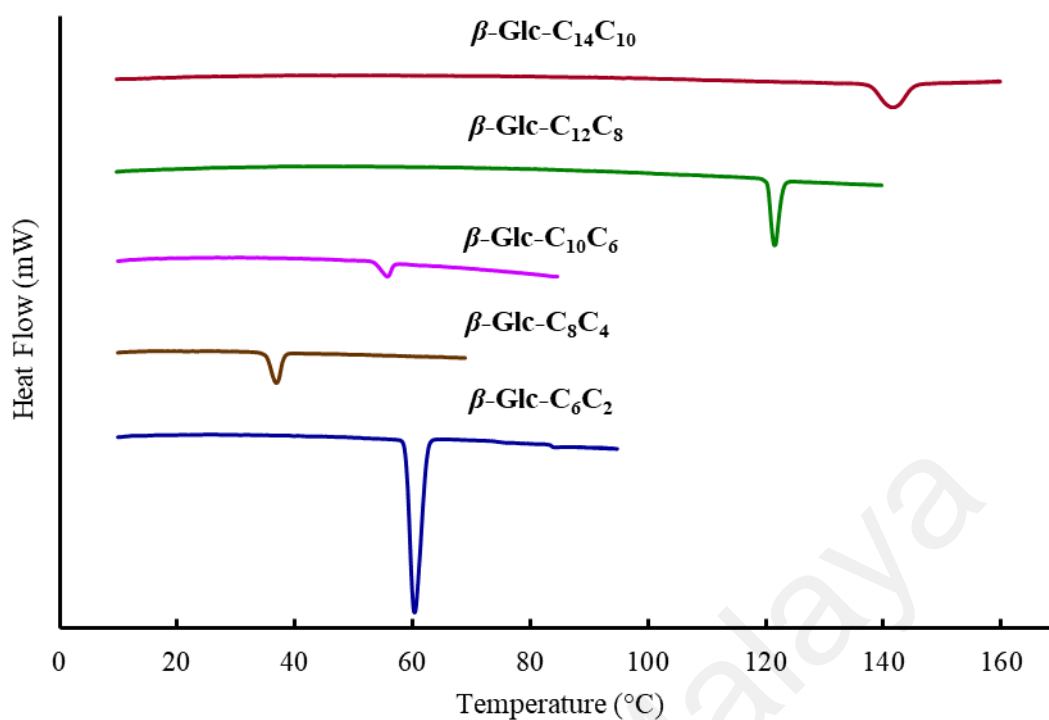


Figure 4.7: DSC thermograms for dry β -D-glucosides at a heating scanning rate of $5\text{ }^{\circ}\text{C min}^{-1}$.

Table 4.3: For comparison, dry Guerbet glucosides and xylosides data obtained using DSC are provided.

			Transition Temperature ($\pm 1\text{ }^{\circ}\text{C}$) [$\Delta H (\pm 0.1\text{ kJ mol}^{-1})$]	
Guerbet Glucosides (Current Work)	n	Molecular Formula	T _c (DSC)	T _c (OPM)
β -Glc-C ₆ C ₂	8	C ₁₄ H ₂₈ O ₆	60 [1.2]	62
β -Glc-C ₈ C ₄	12	C ₁₈ H ₃₆ O ₆	37 [0.3]	-
β -Glc-C ₁₀ C ₆	16	C ₂₂ H ₄₄ O ₆	56 [0.1]	55
β -Glc-C ₁₂ C ₈	20	C ₂₆ H ₅₂ O ₆	122 [0.8]	113
β -Glc-C ₁₄ C ₁₀	24	C ₃₀ H ₆₀ O ₆	142 [1.0]	139
Transition Temperature ($\pm 0.1\text{ }^{\circ}\text{C}$)				
Guerbet Xylosides ^a	n		T _c (DSC)	
β -Xyl-C ₆ C ₂	8		53	
β -Xyl-C ₈ C ₄	12		43	
β -Xyl-C ₁₀ C ₆	16		50	
β -Xyl-C ₁₂ C ₈	20		63	
β -Xyl-C ₁₄ C ₁₀	24		56	

^aData taken from (Liew *et al.*, 2015).

Unlike the first analogue which is β -Glc-C₆C₂, anhydrous β -Glc-C₈C₄ exhibits only L₂ phase with the clearing temperature of 37 °C and $\Delta H = 0.3 \text{ kJ mol}^{-1}$ as obtained using DSC. Likewise, on subsequent heating, there is no other phase transition occurred.

From DSC measurements, the longer branched-chain of β -Glc-C₁₀C₆, β -Glc-C₁₂C₈ and β -Glc-C₁₄C₁₀ give the clearing transition temperatures of 56, 122 and 142 °C with the enthalpy changes of 0.1, 0.8 and 1.0 kJ mol⁻¹, respectively.

A relatively small value of less than 2.0 kJ mol⁻¹ was detected associated with the phase transition enthalpy from liquid crystal phase to clear isotropic phase for the β -D-glucoside homologous series. This signifies a liquid-like and disordered mesomorph state in accordance with the clearing phase transition small amount of energy (Laurent *et al.*, 2003).

The increment of T_C of β -D-glucoside homologous series is subjected to the increased in the number of alkyl chain length except for the shortest β -Glc-C₆C₂. However, the T_C values of these glucosides are lower compared to the corresponding T_C β -D-maltoside homologous series due to a smaller number of hydrogen bonding of the former.

Guerbet glucosides and xylosides are monosaccharides which differ by their sugar head group, namely, a glucose (aldohexose) and a xylose (aldopentose) unit. Even though, both possess the same total number of carbon atoms (C₈–C₂₄) as their non-polar hydrophobic tails. In thermotropic or dry condition, Guerbet glucosides show a similar trend links to the clearing temperatures compared to the Guerbet xylosides. On the other hand, the former exhibits a higher clearing temperature than that of the latter. This is due to the thermotropic clearing temperature is influenced by the total number of hydrogen bonding (Ahmadi *et al.*, 2014). A Guerbet glucoside consists of four OHs, while a similar, Guerbet xyloside has three OHs attached to the sugar head group. Therefore, the former

has extra hydrogen bonding; hence, it requires more thermal energy as a driving force for the Guerbet glucosides to transform to the cleared non-viscous isotropic phase. Similar observation for Guerbet maltosides which are disaccharides with seven OHs show that there is an increment in the clearing phase transition temperatures compared to the Guerbet glucosides. The phase transition clearing temperature (T_C) data between Guerbet glucosides and xylosides is shown in Table 4.3 for comparison purposes.

One key factor which governs the glycosides (glucosides and xylosides) as surfactant is an optimal curvature. This is determined by the relative size of the polar sugar head and non-polar tail groups (Fletcher & Strey, 2002). In a similar fashion, the dichotomy between sugar head and non-polar tail groups of the glycosides is considered one of the main contributors in forming the liquid crystal mesophases either in thermotropic or lyotropic condition (Vill & Hashim, 2002).

4.1.3 Small-Angle X-ray Diffraction

Thermotropic Phases of the Dry Glycolipids

The small-angle synchrotron X-ray diffraction pattern for β -Glc-C₆C₂, after cooling from 80 to 25 °C, is shown in Figure 4.8. The single sharp line has a d -spacing of 20.7 Å; no higher-order peaks are visible due to the beamline configuration. However, lab-based X-ray diffraction experiments (Figure 4.9) show two peaks at S of 0.0481 and 0.0961 Å⁻¹, consistent with a dry L_α phase with a d -spacing of 20.7 Å. The β -Glc-C₈C₄ compound gave only single, broadened X-ray peak (Figure 4.8), implying that it forms an L_2 phase in the dry state, and this is consistent with the OPM results above. The X-ray diffraction pattern from dry β -GlcC₁₀C₆ was collected at the Australian Synchrotron and shows an intense first-order peak with significantly weaker $\sqrt{3}$ and 2 peaks (see Figure

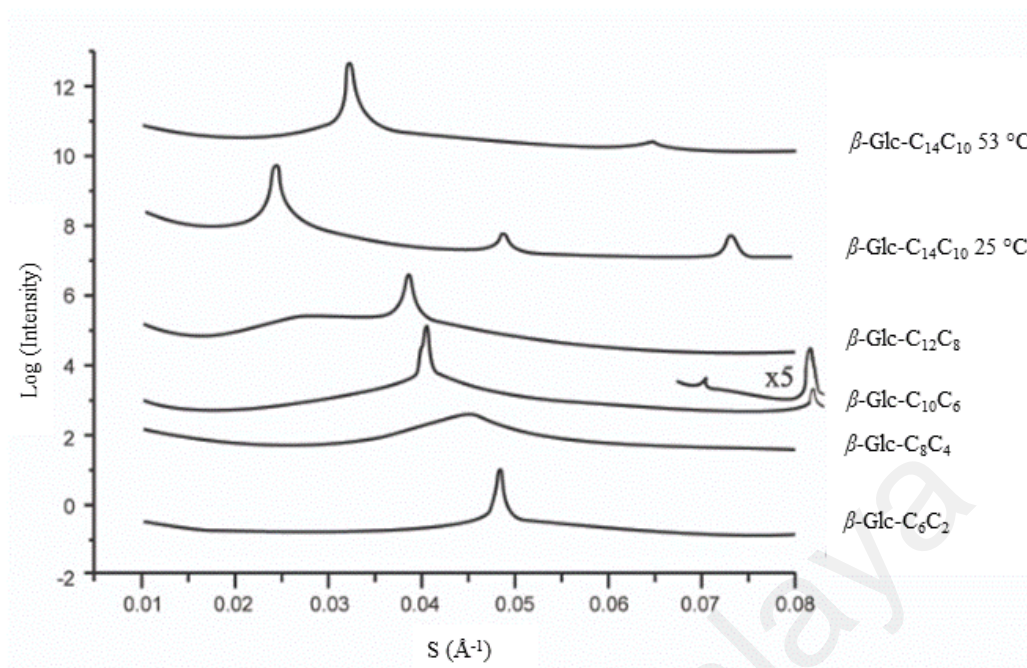


Figure 4.8: Synchrotron small-angle X-ray diffraction patterns from dry β -Glc- $C_{n+4}C_n$ samples at 25 °C unless otherwise stated. Patterns are offset along the y-axis for clarity. Diffraction patterns were collected at Diamond Light Source, with the exception of that from β -Glc- $C_{10}C_6$ which was collected at the Australian Synchrotron.

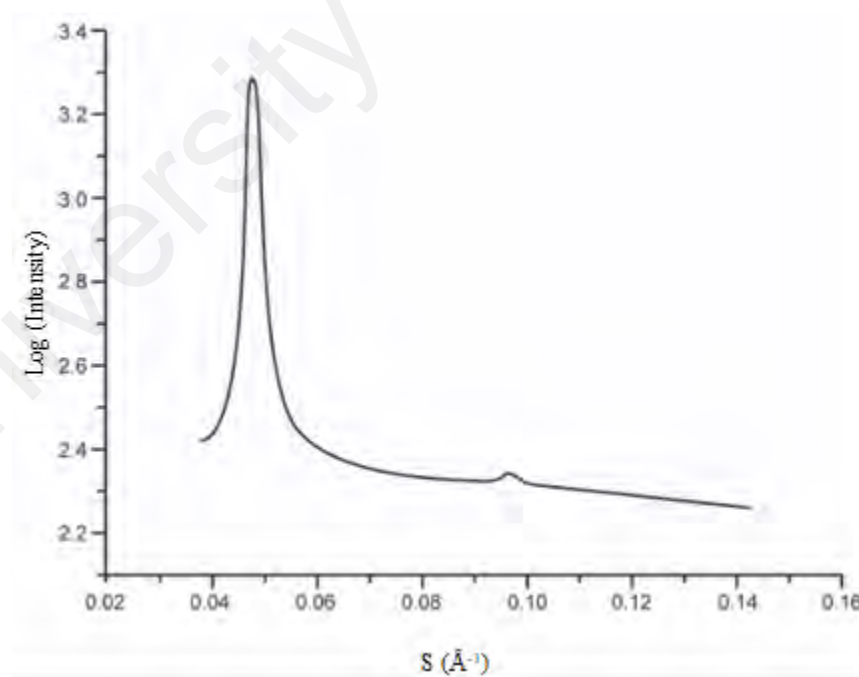


Figure 4.9: Small-angle X-ray diffraction patterns from dry β -Glc- C_6C_2 samples at 30 °C after cooling from 75 °C.

4.8), characteristic of an H_{II} phase which corresponding to lattice parameter of 28.7 Å. There is a small shoulder on the low *S* side of the first order peak; the origin of this is unclear at present, but it represents a minor component relative to the clear H_{II} phase. This is in agreement with the OPM results above; however, earlier diffraction data from this sample, collected at Diamond Light Source showed only a single broadened X-ray peak indicative of an L₂ phase. The reason for this discrepancy is not entirely clear, but it may indicate that the Diamond Light Source sample had absorbed a small amount of water. While the optical texture of dry β -Glc-C₁₂C₈ (Figure 4.5) is typical of a hexagonal phase, its diffraction pattern (Figure 4.8) consists of a single peak (*d*-spacing of 26 Å, corresponding to a 30 Å lattice parameter for a 2-D hexagonal structure) superimposed on a lower-angle diffuse peak whose origin is at present unknown, although it suggests significant interfacial disorder is present within the liquid crystal phase. The characteristic 2-D hexagonal higher-order peaks $\sqrt{3}$, 2, $\sqrt{7}$ etc. are not observed. This has been previously noted for dry H_{II} phases of phospholipids and explained in terms of form factor effects (Seddon, 1990). A dry H_{II} phase can be modelled as a 2-D hexagonal lattice of solid cylinders of uniform electron density (consisting of the dry aggregated headgroups), in a continuum of fluid hydrocarbon chains of uniform electron density. The form factor of a single such cylinder is a Bessel function, whose first node (zero) lies beyond the (10) peak of the hexagonal lattice, but before the next peak in the pattern. Since the form factor lobes beyond the first node are characteristically of very low amplitude for a solid cylinder, the higher-order peaks are too weak to be observed, and only the (10) peak is seen. Increasing the water content introduces a core of lower electron density relative to the head groups, rendering the Bessel function (form factor) more strongly oscillatory, thereby allowing some of the higher-order peaks to become visible (Figure 4.10).

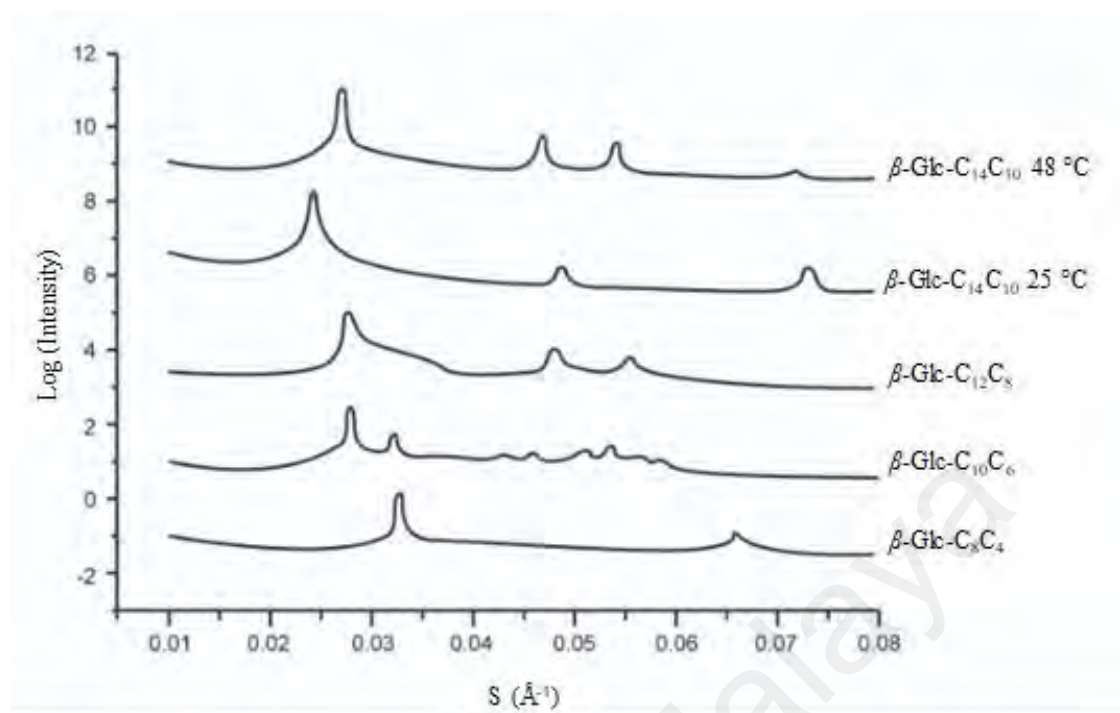


Figure 4.10: Synchrotron small-angle X-ray diffraction patterns from β -Glc- $C_{n+4}C_n$ samples in excess water at 25 °C unless otherwise stated. Patterns are offset along the y-axis for clarity. Diffraction patterns were collected at Diamond Light Source.

The β -Glc- $C_{14}C_{10}$ compound shows three orders of a lamellar phase at 25 °C before heating with a d -spacing of 41.1 Å, presumed to be an ordered gel or crystalline lamellar phase. This pattern transforms upon heating to one consisting of two peaks in the ratio 1, 2. By comparison with the OPM results, it is believed that this arises from a dry H_{II} phase with a lattice parameter of 35.8 Å, with the $\sqrt{3}$ (11) peak missing due to it sitting close to the first node in the form factor, whereas the (20) reflection is far enough into the second form factor lobe to be weakly observed. The results presented so far imply that the shortest chain lipid with a C_6C_2 branched chain promotes a lamellar packing in the absence of water, although not as strongly as the corresponding monoalkylated octyl β -D-glucoside (Vill *et al.*, 1989; Nilsson *et al.*, 1998) whose thermotropic clearing transition temperature is much higher than that observed here. It is well known that chain branching stabilises non-lamellar, curved phases (Nilsson *et al.*, 1998; Nilsson *et al.*,

1997); indeed, it is observed that the longer chain lipids ($C_{14}C_{10}$, $C_{12}C_8$ and $C_{10}C_6$) form hexagonal H_{II} phases, whereas the intermediate chain length C_8C_4 compound gives an inverse micellar L_2 phase.

Lytotropic Phases of the Glycolipids in Excess Water

The branched-chain β -glucoside series was further investigated under excess water conditions. No sharp diffraction peak was observed for the shortest compound (β -Glc- C_6C_2), consistent with it being completely soluble in excess water, forming an L_1 micellar solution. While in dry conditions β -Glc- C_8C_4 exhibits an inverse micellar L_2 phase, in excess water it shows an L_α fluid lamellar structure (Figure 4.10) with a d -spacing of 30.3 Å.

The β -Glc- $C_{10}C_6$ compound solvated in excess water forms an inverse bicontinuous V_{II} cubic phase. Bragg peaks are observed (Figures 4.10 and 4.11) with spacing ratios of $\sqrt{6}$, $\sqrt{8}$, $\sqrt{14}$, $\sqrt{16}$, $\sqrt{20}$, $\sqrt{22}$, $\sqrt{24}$ and $\sqrt{26}$, which are the first eight allowed reflections of space group $Ia3d$ with a lattice parameter of 87.5 Å. The $Ia3d$ cubic phase is based on an underlying G (gyroid) infinite periodic minimal surface (IPMS) and is closely related to the $Im3m$ and $Pn3m$ bicontinuous cubic phases, which are based upon the P and D minimal surfaces respectively. In most systems, only $Pn3m$ (and sometimes $Im3m$) are found in excess water, and if $Ia3d$ is present, it only occurs at a reduced hydration. This is because when the three minimal surfaces are Bonnet related, the G surface is the most compact at filling space, followed by the D and then the P. However, in the present case, surprisingly, the formation of the $Ia3d$ cubic phase in excess water occurs.

The β -Glc- $C_{12}C_8$ compound shows a hexagonal H_{II} pattern in excess water with a lattice parameter of 36.1 Å (Figure 4.9), but with some structured scattering to the high-

angle side of the (10) peak, whose origin is unclear at present. The longest-chain glycolipid, β -Glc-C₁₄C₁₀, was found to adopt an ordered lamellar phase at 25 °C before heating, and a hexagonal H_{II} phase ($a = 36.9$ Å) in excess water at 48 °C (Figure 4.10). The ordered lamellar phase, with a d -spacing of 41.1 Å, is identical to that of the dry compound, indicating that the Krafft point for this lipid lies above room temperature. The d -spacings or lattice parameter for the Guerbet glucoside self-assembly structures in dry and in excess water are listed in Table 4.4.

Table 4.4: Phase assignments and d -spacings or lattice parameter for the dry and excess water β -D-glucosides at 25 °C. Error in d -spacings or lattice parameter is ± 0.1 °C.

Lipid	Dry		Excess Water	
	Phase	d -spacings/ Lattice Parameter (Å)	Phase	d -spacings/ Lattice Parameter (Å)
β -Glc-C ₆ C ₂	L _{α}	20.7	L ₁	-
β - Glc-C ₈ C ₄	L ₂	-	L _{α}	30.3
β - Glc-C ₁₀ C ₆	H _{II}	28.7	V _{II} ($Ia3d$)	87.5
β - Glc-C ₁₂ C ₈	H _{II}	30.0	H _{II}	36.1
β -Glc-C ₁₄ C ₁₀	H _{II}	35.8 ^a	H _{II}	36.9 ^b

^aValues obtained at 53 °C and ^b at 48 °C.

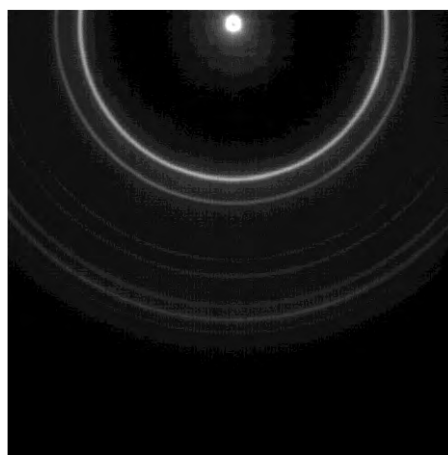


Figure 4.11: Two-dimensional small-angle X-ray diffraction pattern from β -Glc-C₁₀C₆ in excess water, characteristic of a cubic phase of space group $Ia3d$.

4.1.4 Final Remarks

In these experiments, it has been demonstrated that glucosides with Guerbet branched chains (in the dry form and when hydrated in excess water) generally exhibit lamellar phases for chains up to C₁₂, while those with a C₁₆ chain and above show non-lamellar phases including L₂, V_{II} and H_{II}. The prevalence of inverse non-lamellar phases observed for this family of glycosides is due to the relatively large splay of their hydrophobic chains resulting from the chain branching. While straight-chain glycosides form only L _{α} above room temperature, all the Guerbet compounds reported here, with the exception of the longest-chain compound, are liquid crystalline at room temperature in the dry state. The phase behaviour of β -Glc-C₁₀C₆, is noteworthy since it is intermediate between compounds that show a tendency to form L _{α} and H_{II}. In excess water this compound exhibits an inverse bi-continuous cubic phase of space group *Ia3d*, which is very rarely seen in single component amphiphile systems in excess water. It is possible that the asymmetric nature of the Guerbet branched chain stabilises the *Ia3d* phase, but the mechanism of this is not clear at present. Such an excess water *Ia3d* phase could have interesting applications in templating, encapsulation and membrane protein crystallisation.

4.2 Mesophase Structures of Branched-chain Alkyl Maltosides in Dry and Excess Water Conditions

Unique self-assembling properties exhibited by liquid crystals (LCs), which involve an intermediate molecular order between a solid crystal and an isotropic liquid, have made LCs the centre of attention and interest in many areas of research encompassing physics, biology, chemistry and engineering. With such properties of materials, LCs may adopt more than one intermediate state or mesophase i.e.

polymorphisms. Consequently, LCs research offers a wide spectrum of potential applications in both technological and biological applications.

LCs are classified as thermotropic and lyotropic mainly due to their formation controlling factors. Mesomorph states of thermotropic LCs are shown in a certain temperature range in dry conditions (without solvent). Hence, a notable technological application of these LCs is liquid crystal displays (LCDs) which are used for television and display devices in smartphones and laptop screens. The LCs are known as anisotropic materials. This anisotropy is due to the molecule's shape and dictates the resulting alignment. Birefringence is a property of anisotropic LCs. For instance, the values of the anisotropy (Δn) can be up to 0.5 for strongly birefringent LCs. In addition, other properties such as electric and magnetic susceptibility can be used to measure the anisotropy. Hence, the change in birefringence corresponds to the LCs important applications (Vertogen & de Jue, 2012). Consequently, this unique property of LCs has made the exploration on this matter still current, in demand and relevance especially in the world of electronic devices (Ojha *et al.*, 2013). Kaafarani (2011) reviewed optoelectronic applications of discotic liquid crystals (DLCs); in which he reported on the issues of DLCs such as charge-carrier mobilities, transition and mesophase engineering, alignments, theoretical calculations and optoelectronic devices. Furthermore, industrial nematic liquid crystals' thermal diffusivity parameters have been determined using a finite difference method. This method uses a constructed in-house liquid crystal cell and a heating system that measures in situ materials' temperature (Yilmaz & Yildirim, 2009).

In order to unravel more of the usefulness of LCs, the emerging research effort on biosensors has been undertaken; for example, thermotropic liquid crystal-based sensor formats linked with thin films, micro-capillary tubes (Kim & Jang, 2016) and fibres (Enz *et al.*, 2013). In lyotropic LCs, on the other hand, mesomorph states are formed in

solutions. The occurrence of these phases is influenced by solvent's type, concentration and temperature. A good example of lyotropic LCs in everyday life is soap. In addition, Popov *et al.* (2018) reviewed not only on sensor platforms based on thermotropic LCs, they also explained the formation of lyotropic LC-based sensor. A variety of many complex mixtures of molecule, which are able to produce lyotropic mesophases, can be formulated for biosensors, drug delivery vehicles and biomedical applications (van't Hag *et al.*, 2017). In living materials one major component in biological membrane is phospholipids. These lipid molecules are arranged in a stack of lamellar bilayer a lyotropic LC phase. Localised non-lamellar phases, on the other hand, may involve or play a special role in membrane functions. Therefore, in order to understand further the metastability and lipid polymorphism, studies on hydrated saturated diacyl diarachinoylphosphatidylethanolamine (DAPE) and dialkyl didodecylphosphatidylethanolamine (DDPE) were conducted by Seddon and co-workers (1984). DDPE adopts metastable structures of L_{β} and L_{α} at all water contents below 44 °C; moreover, from the L_{α} to H_{II} , other non-lamellar and cubic structures are observed. On the contrary, DAPE produces tilted gel phase; and at below 3 wt% water contents, metastable behaviour is adopted. Investigations on isoprenoid glycolipid lyotropic rich phase behaviours are reviewed related to single-chain and double-chain based isoprenoid glycolipids in view of water contents and temperatures (Hashim *et al.*, 2012). In essence, mesophases or polymorphism displayed by thermotropic and lyotropic LCs (i.e. phospholipids and glycolipids) may be driven by the effect of lipid packing parameter (Hui & Sen, 1989; Khalil & Zarari, 2014).

To date, fundamental research on thermotropic and lyotropic Guerbet glycosides (a glycolipid family) is relatively scanty. Some research on applications include vesicle (Hussen, 2006), nano-emulsion (Ahmad *et al.*, 2014) and hexasome formulations (Ahmad

et al., 2012) and pyroelectricity of thin films (Kwong *et al.*, 2010). Hence, this present research with characterisations of the alkyl maltosides (β -Mal-C₆C₂, β -Mal-C₈C₄, β -Mal-C₁₀C₆, β -Mal-C₁₂C₈ and β -Mal-C₁₄C₁₀) were done using an OPM (phase behaviours of the sample in dry and water penetration scan), DSC (phase transition) and SAXD (phase structures) methods.

4.2.1 Optical Polarising Microscopy

β -Mal-C₆C₂ which has the shortest hydrocarbon chain length (with total 8 carbon atoms) exhibits lamellar crystals (L_C) phase at the room temperature (Figure 4.12a). Upon heating the dry β -Mal-C₆C₂, the compound become cleared $\sim 137^\circ\text{C}$. Upon cooling, birefringent textures appeared in the OPM image (data not shown) which were consistent with an L_α phase. As shown in Figure 4.12b, when water is added, the compound completely dissolved and turning into a non-birefringence texture, indicating the micellar solution (L_I).

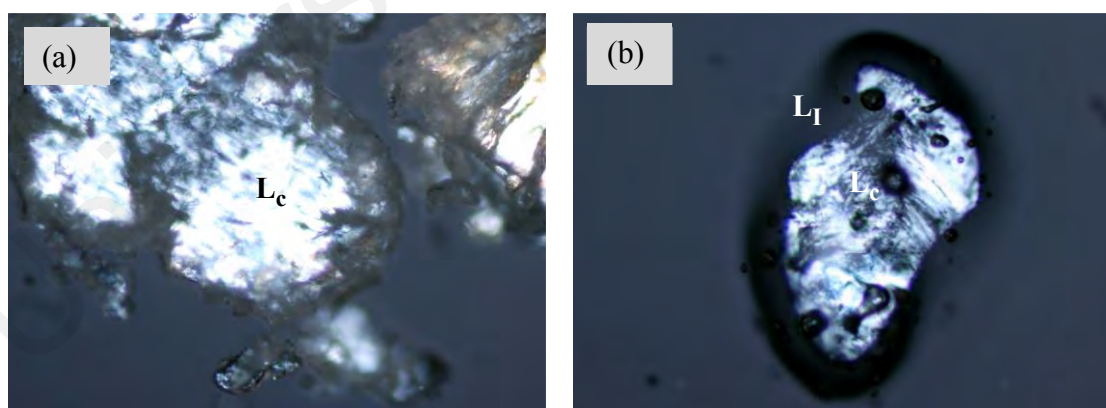


Figure 4.12: OPM textures of β -Mal-C₆C₂ for (a) thermotropic L_C phase; and (b) when it dissolves in water producing L_I solution. 10 \times magnification at room temperature.

Similar to the β -Mal-C₆C₂, the dry β -Mal-C₈C₄ exhibits L_C phase at the room temperature (Figure 4.13a). Upon heating, the compound turned to an isotropic liquid ~ 188 °C and on cooling, an L _{α} phase texture was observed. In the lyotropic study, the sample formed myelin figures, indicating an L _{α} phase (Figure 4.13b).

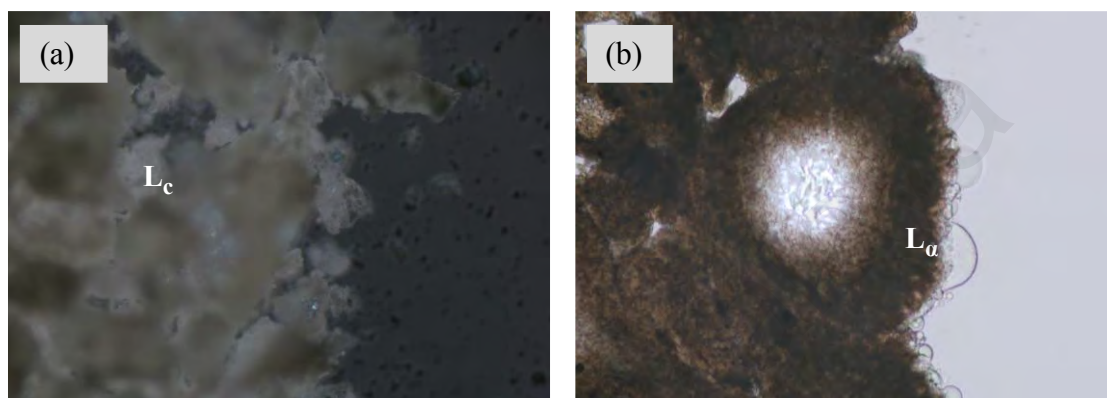


Figure 4.13: OPM textures of β -Mal-C₈C₄ for (a) thermotropic L_C phase; and (b) lyotropic texture by water gradient experiment giving myelin figures of L _{α} phase. 10 \times magnification at room temperature.

The third analogue, β -Mal-C₁₀C₆ which exhibits L_C phase (Figure 4.14a) in an anhydrous state turned to an isotropic liquid ~ 189 °C. On cooling, birefringent textures were observed down to room temperature, suggesting the L _{α} phase. The formation of the L _{α} phase in the samples and SAXS investigations in a later section confirm the existence of this phase. Similar L _{α} texture persisted in the presence of water as shown in Figure 4.14b.



Figure 4.14: OPM textures of β -Mal- $C_{10}C_6$ for (a) thermotropic L_C phase; and (b) contact penetration with water giving L_α birefringence textures. 10 \times magnification at room temperature.

The fourth member, β -Mal- $C_{12}C_8$ exhibits polymorphism upon heating the samples. Initially at the room temperature, β -Mal- $C_{12}C_8$ exhibits L_C (Figure 4.15a). The L_C phase was stable upon heating (Figure 4.15b) before the cubic phase started to appear slowly on further heating as shown in Figure 4.15c. Upon additional increase in temperature, β -Mal- $C_{12}C_8$ transforms to the hexagonal phase (Figure 4.15d) and eventually the sample became clear at $\sim 210^\circ\text{C}$. Contact preparation scan of β -Mal- $C_{12}C_8$ reveals a myelin structure, signifying the formation of the L_α phase as shown in Figure 4.15e. It is anticipated that both cubic and hexagonal phases belong to the inverse structure i.e. V_{II} and H_{II} phases respectively and not the normal type based upon the fact that this branched-chain maltoside has a large critical packing parameter, CPP (>1).

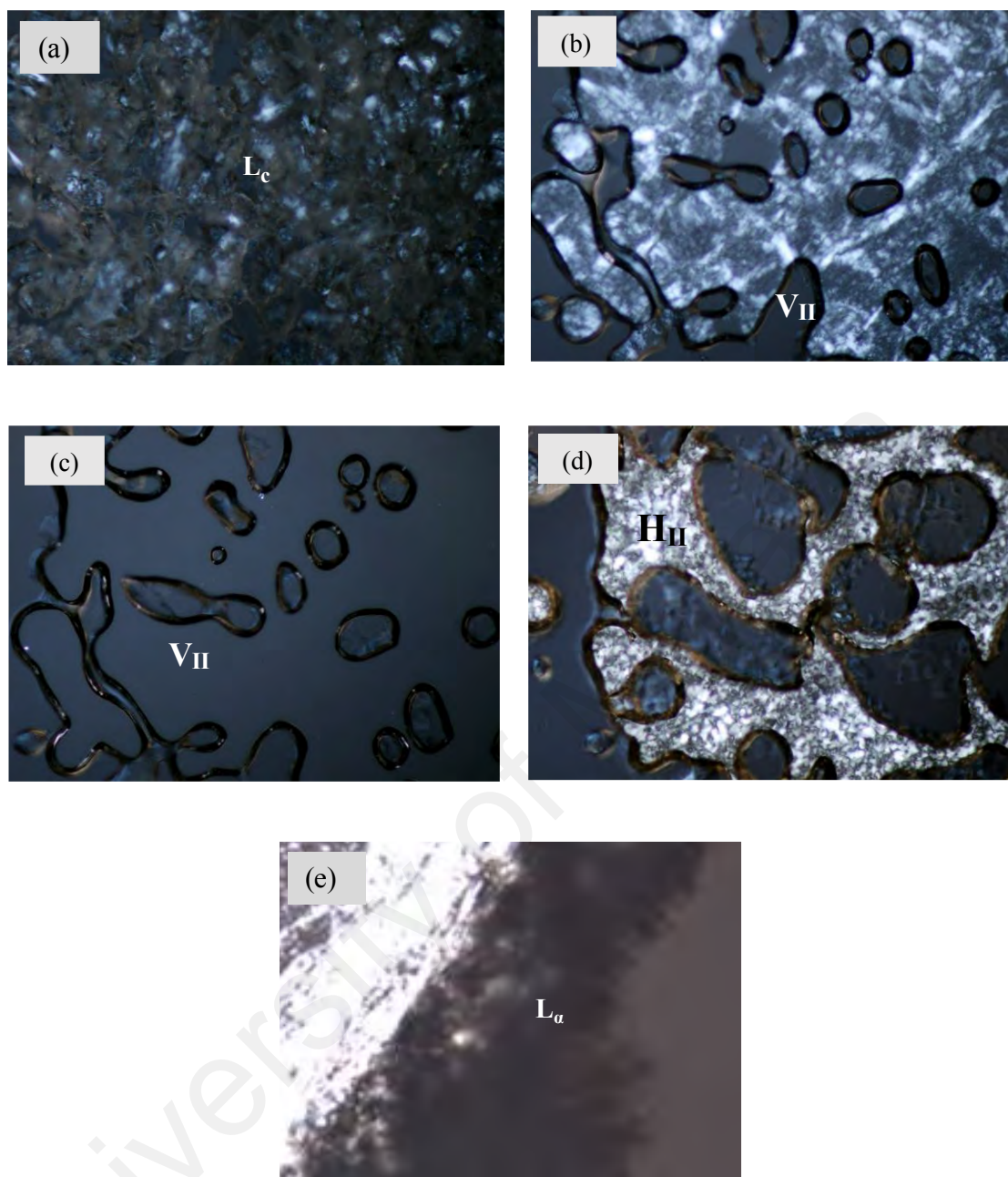


Figure 4.15: Polymorphism of anhydrous β -Mal-C₁₂C₈ observed upon heating under an optical polarising microscope shows (a) L_c phase at 85 °C; (b) isotropic V_{ll} phase slowly form at 123 °C; (c) V_{ll} phase at 162 °C; and (d) H_{ll} texture at 209 °C. (e) An L _{α} phase appears during water penetration experiment at 27 °C with 20 \times magnification.

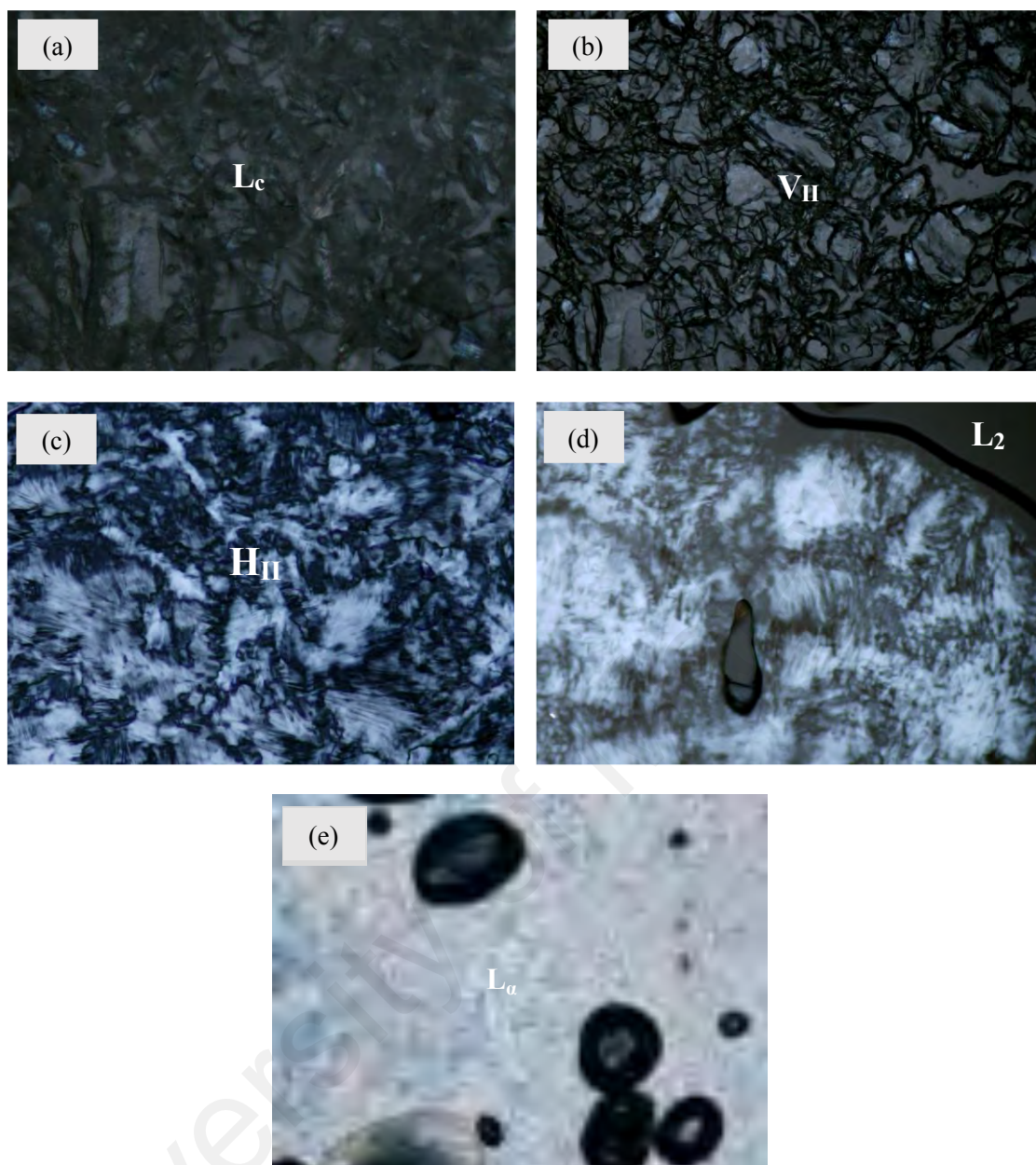


Figure 4.16: OPM textures of β -Mal-C₁₄C₁₀ for (a) thermotropic L_C phase at 25 °C; (b) V_{II} phase at 71 °C; (c) H_{II} phase at 128 °C; (d) L₂ phase at 217 °C; and (e) contact penetration with water giving L_a birefringence textures. 10× magnification at room temperature.

The longest-chain of β -Mal-C₁₄C₁₀ which was initially an L_C phase at room temperature (Figure 4.16a) also exhibits polymorphism L_a-V_{II}-H_{II} upon heating. The sample became clear approximately at a temperature of 225 °C. Figure 4.16b depicts the viscous isotropic V_{II} (cubic) phase OPM texture of β -Mal-C₁₄C₁₀ at 71 °C. Furthermore, the phase transition occurs at 128 °C from V_{II} phase to H_{II} (inverse hexagonal) phase as

shown in Figure 4.16c. On further heating at 216 °C, the dry β -Mal-C₁₄C₁₀ starts to develop L₂ phase which is an inverse micellar and changes completely to isotropic at 218 °C. Figure 4.16e shows that a higher birefringence texture is obtained at a higher water concentration which signifies the formation of the L _{α} phase in this compound. The thermotropic phase transition temperatures measured by OPM are summarised in Table 4.5.

Table 4.5: Thermotropic phase transition temperatures above 25 °C for the dry β -D-maltosides determined by optical polarising microscopy. Note: these transition temperatures are measured after initial heating and cooling during sample preparation.

Glycolipid Maltosides (Current Work)	Phase Transitions and Transition Temperatures
β -Mal-C ₆ C ₂	L _{α} -L ₂ : 137 °C
β - Mal-C ₈ C ₄	L _{α} -L ₂ : 188 °C
β - Mal-C ₁₀ C ₆	L _{α} -L ₂ : 189 °C
β - Mal-C ₁₂ C ₈	L _{α} -V _{II} : 123 °C; V _{II} -H _{II} : 163 °C; H _{II} -L ₂ : 207 °C
β - Mal-C ₁₄ C ₁₀	L _{α} -V _{II} : 71 °C; V _{II} -H _{II} : 128 °C; H _{II} -L ₂ : 216 °C
Glycolipid Maltosides^a	Phase Transitions and Transition Temperatures
β -Mal-C ₆ C ₂	L _{α} -L ₂ : 140 °C
β - Mal-C ₈ C ₄	L _{α} -L ₂ : 195 °C
β - Mal-C ₁₀ C ₆	L _{α} -L ₂ : 190 °C
β - Mal-C ₁₂ C ₈	L _{α} /H _{II} -L ₂ : 196 °C
β - Mal-C ₁₄ C ₁₀	L _{α} -V _{II} : 117 °C; V _{II} -H _{II} : 136 °C; H _{II} -L ₂ : 238 °C

^aData taken from (Saari *et al.*, 2018).

Table 4.5 also compares the phase transitions and transition temperatures of β -D-maltoside homologous series. These compounds possess hydrophilic head group with two

units glucose and hydrophobic tail of Guerbet branched-chain (C_6C_2 , C_8C_4 , $C_{10}C_6$, $C_{12}C_8$, and $C_{14}C_{10}$); thus, producing five series of the carbohydrate liquid crystal compounds. Moreover, the β -D-maltoside compounds, which are also known as amphiphile, have polar head group containing hydroxyl (energetic effect) and randomisation non-polar Guerbet branched-chain (entropic effect) parts. Generally, the head group effect is dominant when the branched-chain part is shorter. However, when the branched-chain is greater in length, both effects are equally dominant; consequently, the β -D-maltoside self-assembly is frustrated and compromised resulting in a thermotropic polymorphism (Saari *et al.*, 2018).

Current investigations show the β -D-maltosides exhibit thermotropic polymorphism such as L_α - V_{II} - H_{II} - L_2 phases. Similarly, the occurrence of these phase transitions also takes place in the previous study done by Saari *et al.* (2018). However, its transition temperature differs a few $^{\circ}\text{C}$ from the previous investigations (Saari *et al.*, 2018). For example, the clearing temperature difference of β -Mal- $C_{12}C_8$ between the current and previous works is 11°C . It might be due to the sample history and small traces amount of water were absorbed by the maltoside hydroxyl group (Boyd *et al.*, 2000). This phenomenon was also shown by 4-cyano-4'-pentylbiphenyl system (Noh *et al.*, 2016). In addition, it further proves the fact that anomeric purity influences the clearing temperature and its mesomorphic structures or behaviours (Vill *et al.*, 1989).

4.2.2 Differential Scanning Calorimetry

Figure 4.17 shows DSC thermograms for all five anhydrous β -D-maltosides at a heating scanning rate of $5^{\circ}\text{C min}^{-1}$. Their DSC phase transition temperature and their corresponding enthalpies are presented in Table 4.6. The phase transition temperatures of those compounds were obtained from the second heating endothermic peak transition

maxima so as to remove the thermal history. In addition, the enthalpy change (ΔH) linked with phase transition was determined via baseline and endothermic or transition peak integration. The complete DSC scans of the five compounds are available in the Appendix.

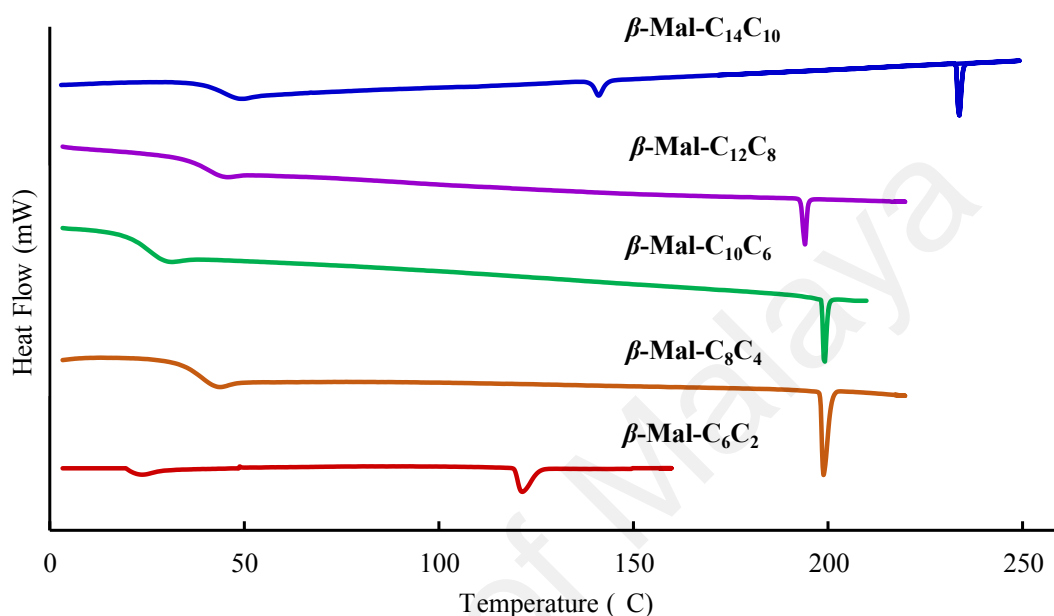


Figure 4.17: DSC thermograms for dry β -D-maltosides at a heating scanning rate of $5\text{ }^{\circ}\text{C min}^{-1}$.

The DSC scans illustrate the typical endothermic peak clearing transition into the isotropic phase. As shown in Figure 4.17, step-shaped peaks related to the glass transition (T_g) are observed instead of the melting transition peaks (T_m). The T_g of the dry maltoside series are in the range of 23 to 49 $^{\circ}\text{C}$. A glass, which does not have a long-range translational order, is an amorphous (Elliott, 1990). Moreover, it can be detected via DSC heating or cooling scans (Ogawa *et al.*, 2013). According to Sagnella and co-workers (2011), liquid crystal phase was obtained associated with the suppressed melting transition which may be due to the occurrence of the glass transition (Sagnella *et al.*, 2011).

It is noteworthy to mention that unlike DSC, in OPM, no morphological changes in textures were observed below and after the T_g . When the liquid crystalline phase

undergoes glass transition, the newly formed glassy crystal phase keeps almost the same structure as in the liquid crystal, which relaxes into a more ordered glassy phase rather slow. Because it takes a long time, no distinct phase changes occurred (see Figures 4.12–4.16); hence, the texture remains the same below and after T_g .

On heating, the dry β -Mal- C_6C_2 , β -Mal- C_8C_4 , β -Mal- $C_{10}C_6$, and β -Mal- $C_{12}C_8$ compounds show their transition temperatures from the liquid crystalline phase to an isotropic phase at 121 °C ($\Delta H = 0.9 \text{ kJ mol}^{-1}$), 199 °C ($\Delta H = 1.6 \text{ kJ mol}^{-1}$), 199 °C ($\Delta H = 0.7 \text{ kJ mol}^{-1}$) and 194 °C ($\Delta H = 0.8 \text{ kJ mol}^{-1}$), respectively. Furthermore, the dry β -Mal- $C_{14}C_{10}$ produces an extra small endothermic peak at 141 °C with ΔH value of 0.6 kJ mol^{-1} . Similarly, this result is in agreement with Saari *et al.* (2018) who observes a cubic to hexagonal phase transition taken place in her work (Saari, *et al.*, 2018). Upon further heating, β -Mal- $C_{14}C_{10}$ became isotropic at 234 °C with the ΔH value of 0.9 kJ mol^{-1} . In overall, the T_C obtained by DSC and with those from OPM are similar to within the error. However, in terms of polymorphism as observed in OPM of β -Mal- $C_{12}C_8$, we did not observe additional phase transition temperatures from liquid crystal to liquid crystal from its thermogram (see Figure 4.17). Possibly, the phase transitions too small to be detected by DSC.

Generally, T_C increases as the alkylated chain is elongated. This is expected due to the longer alkyl chain needs more energy in order to break the bonds in forming the isotropic phase. These maltosides (disaccharide) are expected to have higher T_C compared to those glucosides (monosaccharide) in Section 4.1 because the former has a higher number of hydrogen bonds.

Table 4.6 also provides the selected monoalkylated maltosides thermal behaviour data in comparison with Guerbet maltoside series. For instance, the monoalkylated maltoside series with lesser number of carbon alkyl chain ($n = 8$ and 12) exhibit the T_g .

However, the maltosides with a greater number of carbon alkyl chain ($n = 16$) adopts no T_g . Interestingly, the Guerbet maltosides which contain the same total number of carbon alkyl chain have smaller T_g compared to those of monoalkylated maltosides. This is attributed to the chain branching that reduces the T_g . The chain branching of Guerbet maltosides allows higher mobility of the sugar head part as compared to the alkylated chain. This result is very much in agreement with Achari *et al.* (2014).

Table 4.6: Phase transition temperatures for anhydrous Guerbet and monoalkylated β -D-maltoside determined by DSC.

Guerbet Maltosides (Current Work)	n	Molecular Formula	Transition Temperature (± 1 °C) [ΔH (± 0.1 kJ mol ⁻¹)]		
			T_g	T_{LC-LC}	T_C
β -Mal-C ₆ C ₂	8	C ₂₀ H ₃₈ O ₁₁	23	-	121 [0.9]
β -Mal-C ₈ C ₄	12	C ₂₄ H ₄₆ O ₁₁	43	-	199 [1.6]
β -Mal-C ₁₀ C ₆	16	C ₂₈ H ₅₄ O ₁₁	30	-	199 [0.7]
β -Mal-C ₁₂ C ₈	20	C ₃₂ H ₆₂ O ₁₁	44	-	194 [0.8]
β -Mal-C ₁₄ C ₁₀	24	C ₃₆ H ₇₀ O ₁₁	49	141 [0.6]	234 [0.9]

Monoalkylated Maltosides	n	Transition Temperature (°C)			Ref.
		T_g	T_m	T_C	
β -Mal-C _n	8	~60	89–103 ^a	125 ^a	Boyd <i>et al.</i> , 2000
		54	-	123	Kocherbitov & Söderman, 2004
	12	~60	102	245 ^a	Boyd <i>et al.</i> , 2000
		65	-	244	Ericsson <i>et al.</i> , 2005a
	16	-	105	- ^b	Ericsson <i>et al.</i> , 2005b

^aOPM data and ^bnot reported (original paper).

4.2.3 Small-angle X-ray Diffraction

Thermotropic Phases of the Dry Maltosides

The X-ray diffraction results of β -D-maltosides series were identified upon heating and cooling between temperatures ranging from 0–80–0 °C. The L_C phase is adopted for the dry β -D-maltosides compounds within the studied temperatures (see Figures 4.18–4.21 for example). The d -spacing values of the L_C phase for these dry β -D-maltoside are in a range from 29 to 34 Å. The occurrence of the same L_C phase over the temperature range is confirmed by the OPM results (see Figures 4.12a, 4.13a, 4.14a, 4.15a and 4.16a).

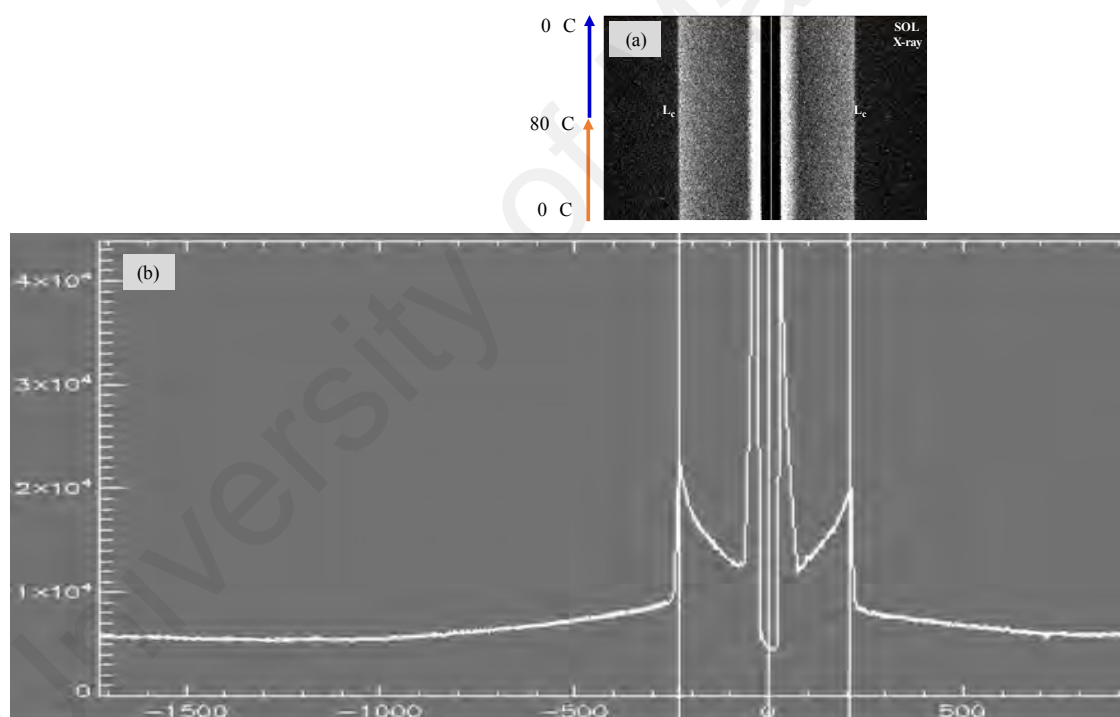


Figure 4.18: A representative L_C phase (a) Bragg's diffraction pattern image of dry β -Mal- C_8C_4 upon heating and cooling at temperatures ranging from 0–80–0 °C which corresponds to the (b) image integrated intensity plots.

It is well known that chain branching stabilises non-lamellar, curved phases (Nilsson *et al.*, 1998, Nilsson *et al.*, 1997). However, the chain length effect for these Guerbet branched-chains is insufficient to counter the strong influence of the bulky

maltose head groups, which support the formation of the lamellar layers (in this case, crystalline). This is due to the fact that the molecular balance between the hydrophobic chain moiety bound to the ether bond and the maltose head group gives a more rod-like packing with equivalent balance between these two parts i.e. $CPP = 1$. Hence, the formation of lamellar layers (L_C phase) is more favoured.

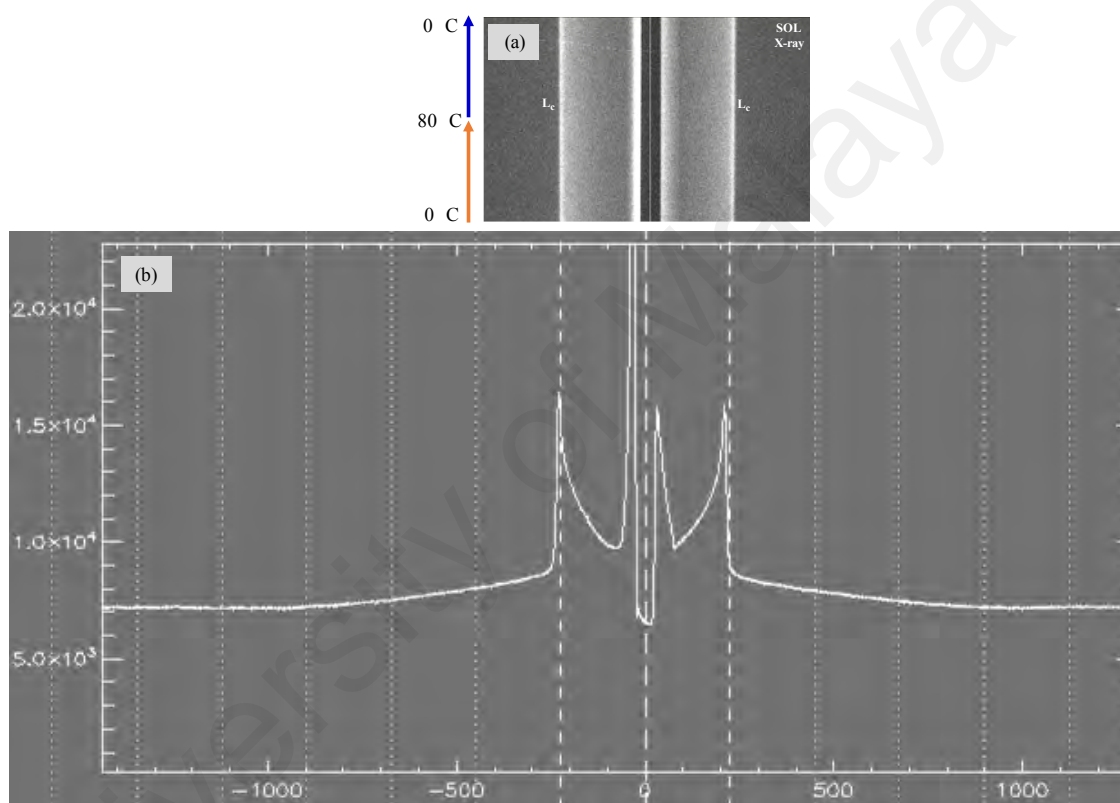


Figure 4.19: A representative L_C phase (a) Bragg's diffraction pattern image of dry β -Mal- $C_{10}C_6$ upon heating and cooling at temperatures ranging from 0–80–0 °C which corresponds to the (b) image integrated intensity plots.

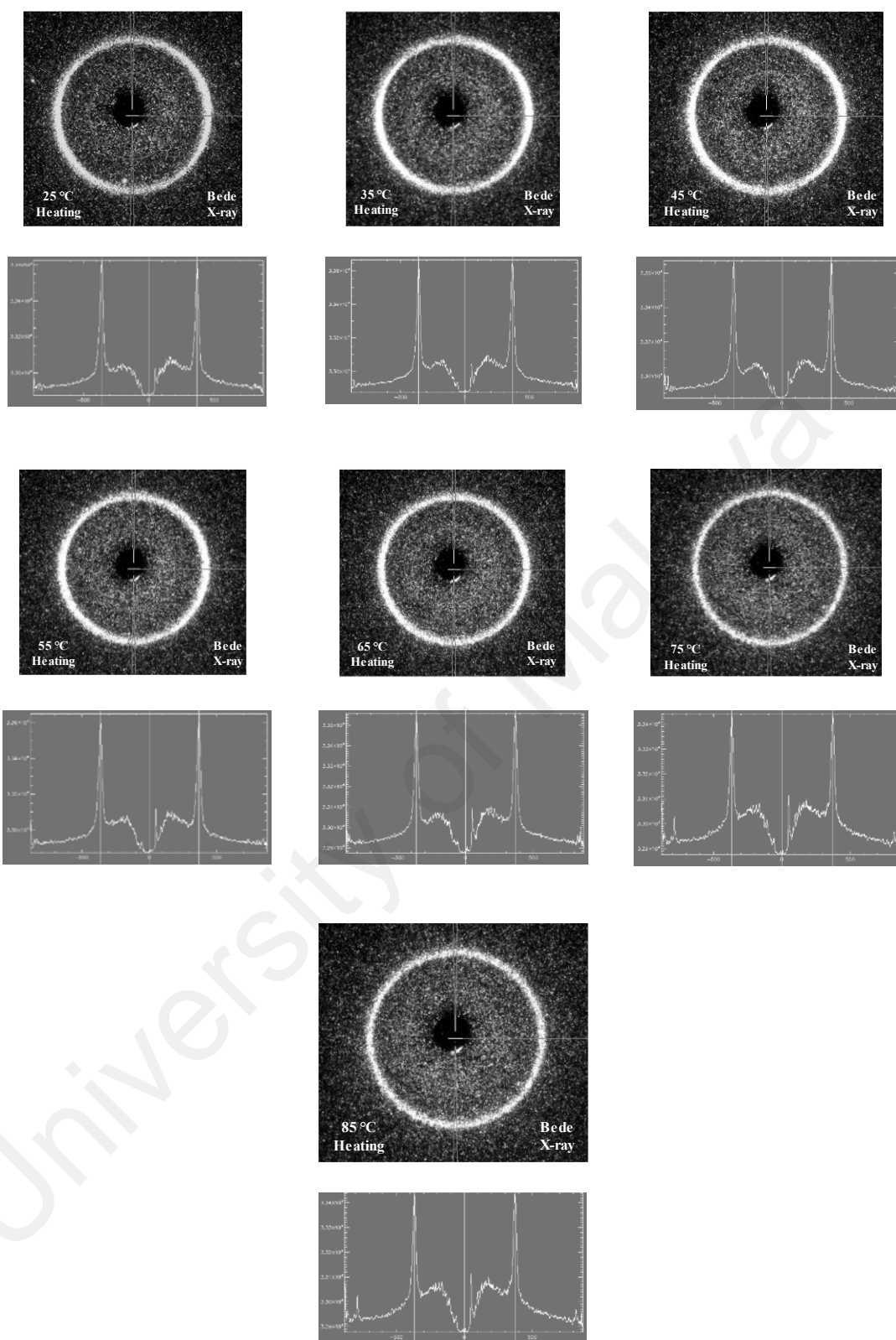


Figure 4.20: A representative LC phase Bragg's diffraction patterns image of dry β -Mal-C₁₂C₈ at different temperatures (top) which correspond to image integrated intensity plot (bottom).

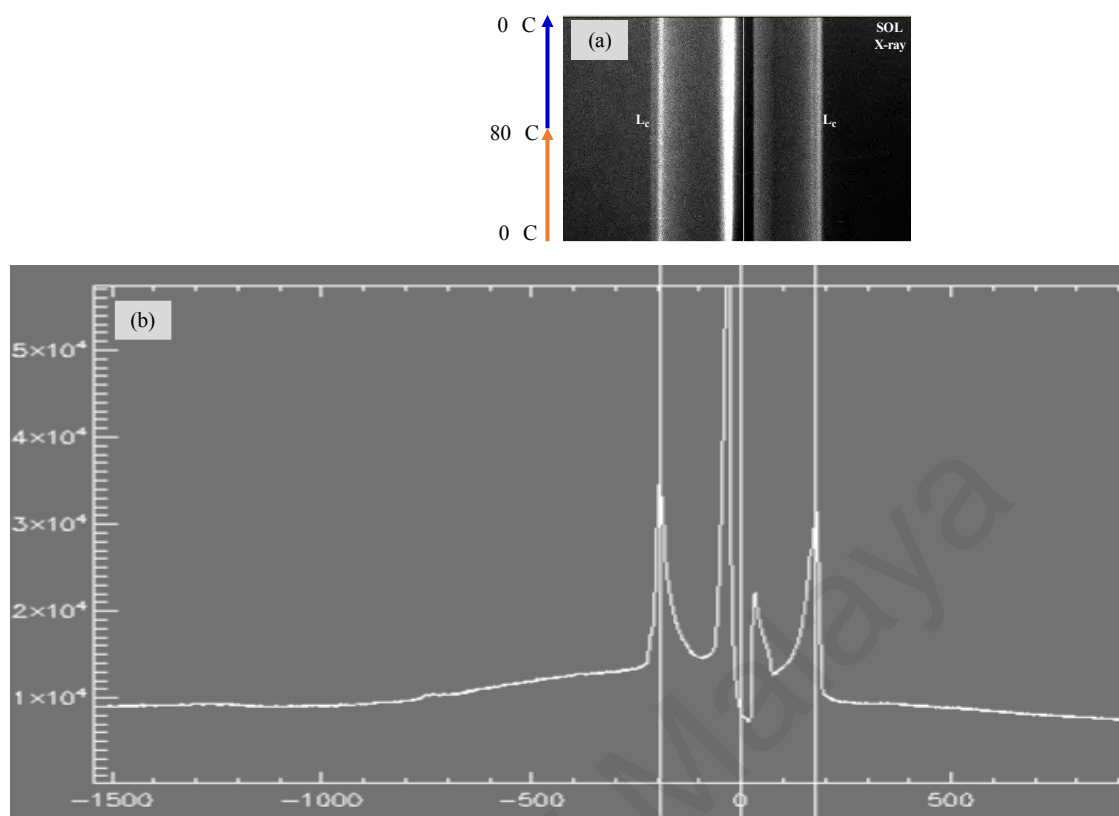


Figure 4.21: A representative L_c phase (a) Bragg's diffraction pattern image of dry β -Mal- $C_{14}C_{10}$ upon heating and cooling at temperatures ranging from 0–80–0 °C which corresponds to the (b) image integrated intensity plots.

Lyotropic Phases of the Maltosides in Excess Water

Selected X-ray diffraction results of β -D-maltosides series in excess water are provided in this sub-section. For shorter chain Guerbet maltosides e.g. β -Mal- C_8C_4 , only the parasitic scatter is observed as depicted in Figure 4.22. This scatter is a non-diffraction X-ray scattering which may well be due to the effect of air molecule and X-ray interaction or objects beam reflection in the beam path (Conn *et al.*, 2006). Another possible explanation for this is that, the sample is not on the beamstop. Figures 4.23-4.26 show the equally spaced peaks (ratio 1 and 2) of a fluid lamellar phase (L_α) observed for longer chain Guerbet maltosides i.e. β -Mal- $C_{10}C_6$, β -Mal- $C_{12}C_8$ and β -Mal- $C_{14}C_{10}$ compounds. The same phase remains in existence throughout the variation of temperatures which is confirmed by OPM (Figures 4.14b, 4.15e and 4.16e). It is worth mentioning that in

general, the L_α phase remains stable upon pressure variation as depicted in Figure 4.24. The d -spacings for the Guerbet maltoside self-assembly structures in dry and in excess water are listed in Table 4.7.

Table 4.7: Phase assignments and d -spacings for the dry and excess water β -D-maltosides at temperatures ranging from 0–80–0 °C.

Lipid	Dry		Excess Water	
	Phase	d -spacings (Å)	Phase	d -spacings (Å)
β -Mal-C ₆ C ₂	L _C	-	L ₁	-
β -Mal-C ₈ C ₄	L _C	31	L _{α}	Not detected
β -Mal-C ₁₀ C ₆	L _C	30	L _{α}	40
β -Mal-C ₁₂ C ₈	L _C	34	L _{α}	42
β -Mal-C ₁₄ C ₁₀	L _C	29	L _{α}	45

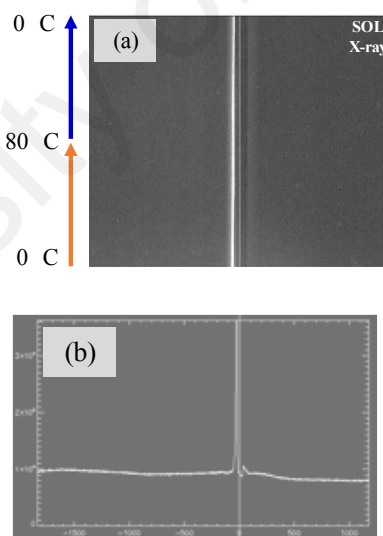


Figure 4.22: No appearance of (a) Bragg's diffraction peak for an excess water sample of β -Mal-C₈C₄ which corresponds to (b) a parasitic scatter.

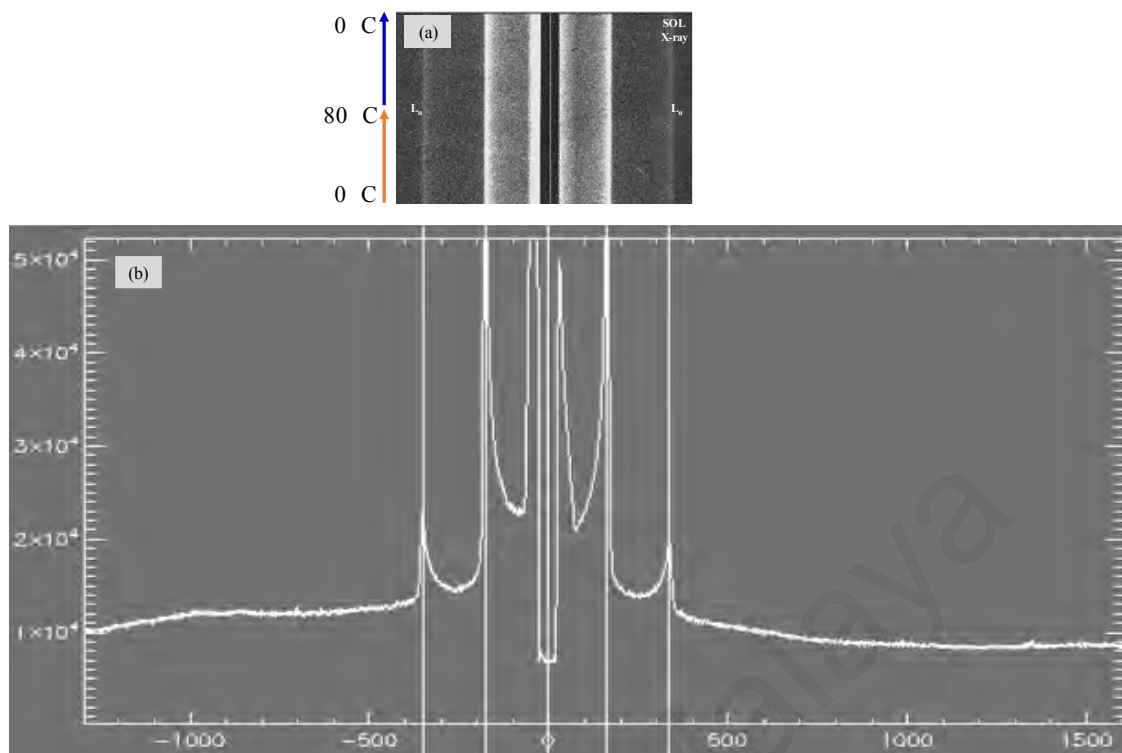


Figure 4.23: A representative L_α phase (a) Bragg's diffraction pattern image of β -Mal- $C_{10}C_6$ in excess water upon heating and cooling at temperatures ranging from 0–80–0 °C which corresponds to the (b) image integrated intensity plots.

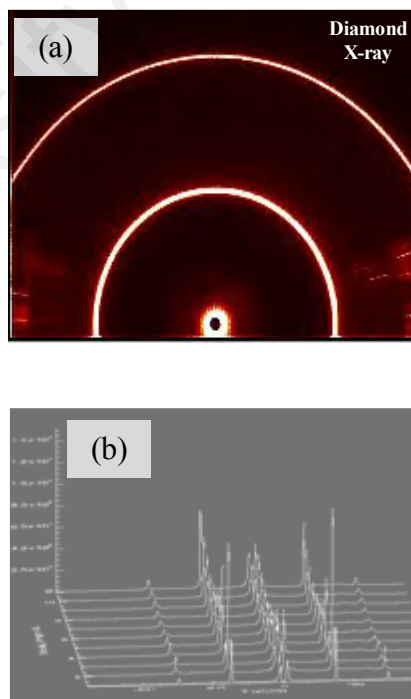


Figure 4.24: A representative L_α phase (a) Bragg's diffraction pattern synchrotron image of β -Mal- $C_{10}C_6$ in excess water sample with pressure which corresponds to the (b) stackplot image analysis.

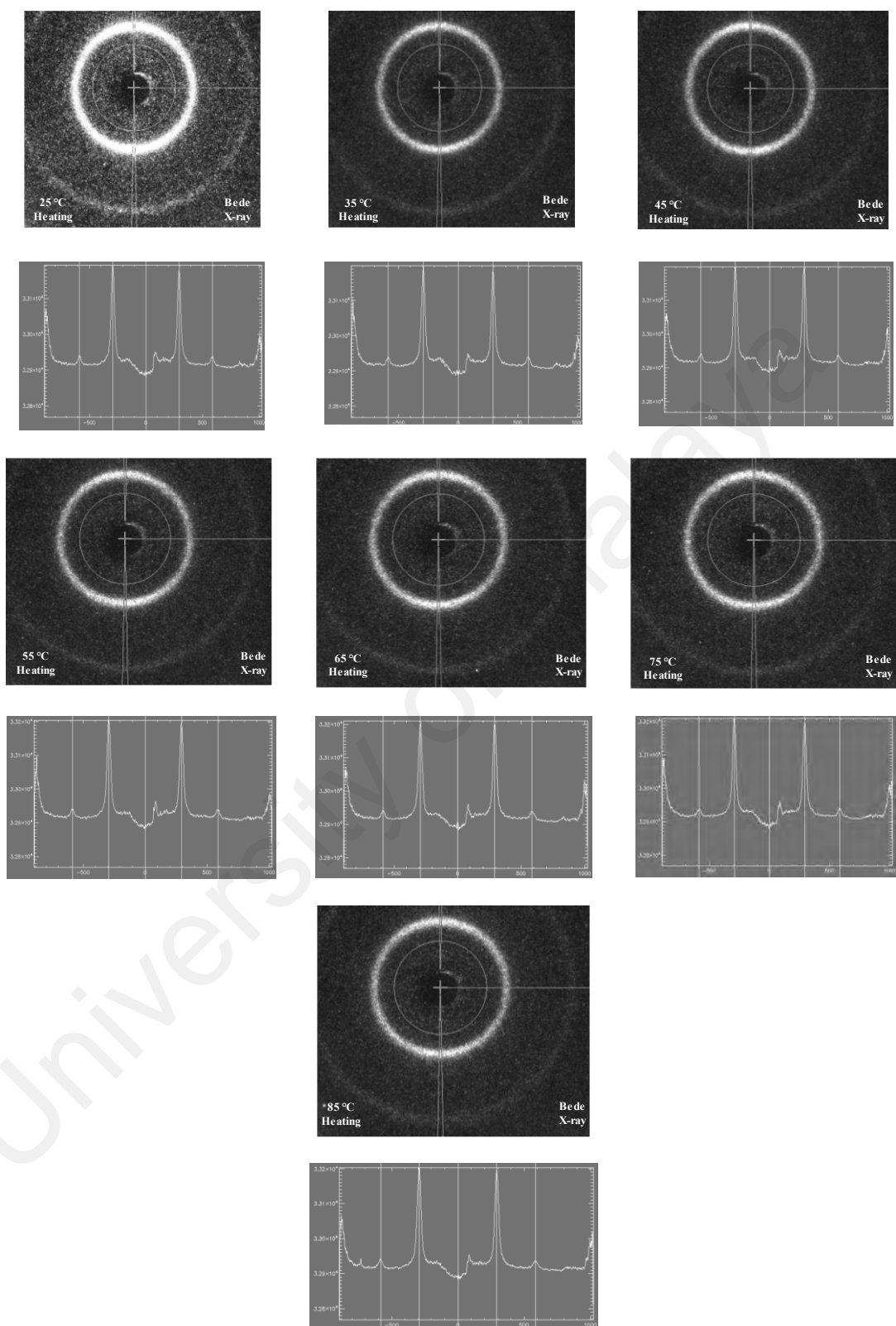


Figure 4.25: A representative L_α phase Bragg's diffraction patterns of β -Mal-C₁₂C₈ in excess water at different temperatures (top) which correspond to image integrated intensity plot (bottom).

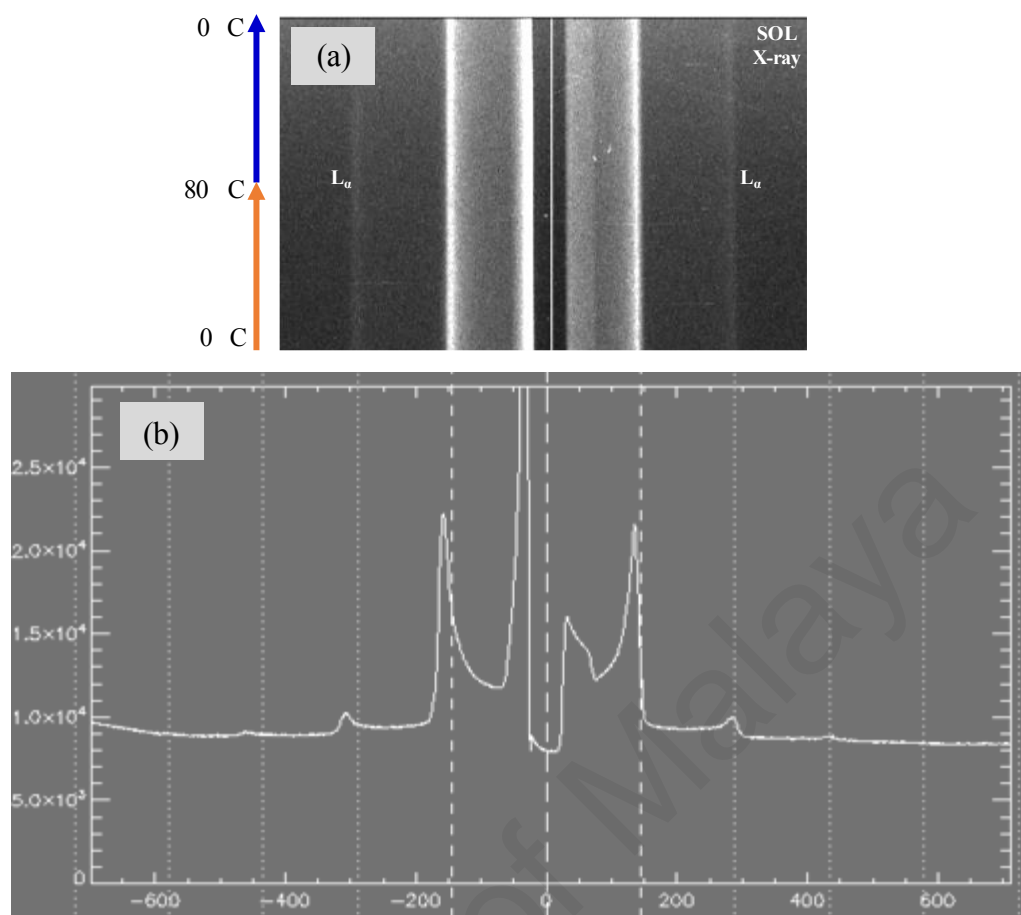


Figure 4.26: A representative L_α phase (a) Bragg's diffraction pattern image of β -Mal-C₁₄C₁₀ in excess water upon heating and cooling at temperatures ranging from 0–80–0 °C which corresponds to the (b) image integrated intensity plots.

4.2.4 Hydration of the Fluid Lamellar Phase

In addition to provide more understanding of membrane functions study, this part of the work focuses on fluid lamellar L_α phase in the presence of excess water (lyotropic) exhibited by the longer chain Guerbet maltosides i.e. β -Mal-C₁₀C₆, β -Mal-C₁₂C₈ and β -Mal-C₁₄C₁₀. This study also presented the d -spacing value at different temperatures (0–80 °C) for these three maltosides in excess water conditions. The dry condition data is also included for comparison. The area per molecule and water content were then estimated for compounds under studied.

In the calculation of the estimated area per molecule and weight percent of water of the fully hydrated maltoside bilayers, the X-ray d -spacings of the dry and excess water

conditions are plotted as functions of temperatures upon heating and cooling between 0 and 80 °C in order to determine the water layer thickness (Δd) for each maltosides as shown in Figures 4.27 to 4.29.

The area per molecule (Seddon *et al.*, 1997) and volume fraction of water of L_α phase from the measured d -spacings in dry and excess water conditions, and density of the maltosides (Nguan *et al.*, 2010) can be estimated by using Equation 4.1 as follows:

$$\frac{v_w}{v_{total}} = \frac{d_w}{d_o} = \frac{\Delta d}{d_{excess}} \quad \text{(Equation 4.1)}$$

where v_w and v_{total} partial specific volumes of water and total (lipid + water), d_w and Δd are the water layer thickness ($d_{excess} - d_o$), and d_o and d_{excess} are d -spacings in dry and excess water conditions. The volume percent of water is approximately the same as weight percent of water if the density of the maltosides is equal to the density of water.

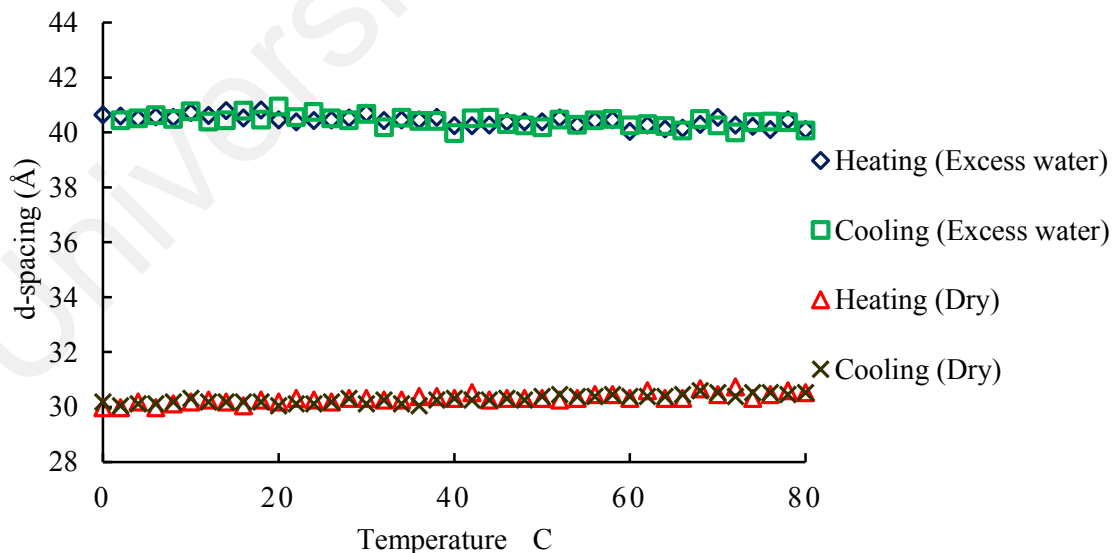


Figure 4.27: A graph of d -spacing versus temperature of β -Mal- $C_{10}C_6$ in dry and excess water conditions upon heating and cooling processes.

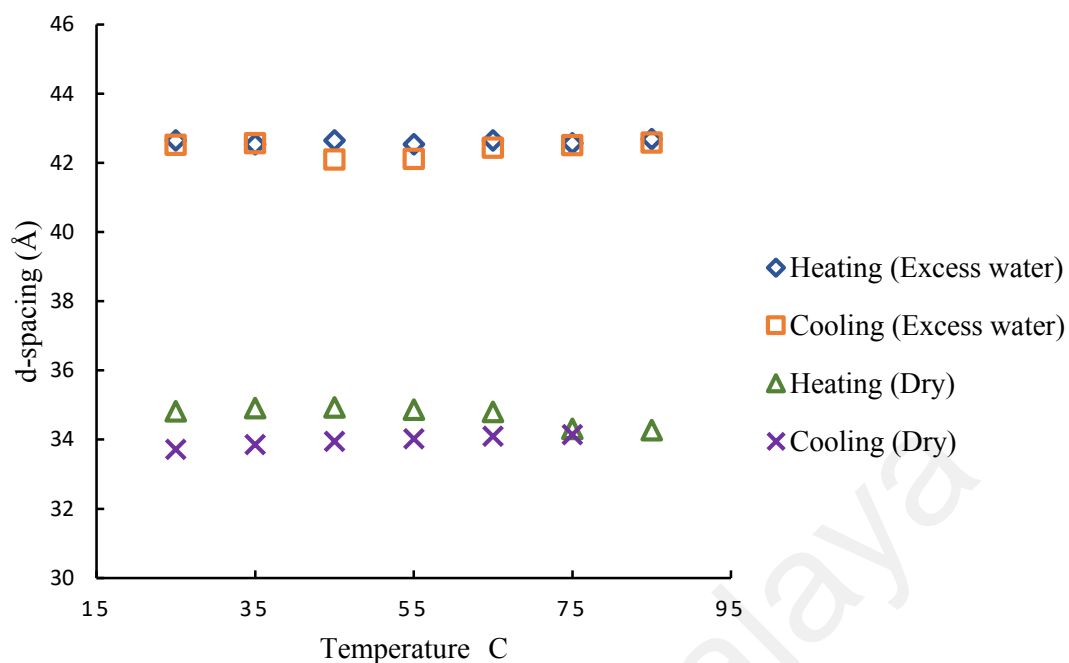


Figure 4.28: A graph of *d*-spacing versus temperature of β -Mal- $C_{12}C_8$ in dry and excess water conditions upon heating and cooling processes.

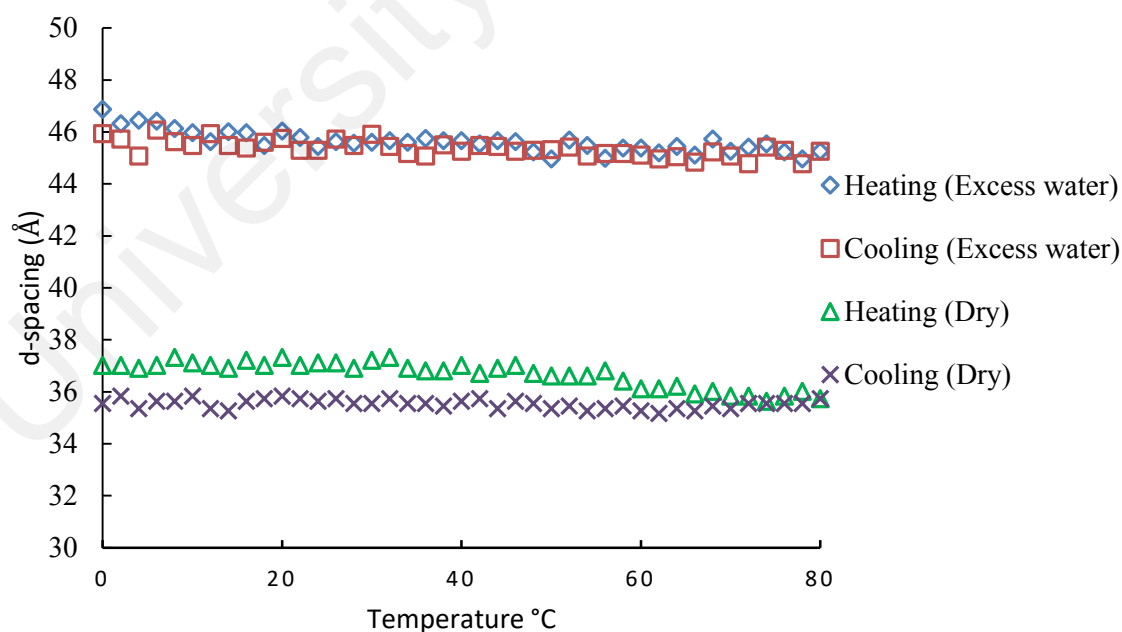


Figure 4.29: A graph of *d*-spacing versus temperature of β -Mal- $C_{14}C_{10}$ in dry and excess water conditions upon heating and cooling processes.

In excess water, for all maltosides, upon heating and cooling between 0 and 80 °C the only stable state formed is an L_α phase as demonstrated in Table 4.8. This can be explained by the increased chain length region surface area which lowers the sugar domain packing stress (Nguan *et al.*, 2010). Even though the type of phase occurred is the same for all maltosides, the concomitant increases in area per molecule are observed from 56.5 to 59.7 Å². These are considerably lower than the obtainable value 72.2 Å² of fully hydrated 1,2dioleoyl-*sn*-glycero-3-phosphatidylcholine (DOPC). Indeed, the larger molecular weight of DOPC (786) indicates the greater molecular volume (1303 Å³) (Tristram-Nagle *et al.*, 1998) and thus, requires greater an area per molecule. This result is consistent with those β -Mal-C₁₀C₆ (M: 567 g mol⁻¹), β -Mal-C₁₂C₈ (M: 623 g mol⁻¹) and β -Mal-C₁₄C₁₀ (M: 679 g mol⁻¹) which exhibit an increment in the area of the molecule when the chain length of the hydrocarbons and the molecular volumes are increased (Nguan *et al.*, 2010).

Table 4.8: The structural parameters of the fluid lamellar L_α phase of Guerbet maltosides at full hydrations varying at temperatures 0–80 °C except for β -Mal-C₁₂C₈ (25–85 °C) (heating and cooling). X-ray data were taken from SOL (β -Mal-C₁₀C₆, β -Mal-C₁₄C₁₀) and Bede (β -Mal-C₁₂C₈).

Lipid	Phase	Chain Length	Water Layer Thickness (Δd)[Å] (± 0.2)	Area per Molecule [Å ²] (± 1.7)	Weight % of Water (± 3)
β -Mal-C ₁₀ C ₆	L_α	C ₁₆	10	56.5	25
β -Mal-C ₁₂ C ₈	L_α	C ₂₀	8	56.9	19
β -Mal-C ₁₄ C ₁₀	L_α	C ₂₄	9	59.7	20

One important factor that affects water spacing is the fluctuation pressures of the interbilayer interactions exist in the fully hydrated L_α phase (Tristram-Nagle *et al.*, 1998). Moreover, McIntosh and Simon (1993) found that the flexible L_α lipid with bigger

fluctuation pressure resulted in a larger water spacing in comparison with rigid gel or sub gel lipid. As shown in Table 4.8, the water layer thickness L_α phase of β -Mal-C₁₀C₆, β -Mal-C₁₂C₈ and β -Mal-C₁₄C₁₀ are 10, 8 and 9 Å, respectively. This small decrement and increment in Δd arises probably due to the higher interbilayer fluctuation pressures as mentioned earlier and a change in free energy leads to the layer to bend (Seddon & Templer, 1993).

The weight percent of 25 wt% of water for β -Mal-C₁₀C₆, 19 wt% of water for β -Mal-C₁₂C₈ and 20 wt% of water for β -Mal-C₁₄C₁₀ indicate the solvation of all maltosides. It is interesting to note that, the β -Mal-C₁₂C₈ and β -Mal-C₁₄C₁₀ show a reduction in weight percent of water as the chain length increases as compared to the β -Mal-C₁₀C₆. This suggests that the interaction factors needed to be considered are the freely water entering the fluid space between bilayers, the intercalated water into the head groups bilayers (McIntosh & Simon, 1986); and the interbilayer interactions namely; van der Waals interaction (Costigan *et al.*, 2000), fluctuation pressure (Tristram-Nagle *et al.*, 1998), hydration force (McIntosh, 1996) and the steric thickness (Kučerka *et al.*, 2005).

4.2.5 Final Remarks

Knowledge of the fundamental parameters, for instance, the surface area per molecule and amount of water per lipid molecule (Hamid *et al.*, 2014) are essential to bio membrane of lipids. Hence, in this work, the thermotropic and lyotropic phase behaviours of lamellar layer/phase have been investigated. In dry condition at all temperatures, all maltosides exhibit lamellar layer of L_C phase. On the contrary, in excess water the maltosides produce a fluid lamellar L_α phase. Values of area per molecule and water content for the fully hydrated L_α phase are 56.5 Å² at 25 wt% for β -Mal-C₁₀C₆; 56.9 Å² at 19 wt% for β -Mal-C₁₂C₈ and 59.7 Å² at 20 wt% for β -Mal-C₁₄C₁₀.

4.3 Structural Parameters of Branched-chain β -Glc-C₁₂C₈ and β -Mal-C₁₂C₈ at Fixed Hydration of Water Conditions

Maintaining a cell membrane fluidity is subjected to the important role of water in biological processes or function (Goodby, 1998). This is due to the fact that the cell membrane lipid physical state is related to its fluidity. Hence, this membrane lipid fluidity gives a perfect balance between the membrane ordered structure's rigidity and complete fluidity. Furthermore, fluidity also permits the molecular interactions within membrane and takes part in the membrane assembly.

The cell membrane is described as the fluid mosaic model that consists of different types of molecules (Koynova & Tenchov, 2013). For instance, such molecules are phospholipids and glycolipids (Jewell, 2011). These molecules are amphitropic and able to self-organise to lyotropic structures of mesophases. One of the structures is a fluid lamellar phase. It is well known that the biological cell membrane is mainly made up of bilayers (lamellar phase). Floating icebergs on the ocean is an analogy of these bilayers which are constantly on the move in order to regulate the function of the cell membrane.

Thermodynamic parameters, for example, water content and temperatures remain the subject of interest in order to understand the highly swollen fluid lamellar phase lipid bilayers that can act as a thin elastic sheet (Kučerka *et al.*, 2011; Kobayashi & Fukada, 1998; Rand, 1992). Detailed study of the hydration of cell membrane and structured parameters; for instance, water layer and lipid bilayer thickness, as well as surface area per molecule are of importance in order to further understand functionally its structure and the cell membrane (Perera *et al.*, 1996). A study on the bilayer parameters; for instance, area per lipid molecule and bilayer thickness, plays a key role in order to gain insight of bio-membrane asymmetric lipid distribution. This is due to the unequal lipid surface area in both bilayer leaflets which is linked to the number of lipid molecules

(Marquardt *et al.*, 2015). Moreover, according to (Liu & Conboy, 2005) and (John *et al.*, 2002), there is a flip/flop rate dependency on bilayer thickness. For example, the flip/flop rate is reduced with longer acyl chains of phospholipids. Furthermore, in 2011, a research was done by Kučerka and co-workers on the simultaneous analysis of small-angle neutron and X-ray scattering data with regard to the effect of temperature on the phosphatidylcholine fluid phases of lipid areas and bilayer thicknesses. Similarly, asymmetric lipid vesicles data were obtained using the same techniques in order to produce low and high-resolution models. Both models give details of inner and outer bilayer leaflets scattering electron density profile that correspond to the structural parameters such as hydrocarbon thickness and individual area per lipid molecules (Eicher *et al.*, 2017). There are two lipid bilayer structural parameters namely, the number of water molecules per lipid and its distribution relative to the lipid molecule. In order to construct the phase diagram of lipid-water system (Seddon *et al.*, 1984; McIntosh & Simon, 1986; Zahid *et al.*, 2013) as well as comprehend the attractive and repulsive intermolecular forces between membranes (Rau & Parsegian, 1992; Kanduc & Netz, 2015), it is necessary to know the number of water molecules per lipid. Water distribution relative to the lipid molecule corresponds to the bioenergetic processes *via* water-proton interaction at water and membrane interfaces (Nguyen *et al.*, 2018). In addition, Kučerka *et al.* (2019) reviewed the functions and structures of bio-membrane affected by water including biomimetic membranes, interaction of membrane-ion, bio-membrane linked with cholesterol and anaesthetic effects.

Thus, the structural parameters of biosurfactant β -Glc-C₁₂C₈ and β -Mal-C₁₂C₈ over the selected temperatures were investigated in order to calculate the water layer thickness, bilayer thickness and area per molecule. The values of such parameters were determined upon varying the water contents via small-angle X-ray diffraction.

4.3.1 Structural Parameters Determination

The structural parameters of fluid lamellar (L_α) phase and inverse hexagonal (H_{II}) were calculated at 25, 40, 60, and 80 °C (Luzzati, 1968). These parameters are described as illustrated in the schematic drawing of L_α and H_{II} as shown in Figure 4.30.

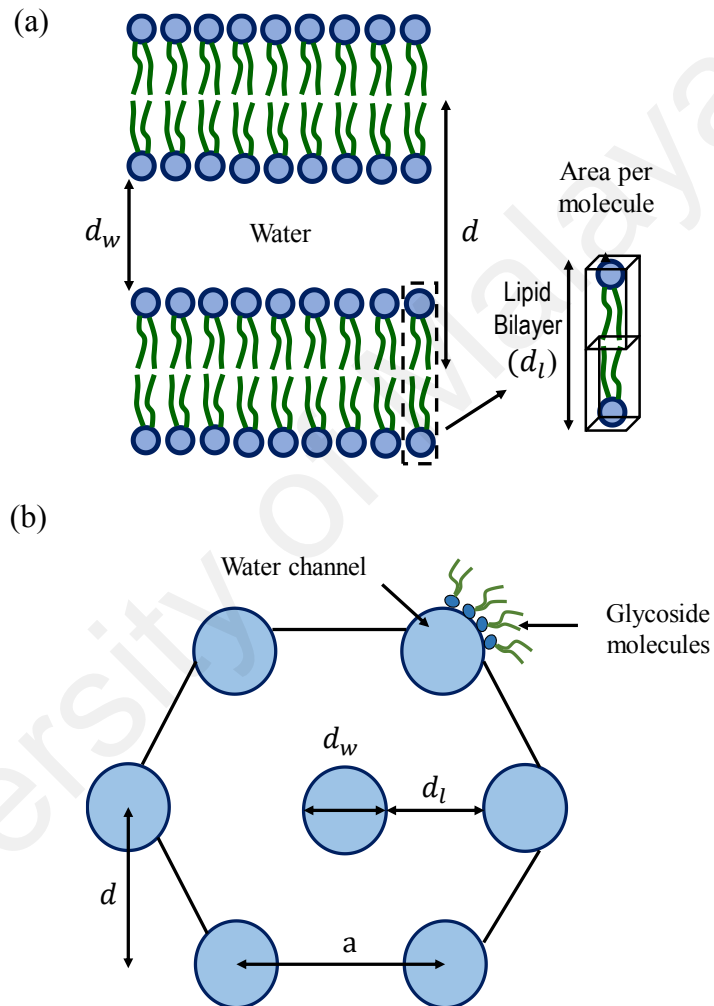


Figure 4.30: (a) The bilayer lamellar; and (b) the thickness of water layer of hexagonal phase dimension schematic diagram. Redrawn from (Costigan *et al.*, 2000).

Densities of glycoside and water, glycoside concentration, and d -spacings (d) of the L_α and H_{II} phase are needed for the calculation of those structural parameters. Volume fraction of the maltoside Φ_l is calculated using Equation 4.2 as follows:

$$\Phi_l = \left[1 + \left(\frac{V_w}{V_l} \right) \left(\frac{1 - C_l}{C_l} \right) \right]^{-1} \quad (\text{Equation 4.2})$$

where (C_l) is the total glycoside weight concentration [glycoside / (glycoside + water)] and V_w and V_l are the partial specific volumes of water and glycoside, respectively. The maltoside of L_α phase and the lipid layer thickness (d_l) is calculated using Equation 4.3:

$$d_l = d\Phi_l \quad (\text{Equation 4.3})$$

where d_l is the bilayer thickness, d is the d -spacing and the water layer thickness is $d_w = d - d_l$. The cross-sectional area per maltoside (S) is given by Equation 4.4 as follows:

$$S = \frac{2M_r V_l}{N_A d_l} \quad (\text{Equation 4.4})$$

where M_r is the maltoside molecular mass and N_A is Avogadro's number. For the H_{II} phase, the diameter of the water cylinders (d_w) is given in Equation 4.5:

$$d_w = \left[\left(\frac{2\sqrt{3}}{\pi} \right) (1 - \Phi) a^2 \right]^{\frac{1}{2}} \quad (\text{Equation 4.5})$$

where a is the lattice spacing of the H_{II} phase ($a = (2/\sqrt{3})d$). The glycoside layer thickness (along the line connecting the cylinder axes) is given by Equation 4.6:

$$d_l = a - d_w \quad (\text{Equation 4.6})$$

The area per molecule at the glycoside/water interface is given by Equation 4.7:

$$S = 2\pi d_w M_r \bar{v}_l / (\sqrt{3} a^2 \Phi N_A) \quad (\text{Equation 4.7})$$

4.3.2 Small-Angle X-ray Diffraction

X-ray diffraction data of β -Glc-C₁₂C₈ and β -Mal-C₁₂C₈ at varied water contents and temperatures were collected and analysed. At all water contents and temperatures, only the first order of L _{α} phase reflection was observed for β -Mal-C₁₂C₈. This might be due to the liquid crystalline thermal disorder (Seddon & Templer, 1995). The appearance of L _{α} phase was previously confirmed using the contact penetration method under the optical polarising microscope (Hamid *et al.*, 2014). Figure 4.31 illustrates the images of X-ray diffraction patterns (L _{α} phase) of β -Mal-C₁₂C₈ at different temperatures containing 10 water molecules per maltoside. The d -spacing obtained is the only difference among the samples at all hydrations and temperatures.

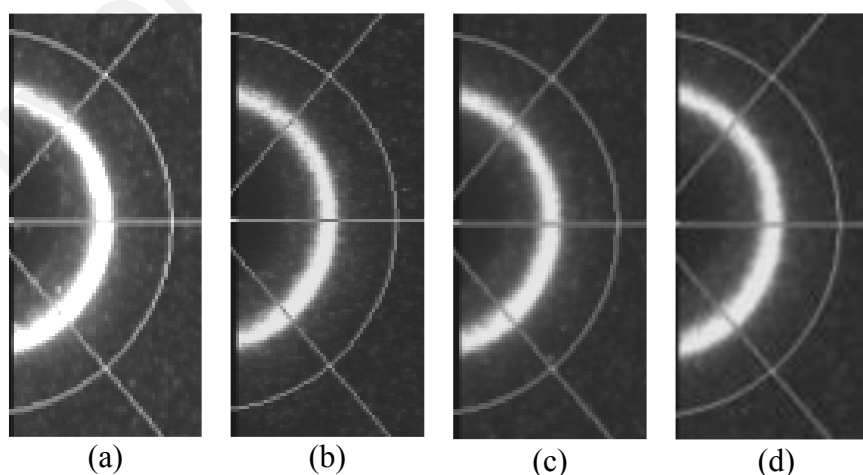


Figure 4.31: X-ray diffraction patterns (L _{α} phase) of 10 water molecules of β -Mal-C₁₂C₈ at (a) 25 °C; (b) 40 °C; (c) 60 °C; and (d) 80 °C.

At all water contents and temperatures, only the first and second order of hexagonal reflection were observed for β -Glc- $C_{12}C_8$. Figure 4.32 depicts the images of X-ray diffraction patterns of samples at different temperatures containing 10 water molecules per glucosides. The structural parameters of the L_α and H_{II} phases at fixed hydration were calculated at 25, 40, 60 and 80 °C. These parameters are provided as shown in Tables 4.9 (maltoside) and 4.10 (glucoside). Figures 4.33–4.35 show the water layer thickness, bilayer thickness and area per molecule dependency with volume fraction of water of the fluid L_α phase (β -Mal- $C_{12}C_8$). In contrast, Figures 4.36–4.38 show the water layer thickness, bilayer thickness and area per molecule dependency with volume fraction of water of the H_{II} phase (β -Glc- $C_{12}C_8$).

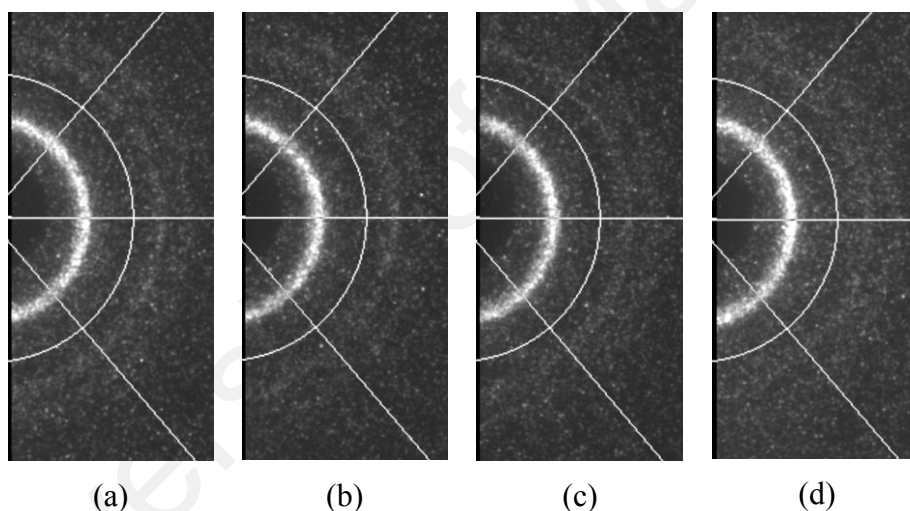


Figure 4.32: X-ray diffraction patterns (H_{II} phase) of 10 water molecules of β -Glc- $C_{12}C_8$ at (a) 25 °C; (b) 40 °C; (c) 60 °C; and (d) 80 °C.

Table 4.9: Structural parameters of β -Mal-C₁₂C₈ at different temperatures. d is the d -spacing, ϕ_w is the volume fraction of water, d_w water layer thickness, d_l monolayer thickness, S area per molecule at the maltoside/water interface.

25 °C							
Water Molecules per Maltoside	wt% H₂O	Phase	d (Å)	ϕ_w	d_w (Å)	d_l (Å)	S (Å²)
2	6	L _{α}	34.00	0.05	1.65	32.35	59.79
4	10	L _{α}	36.20	0.11	4.09	32.11	60.24
6	15	L _{α}	37.80	0.15	5.86	31.94	60.56
8	19	L _{α}	38.70	0.19	7.48	31.22	61.95
10	22	L _{α}	39.00	0.24	9.20	29.60	65.35
12	26	L _{α}	43.00	0.27	11.62	31.68	61.06
14	29	L _{α}	43.00	0.3	12.83	29.97	64.54
40 °C							
Water Molecules per Maltoside	wt% H₂O	Phase	d (Å)	ϕ_w	d_w (Å)	d_l (Å)	S (Å²)
2	6	L _{α}	34.90	0.05	1.69	33.21	58.25
4	10	L _{α}	36.60	0.11	4.13	32.46	59.58
6	15	L _{α}	39.00	0.15	6.04	32.96	58.70
8	19	L _{α}	40.30	0.19	7.79	32.51	59.49
10	22	L _{α}	38.90	0.24	9.20	29.60	65.35
12	26	L _{α}	43.00	0.27	11.54	31.46	61.49
14	29	L _{α}	42.20	0.30	12.65	29.55	65.46
60 °C							
Water Molecules per Maltoside	wt% H₂O	Phase	d (Å)	ϕ_w	d_w (Å)	d_l (Å)	S (Å²)
2	6	L _{α}	35.20	0.05	1.71	33.49	57.75
4	10	L _{α}	36.50	0.11	4.12	32.38	59.75
6	15	L _{α}	38.60	0.15	5.98	32.62	59.31
8	19	L _{α}	39.50	0.19	7.63	31.87	60.70
10	22	L _{α}	38.60	0.24	9.15	29.45	65.69
12	26	L _{α}	42.80	0.27	11.49	31.31	61.78
14	29	L _{α}	41.50	0.30	12.44	29.06	66.56
80 °C							
Water Molecules per Maltoside	wt% H₂O	Phase	d (Å)	ϕ_w	d_w (Å)	d_l (Å)	S (Å²)
2	6	L _{α}	35.50	0.05	1.72	33.78	57.27
4	10	L _{α}	36.20	0.11	4.09	32.11	60.24
6	15	L _{α}	37.30	0.15	5.78	31.52	61.37
8	19	L _{α}	38.40	0.19	7.42	30.98	62.44
10	22	L _{α}	38.10	0.24	9.03	29.07	66.55
12	26	L _{α}	41.10	0.27	11.03	30.07	64.33
14	29	L _{α}	40.00	0.30	11.99	28.01	69.06

Table 4.10: Structural parameters of β -Glc-C₁₂C₈ at different temperatures. d is the d -spacing, ϕ_w is the volume fraction of water, d_w water layer thickness, d_l monolayer thickness, S area per molecule at the glucoside/water interface.

25 °C							
Water Molecules per Glucoside	wt% H₂O	Phase	d (Å)	ϕ_w	d_w (Å)	d_l (Å)	S (Å²)
2	7	H _{II}	36.30	0.09	38.60	87.20	7.56
4	14	H _{II}	33.30	0.16	48.00	67.30	12.10
6	19	H _{II}	35.80	0.22	60.90	63.10	14.40
8	24	H _{II}	37.00	0.25	66.80	61.40	15.30
10	28	H _{II}	36.00	0.27	68.20	56.40	17.10
12	32	H _{II}	35.50	0.31	72.30	50.60	19.80
14	35	H _{II}	36.20	0.34	76.70	48.70	20.90
40 °C							
Water Molecules per Glucoside	wt% H₂O	Phase	d (Å)	ϕ_w	d_w (Å)	d_l (Å)	S (Å²)
2	7	H _{II}	45.60	0.09	48.50	109.50	6.020
4	14	H _{II}	33.20	0.16	47.90	67.10	12.20
6	19	H _{II}	35.60	0.22	60.60	62.80	14.40
8	24	H _{II}	37.00	0.25	66.80	61.40	15.30
10	28	H _{II}	35.90	0.27	68.10	56.30	17.10
12	32	H _{II}	35.50	0.31	72.30	50.60	19.80
14	35	H _{II}	36.20	0.34	76.70	48.70	20.90
60 °C							
Water Molecules per Glucoside	wt% H₂O	Phase	d (Å)	ϕ_w	d_w (Å)	d_l (Å)	S (Å²)
2	7	H _{II}	26.50	0.09	28.20	63.60	10.40
4	14	H _{II}	32.20	0.16	46.50	65.10	12.60
6	19	H _{II}	35.10	0.22	59.70	61.90	14.70
8	24	H _{II}	36.90	0.25	66.60	61.20	15.30
10	28	H _{II}	34.00	0.27	64.50	53.30	18.10
12	32	H _{II}	35.10	0.31	71.50	50.10	20.00
14	35	H _{II}	35.50	0.34	75.20	47.80	21.30
80 °C							
Water Molecules per Glucoside	wt% H₂O	Phase	d (Å)	ϕ_w	d_w (Å)	d_l (Å)	S (Å²)
2	7	H _{II}	26.20	0.09	27.80	62.90	10.50
4	14	H _{II}	30.20	0.16	43.60	61.00	13.40
6	19	H _{II}	33.60	0.22	57.20	59.20	15.30
8	24	H _{II}	34.50	0.25	62.30	57.20	16.40
10	28	H _{II}	35.30	0.27	66.90	55.30	17.40
12	32	H _{II}	34.40	0.31	70.10	49.10	20.40
14	35	H _{II}	34.50	0.34	73.10	46.40	22.00

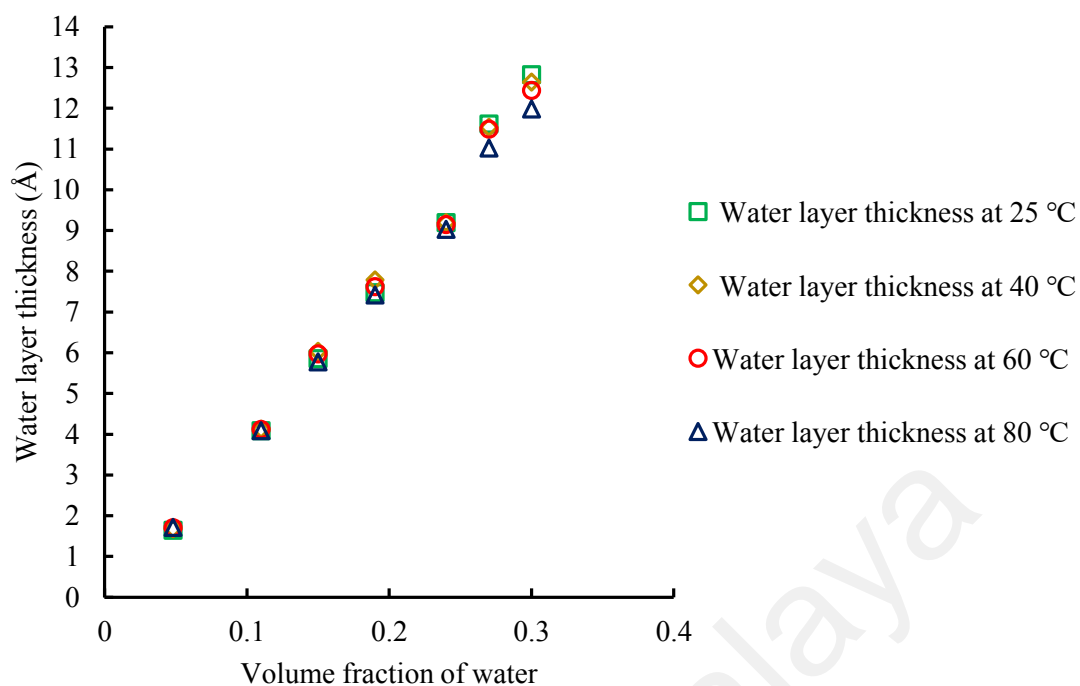


Figure 4.33: Water layer thickness against fraction of water at different temperatures for L_α phase of the β -Mal- $C_{12}C_8$.

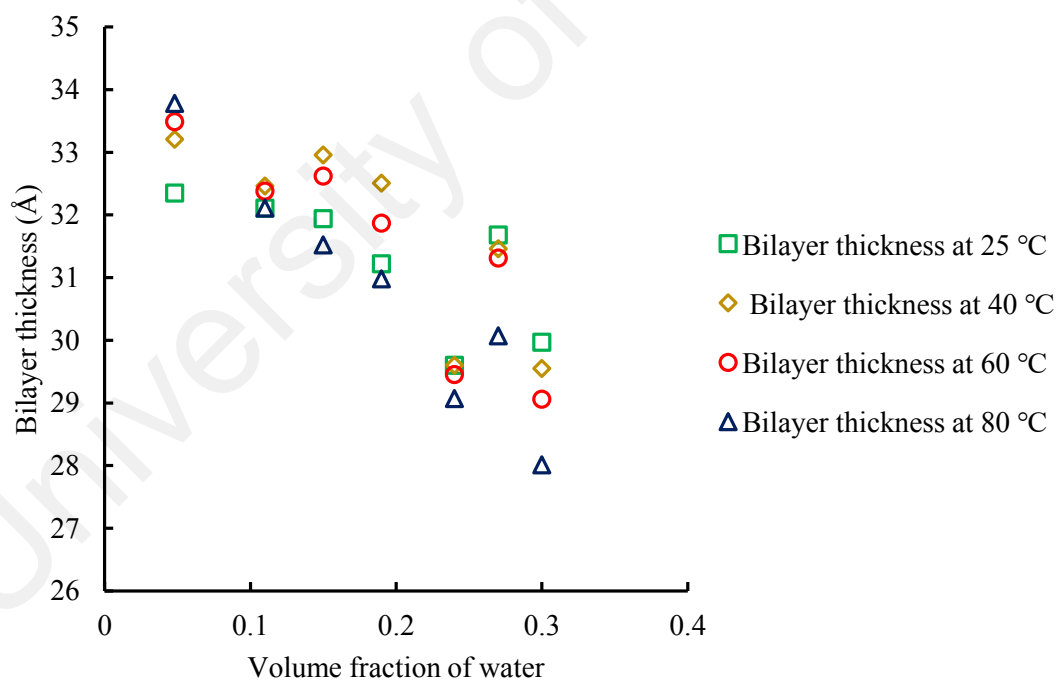


Figure 4.34: Bilayer thickness against fraction of water at different temperatures for L_α phase of the β -Mal- $C_{12}C_8$.

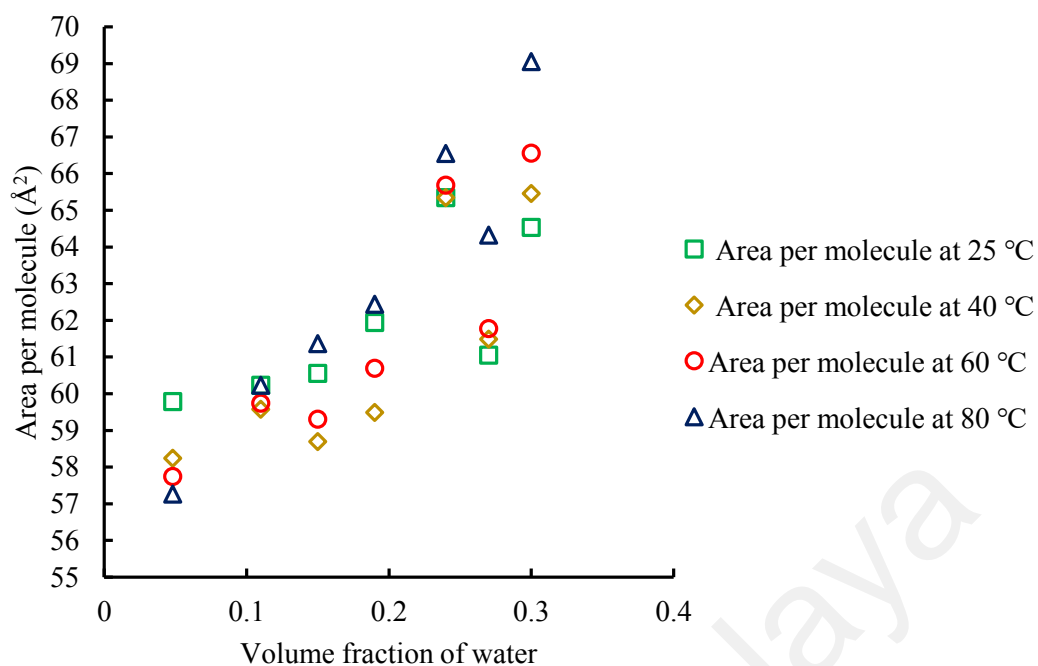


Figure 4.35: Area per molecule against fraction of water at different temperatures for L_α phase of the β -Mal- $C_{12}C_8$.

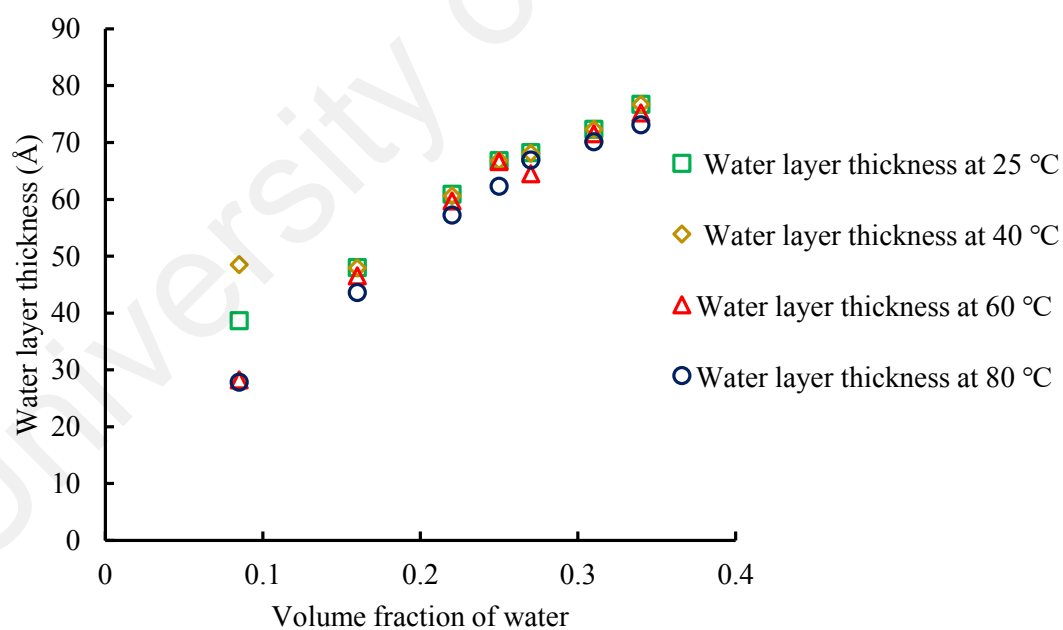


Figure 4.36: Water layer thickness against fraction of water at different temperatures for H_{II} phase of the β -Glc- $C_{12}C_8$.

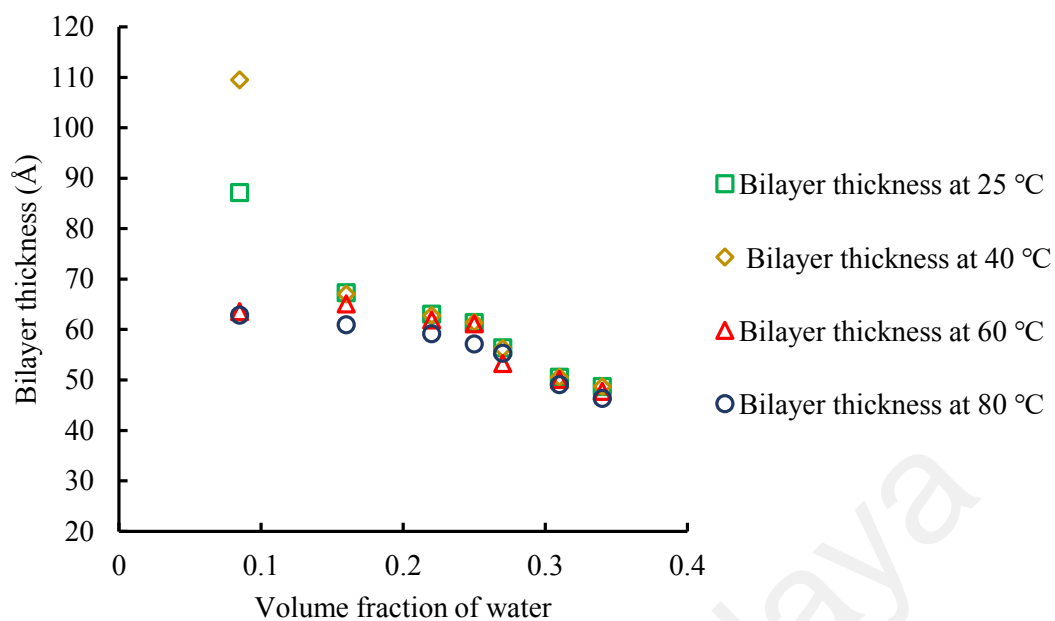


Figure 4.37: Bilayer thickness against fraction of water at different temperatures for H_{II} phase of the β -Glc- $C_{12}C_8$.

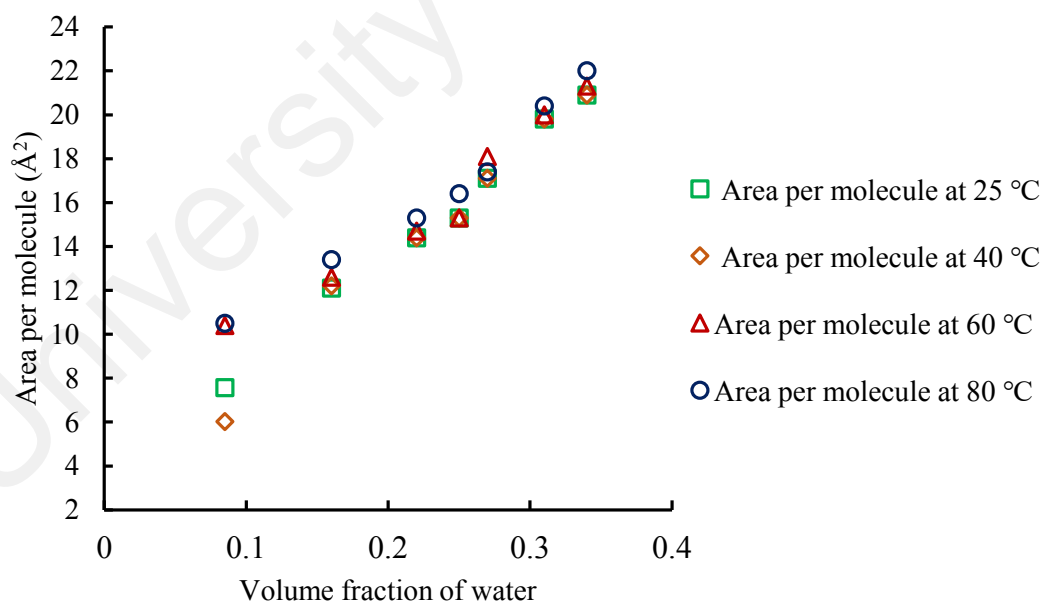


Figure 4.38: Area per molecule against fraction of water at different temperatures for H_{II} phase of the β -Glc- $C_{12}C_8$.

From Figures 4.33 and 4.36, they show that the water layer thickness (d_w) values are directly proportional to the volume fraction of water (ϕ_w). This is related to the swelling ability of the L_α and H_{II} phases until no further water is dissolved (Kobayashi & Fukada, 1998). Consequently, the diameter of the water layer thickness increases as the volume fraction of water increases because the system has yet to reach the excess water point. The increase of area per molecule (S) at the head group as the volume fraction of water increases, implies that both glucose and maltose head groups hydrations increase when the water availability is high (Figures 4.35 and 4.38). However, the bilayer thickness of lipid is inversely proportional to the volume fraction of water as shown in Figures 4.34 and 4.37. This might be due to the increment of the packing frustration and the lamellar lipid layer getting less ordered in order to avoid the occurrence of polar water molecules. Moreover, a comparison between the calculated and experimental data of the glycolipid lyotropic liquid crystal assemblies were done by Ngan and co-workers (2010). They found a similar pattern of results as obtained in this study.

The water layer thickness, bilayer thickness and area per molecule dependency with temperatures (i.e. 25, 40, 60 and 80 °C) of the L_α and H_{II} phases are shown in Figures 4.39–4.41 and 4.42–4.44, respectively.

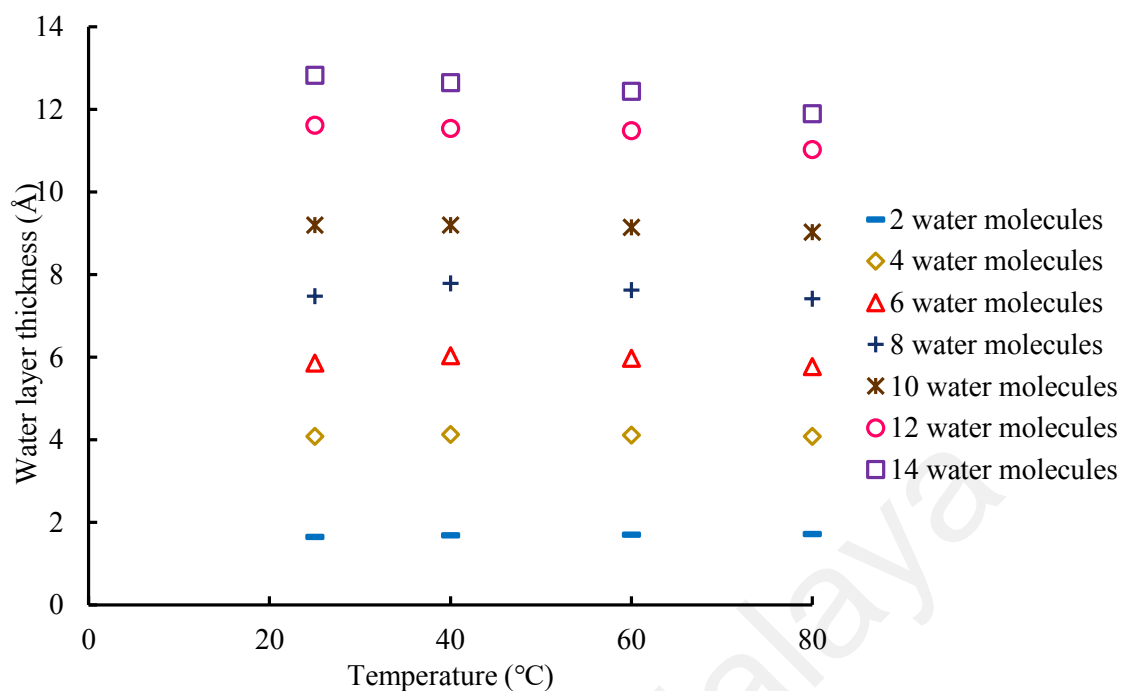


Figure 4.39: Water layer thickness against different temperatures for L_α phase of the β -Mal- $C_{12}C_8$.

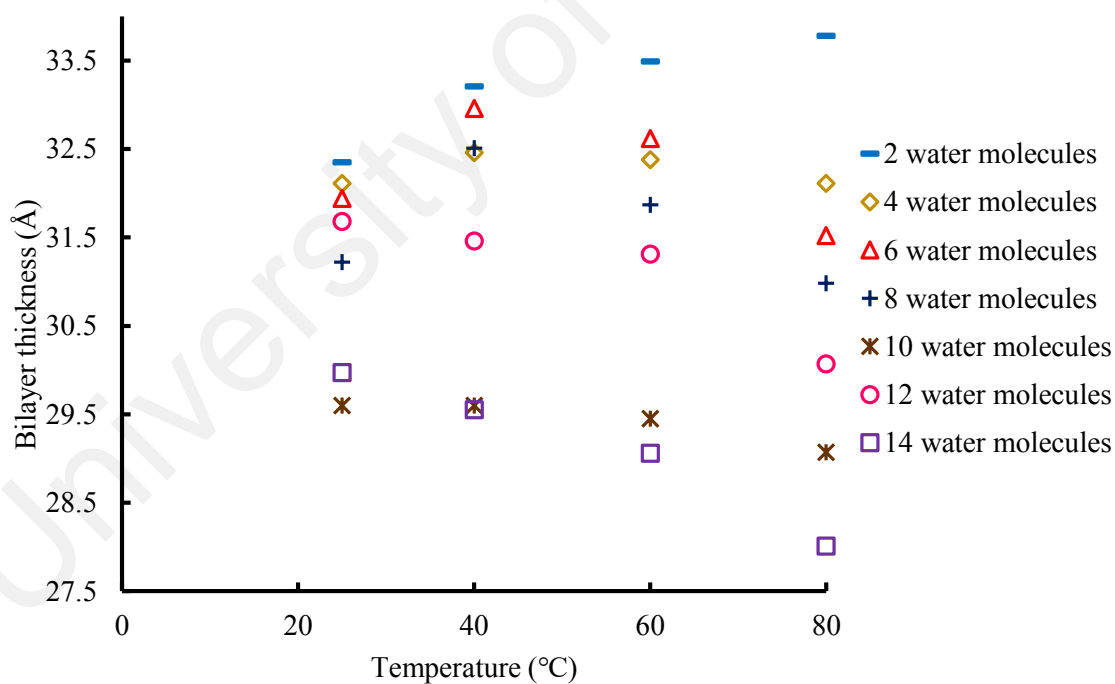


Figure 4.40: Bilayer thickness against different temperatures for L_α phase of the β -Mal- $C_{12}C_8$.

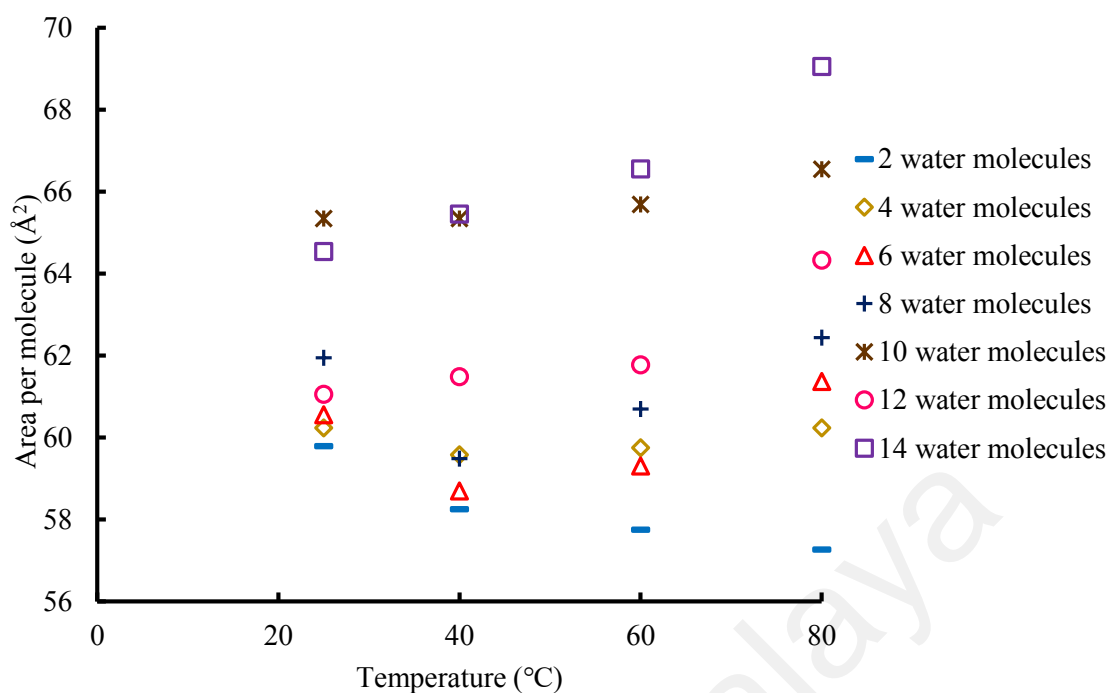


Figure 4.41: Area per molecule against different temperatures for L_α phase of the β -Mal- $C_{12}C_8$.

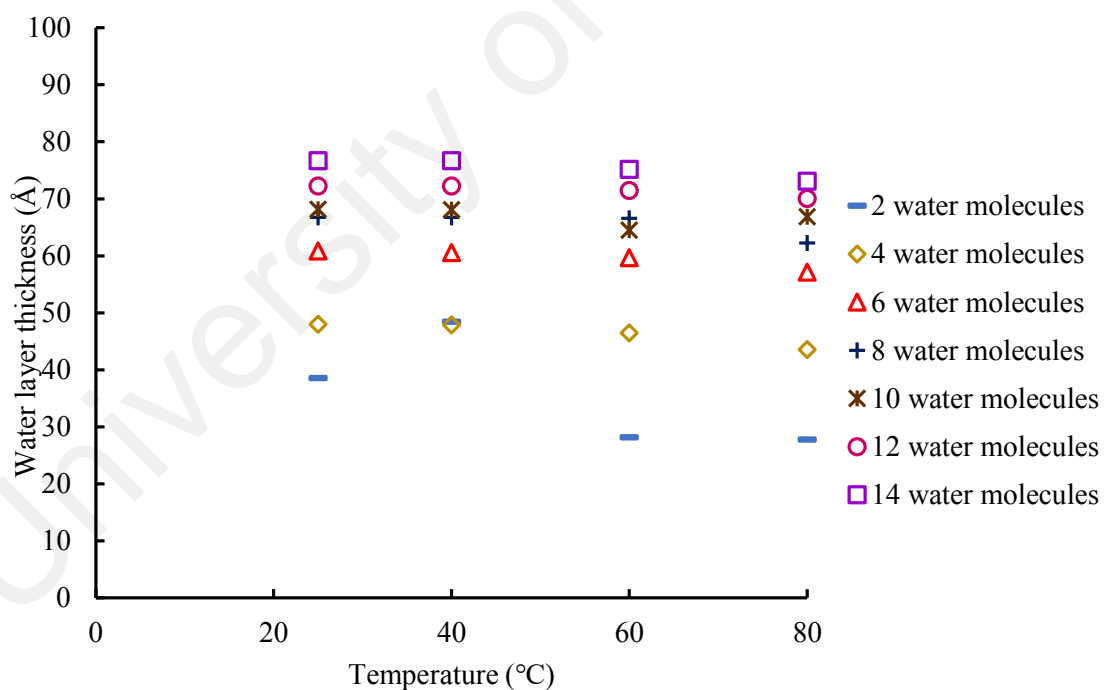


Figure 4.42: Water layer thickness against different temperatures for H_{II} phase of the β -Glc- $C_{12}C_8$.

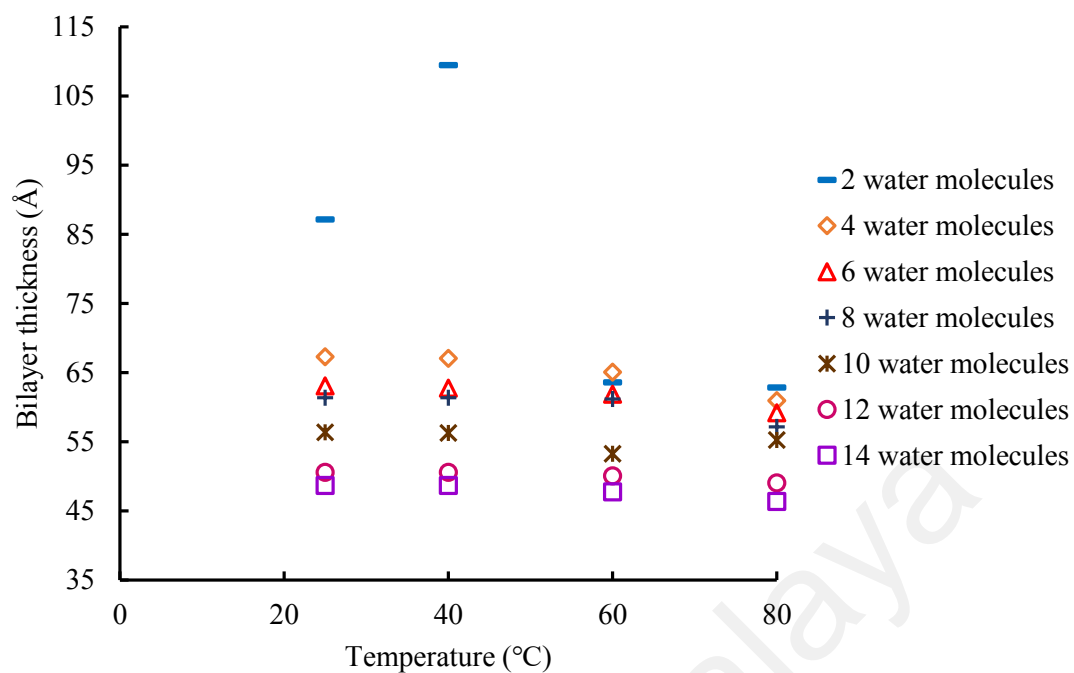


Figure 4.43: Bilayer thickness against different temperatures for H_{II} phase of the β -Glc- $C_{12}C_8$.

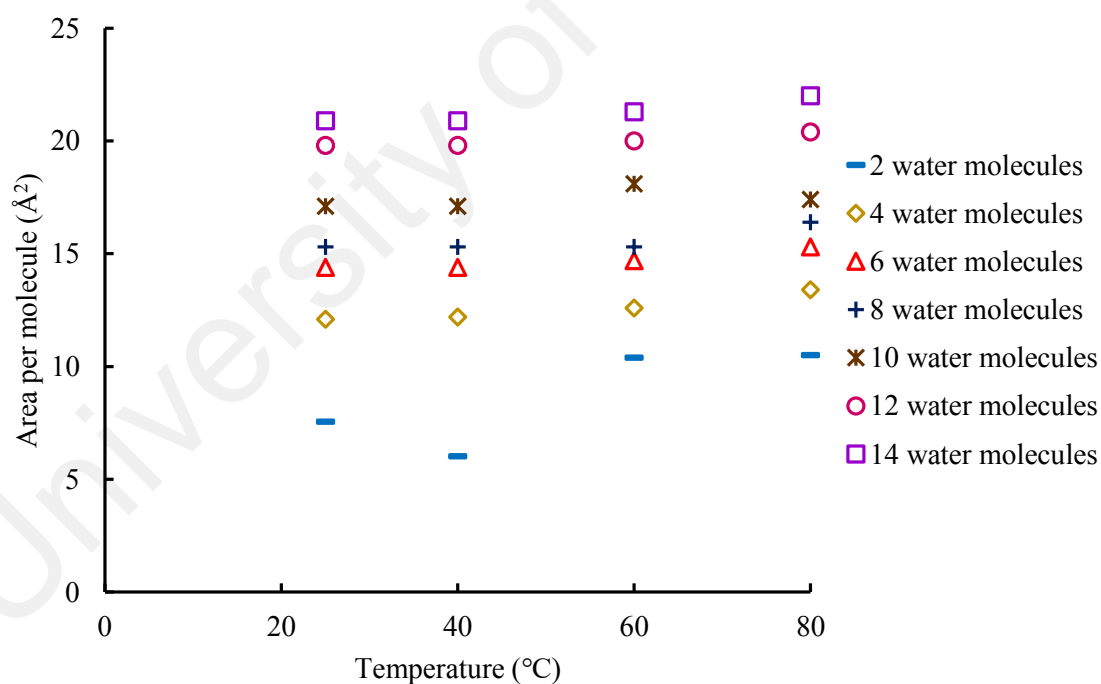


Figure 4.44: Area per molecule against different temperatures for H_{II} phase of the β -Glc- $C_{12}C_8$.

Figures 4.39 and 4.42 show the increasing in temperatures from 25 to 80 °C, the water layer thickness decreases for 10–14 water molecules per lipid (at fixed hydration). Conversely, from 25 to 40 °C, there is a small increment in the water layer thickness and then it decreases with increasing temperatures (60–80 °C) for 4–8 water molecules per lipid. With increasing temperature, however, the inter-bilayer water spacing of the oriented multilamellar vesicles (MLV) also increases in full hydration state (Pan *et al.*, 2008).

For bilayer thickness as provided in Figures 4.40 and 4.43, 4–14, water molecules per lipid decrease with the increasing temperature ranging from 25 to 80 °C. However, 2 water molecules per lipid show linearity with the temperatures. Chen and Hung (1996) reported that the hydrophobic dilauroyl-phosphocholine (DLPC) hydrocarbon chain expanded its ordering portion upon losing water molecules. In Figures 4.41 and 4.44, an area per molecule at the sugar head group of the fluid L_α and H_{II} phases of all water contents increases at temperatures of 40 °C and above. This result was consistent with the works of Nguan and co-workers (2010) Chen and Hung (1996). In contrast, the area per molecule decreases (2–8 water molecules/lipid) from 25 to 40 °C.

Phase Stability of Fluid Lamellar Phase

Lipid maltoside favours the fluid L_α phase at all temperatures and water contents. The L_α phase is stable due to the controlling factors namely, transverse and lateral interactions. The former refers to the interaction occurred between the adjacent lipid layers. The interactions include van der Waals (Costigan *et al.*, 2000), hydration (McIntosh, 1996), fluctuation (Tristram-Nagle *et al.*, 1998) and steric thickness (Kučerka, *et al.*, 2005). However, the latter is the lateral interaction that exists within a lipid bilayer. The interactions, which are the lateral stress, repulsions and attractions, exist at the head

group-head group and the hydrocarbon chain-hydrocarbon chain. Moreover, an interfacial area per molecule is regulated by the interaction within a lipid bilayer. Ngan and co-workers (2010) stated that maltosides produced a $\text{SmA}/\text{L}_\alpha$ phase due to the disaccharide head group. The stabilised $\text{SmA}/\text{L}_\alpha$ phase was favoured because of the extensive glycolipid head group attractive interactions.

One of the factors that determine the lipid polymorphism is the bilayer stress profile of packing geometry and frustration. This bilayer stress is affected by the thermodynamic parameters which are hydration and temperature. According to Sadoc and Charvolin (1986), frustration arises due to the opposing and compromising of two physical forces. None of them are fully satisfied. Figure 4.45 illustrates the schematic diagram of frustration.

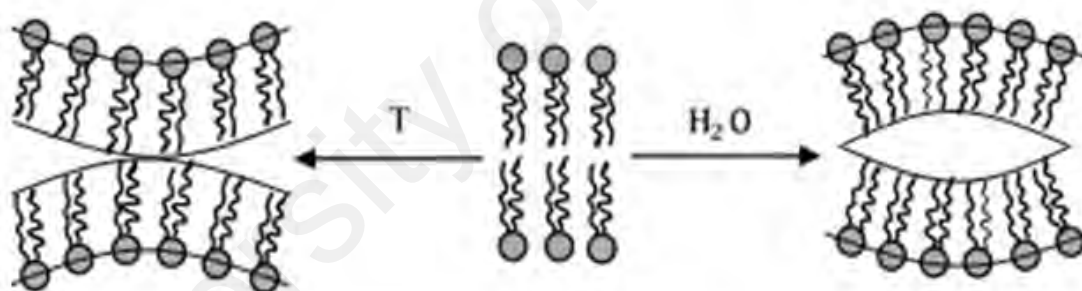


Figure 4.45: Schematic diagram of frustration. Redrawn from (Sadoc & Charvolin, 1986).

The non-polar hydrocarbon chain and area per molecule at the polar head group tend to be more disordered and expanded with increasing temperature, respectively. In contrast, there is an increase in the lateral repulsions between the polar headgroups with increasing degree of hydrations. Hence, both the area per molecule and water-hydrocarbon contact tend to increase. Therefore, the hydrophobic effect promotes the hydrocarbon chain move towards its chain region. This is also another possible reason for

a lipid bilayer thinning in which the hydrophobic hydrocarbon fills up the empty space driven by the enlargement of the solvated polar head group (Chen & Hung, 1996).

It is very important to consider the interfacial tension between the polar head group and non-polar hydrocarbon chain of the lyotropic fluid L_α phase. Area per molecule, mean curvature (H) and Gaussian Curvature (K) are the three factors that characterise the interfacial tension. These curvatures are described by the two principal curvatures C_1 and C_2 (Seddon & Templer, 1995; Rappolt & Pabst, 2008). For a lipid monolayer, the value of H more than zero indicates its curvature move towards the non-polar hydrocarbon chain, however, the value of H less than zero signifies its curvature move towards the polar head group. The fluid L_α phase is known as the flat bilayer that has zero principal curvatures and Gaussian curvature. Hence, the surface of the L_α phase is parabolic.

4.3.3 Final Remarks

The plasma membrane study still remains an important area which needs to be considered as it carries many cellular functions. Therefore, this study has focused on the effects of hydration and temperature on the Guerbet branched-chain maltoside and glucoside. At all varied water contents and temperatures, the maltoside and glucoside exhibited only the fluid L_α dan H_{II} phases, respectively. Increasing volume fraction of water or number of waters per lipid produced the increment in the d_w and S , and decreased in d . At a higher temperature, d_w and d were shrunk, but the S was expanded.

CHAPTER 5: CONCLUSIONS AND RECOMMENDATIONS

In conclusion, three different techniques were utilised in order to investigate the five homologous series of branched-chain Guerbet β -D-glucosides phase behaviours in dry and excess water conditions; phase behaviours of five homologous series of branched-chain Guerbet β -D-maltosides and their lamellar hydration properties; and sugar head groups of β -Glc-C₁₂C₈ and β -Mal-C₁₂C₈ with the same total number of chain length (-C₁₂C₈) on their mesophase structural parameters at fixed water hydration.

There are five branched-chain β -D-glucosides under study, namely, β -Glc-C₆C₂, β -Glc-C₈C₄, β -Glc-C₁₀C₆, β -Glc-C₁₂C₈ and β -Glc-C₁₄C₁₀. In OPM, the dry conditions, β -Glc-C₆C₂ shows a phase transition from a lamellar crystalline L_C phase to an inverse micellar L₂ solution at 62 °C upon heating. When cooled, L _{α} phase forms by β -Glc-C₆C₂. Moreover, the lyotropic phase behaviour adopted by this compound via a contact penetration scan is L₁ micellar solution. The β -Glc-C₈C₄, however, exhibits an inverse micellar L₂ solution and a fluid lamellar L _{α} phase in thermotropic and lyotropic conditions, respectively. An inverse hexagonal H_{II} phase appears at below 49 °C (dry condition) and a cubic V_{II} phase (water contact penetration) are adopted by the β -Glc-C₁₀C₆. The dry β -Glc-C₁₂C₈ and β -Glc-C₁₄C₁₀ compounds form hexagonal H_{II} phase both in dry and excess water. For DSC measurements, five homologous series of branched-chain Guerbet β -D-glucosides show the clearing transition temperatures of 60 °C (β -Glc-C₆C₂), 37 °C (β -Glc-C₈C₄), 56 °C (β -Glc-C₁₀C₆), 122 °C (β -Glc-C₁₂C₈) and 142 °C (β -Glc-C₁₄C₁₀). These T_C (DSC) are in agreement with T_C (OPM) (see Table 4.3). For X-ray results, the β -Glc-C₆C₂ compound produces L _{α} (dry) and normal micellar L₁ (excess water) with 20.7 Å and a non-detected *d*-spacings, respectively. However, the β -Glc-C₈C₄ compound displays an inverse micellar L₂ (dry) and L _{α} (excess water) with a non-detected

d -spacing and 30.3 Å, respectively. The β -Glc-C₁₀C₆ compound gives an inverse hexagonal H_{II} phase with lattice parameter of 28.7 Å and cubic V_{II} ($Ia3d$) phase with lattice parameter of 87.5 Å. Furthermore, the hexagonal H_{II} phase appears in dry (30.0 Å, 36.6 Å) and excess water (35.8 Å, 36.9 Å) conditions for both the β -Glc-C₁₂C₈ and β -Glc-C₁₄C₁₀, respectively.

A series of branched-chain β -D-maltosides by referring to the β -Mal-C₆C₂, β -Mal-C₈C₄, β -Mal-C₁₀C₆, β -Mal-C₁₂C₈ and β -Mal-C₁₄C₁₀ mesophases and their lamellar hydration properties were studied. For OPM results, the dry β -Mal-C₆C₂ shows a phase transition from a lamellar L_C to an inverse micellar L₂ at 137 °C and a normal micellar L_I when dissolved in water. Likewise, the dry β -Mal-C₈C₄ exhibits a lamellar crystalline L_c phase at room temperature with the clearing temperature of 188 °C. However, in lyotropic condition, the sample forms an L _{α} phase. The dry β -Mal-C₁₀C₆ which is the third analogue shows L_c phase (T_c, ~189 °C) and L _{α} texture in lyotropic condition. The longer chain of β -Mal-C₁₂C₈ and β -Mal-C₁₄C₁₀ compound adopt polymorphisms such as L _{α} -V_{II}-H_{II}-L₂ are as shown in Table 4.5. A DSC technique was used to detect T_g and T_C for thermotropic branched-chain β -D-maltoside series. The T_g values of β -Mal-C₆C₂, β -Mal-C₈C₄, β -Mal-C₁₀C₆, β -Mal-C₁₂C₈ and β -Mal-C₁₄C₁₀ are 23 °C, 43 °C, 30 °C, 44 °C and 49 °C, respectively. Moreover, the T_C values of β -Mal-C₆C₂, β -Mal-C₈C₄, β -Mal-C₁₀C₆, β -Mal-C₁₂C₈ are 121 °C, 199 °C, 199 °C and 194 °C, respectively. However, two transition peaks were observed for β -Mal-C₁₄C₁₀ referring to 141 °C (ΔH , 0.6 kJ mol⁻¹) and 234 °C (ΔH , 0.9 kJ mol⁻¹). SAXS results show the appearance of L_C in dry and L _{α} in excess water conditions for the branched-chain β -D-maltoside series. The only difference among the β -D-maltosides is the d -spacing value for dry and excess water conditions ranging from 20 to 45 Å. Since the β -Mal-C₁₀C₆, β -Mal-C₁₂C₈ and β -Mal-C₁₄C₁₀ exhibit L_C in dry and L _{α} in excess water, the change in d -spacing can be used in the structural parameter

calculations which in turn is the area per molecule and water content are estimated. Among the three compounds, the β -Mal-C₁₀C₆ gives the highest wt % of water which is 25% and β -Mal-C₁₂C₈ shows the lowest value which is 19%. However, the β -Mal-C₁₄C₁₀ produces the highest value for an area per molecule (59.7 Å²).

For all degrees of hydration, the structural parameters of β -Mal-C₁₂C₈ and β -Glc-C₁₂C₈ show their dependency on varied temperatures. The L _{α} of β -Mal-C₁₂C₈ and H_{II} of β -Glc-C₁₂C₈ swell upon the addition of water. Therefore, the water layer thicknesses for both compounds are increased. Bilayer thickness and area per molecule values of both β -Mal-C₁₂C₈ and β -Glc-C₁₂C₈ are inversely and directly proportional to the volume fraction of water upon the increment of temperatures respectively.

As a recommendation for future works, there is a need to carry out a binary phase diagram of those compounds in a specific weight percent of water versus temperature so as to find out the effect of pressure-jump amplitude on the rate of transition in excess water conditions.

REFERENCES

- Achhari, V. M., Bryce, R. A., & Hashim, R. (2014). Conformational dynamics of dry lamellar crystals of sugar-based lipids: An atomistic simulation study. *PLoS ONE*, 9(6), Article #e101110.
- Agoston, K., Dobo, A., Rako, J., Kerekgyarto, J., & Szurmai, Z. (2001). Anomalous Zemplen deacylation reactions of α - and β -D-mannopyranoside derivatives. *Carbohydrate Research*, 330(2), 183–190.
- Ahmad, N., Ramsch, R., Esquena, J., Solans, C., Tajuddin, H. A. & Hashim, R. (2012). Physicochemical Characterization of Natural-like Branched-Chain Glycosides toward Formation of Hexosomes and Vesicles. *Langmuir*, 28, 2395–2403.
- Ahmad, N., Ramsch, R., Llinas, M., Solans, C., Hashim, R., & Tajuddin, H. A. (2014). Influence of nonionic branched-chain alkyl glycosides on a model nano-emulsion for drug delivery systems. *Colloids Surface B Biointerfaces*, 115, 267–274.
- Ahmadi, S., Achhari, V. M., Nguan, H., & Hashim, R. (2014). Atomistic simulation studies of the α/β -glucoside and galactoside in anhydrous bilayers: Effect of the anomeric and epimeric configurations. *Journal of Molecular Modeling*, 20(3), Article #2165.
- Akabori, K., & Nagle, J. F. (2015). Structure of the DMPC lipid bilayer ripple phase. *Soft Matter*, 11(5), 918–926.
- Allec, N., Choi, M., Yesupriya, N., Szychowski, B., White, M. R., Kann, M. G., Garcin, E. D., Daniel, M. C., & Badano, A. (2015). Small-angle X-ray scattering method to characterize molecular interactions: Proof of concept. *Scientific Reports*, 5(1), 1–12.
- Amar-Yuli, I., Wachtel, E., Shoshan, E. B., Danino, D., Aserin, A., & Garti, N. (2007). Hexosome and hexagonal phases mediated by hydration and polymeric stabilizer. *Langmuir*, 23(7), 3637–3645.
- An, J., Hina, S., Yang, Y., Xue, M., & Liu, Y. (2016). Characterization of liquid crystals: A literature review. *Reviews on Advanced Materials Science*, 44(4), 398–406.
- Andrienko, D. (2018). Introduction to liquid crystals. *Journal of Molecular Liquids*, 267, 520–541.
- Arachea, B. T., Sun, Z., Potente, N., Malik, R., Isailovic, D., & Viola, R. E. (2012). Detergent selection for enhanced extraction of membrane proteins. *Protein Expression and Purification*, 86(1), 12–20.
- Aripin, N. F. K., Hashim, R., Heidelberg, T., Kweon, D. K., & Park, H. J. (2013). Effect of vesicle's membrane packing behaviour on skin penetration of model lipophilic drug. *Journal of Microencapsulation*, 30(3), 265–273.

- Arsov, Z., Gonzalez-Ramirez, E. J., Goni, F. M., Tristram-Nagle, S., & Nagle, J. F. (2018). Phase behavior of palmitoyl and egg sphingomyelin. *Chemistry and Physics of Lipids*, 213, 102–110.
- Balzer, D., & Luders, H. (2000). *Nonionic surfactants: Alkyl polyglucosides* (Vol. 91). New York: Marcel Dekker.
- Biffi, A., Capotondo, A., Fasano, S., del Carro, U., Marchesini, S., Azuma, H., Malaguti, M. C., Amadio, S., Brambilla, R., Grompe, M., Bordignon, C., Quattrini, A., & Naldini, L. (2006). Gene therapy of metachromatic leukodystrophy reverses neurological damage and deficits in mice. *Journal of Clinical Investigation*, 116(11), 3070–3082.
- Boyd, B. J., Drummond, C. J., Krodziewska, I., & Grieser, F. (2000). How chain length, headgroup polymerization, and anomeric configuration govern the thermotropic and lyotropic liquid crystalline phase behavior and the air-water interfacial adsorption of glucose-based surfactants. *Langmuir*, 16, 7359–7367.
- Bragg, W. H., & Bragg, W. L. (1913). The reflection of X-rays by crystals. *Proceedings of the Royal Society A*, 88(605), 428–438.
- Brooks, N. J., Hamid, H. A. A., Hashim, R., Heidelberg, T., Seddon, J. M., Conn, C. E., Mirzadeh Hussein, S. M., Zahid, N. I., & Hussien, R. S. D. (2011). Thermotropic and lyotropic liquid crystalline phases of Guerbet branched-chain-D-glucosides. *Liquid Crystals*, 38(11–12), 1725–1734.
- Bushby, R. J., & Kawata, K. (2011). Liquid crystals that affected the world: Discotic liquid crystals. *Liquid Crystals*, 38(11–12), 1415–1426.
- Cachon-Gonzalez, M. B., Wang, S. Z., Lynch, A., Ziegler, R., Cheng, S. H., & Cox, T. M. (2006). Effective gene therapy in an authentic model of Tay-Sachs-related diseases. *Proceeding of the National Academy of Sciences*, 103(27), 10373–10378.
- Cameotra, S. S., & Makkar, R. S. (2004). Recent applications of biosurfactants as biological and immunological molecules. *Current Opinion in Microbiology*, 7(3), 262–266.
- Canda, F., Debeauvais, F., & Wittmann, J. (1982). Structural properties and topological defects of swollen polymeric mesophases: Low angle X-ray diffraction and optical microscopic studies. *Journal of Colloid and Interface Science*, 87(2), 356–374.
- Carlton, R. A. (Ed.) (2011). *Polarized light microscopy in Pharmaceutical microscopy*. New York: Springer-Verlag.
- Cecutti, C., Focher, B., Perly, B., & Zemb, T. (1991). Glycolipid self-assembly: Micellar structure. *Langmuir*, 7(11), 2580–2585.
- Cevc, G. (1993). *Phospholipids handbook*. New York: Marcel Dekker.

- Changizi, V., Oghabian, M. A., Speller, R., Sarkar, S., & Kheradmand, A. A. (2005). Application of small angle X-ray scattering (SAXS) for differentiation between normal and cancerous breast tissue. *International Journal of Medical Sciences*, 2(3), 118–121.
- Chen, F. Y., & Hung, W. C. (1996). Structural changes of lipid membrane induced by dehydration. *Chinese Journal of Physics*, 34(6), 1363–1372.
- Chen, Y., Ma, P., & Gui, S. (2014). Cubic and hexagonal liquid crystals as drug delivery systems. *Biomed Research International*, 2014, Article #815981.
- Chester, M. A. (1997). Nomenclature of glycolipids. *Pure and Applied Chemistry*, 69(12), 2475–2487.
- Collings, P. J., & Hird, M. (1997). *Introduction to liquid crystal: Chemistry and physics*. London, England: Taylor & Francis.
- Conn, C. E., Ces, O., Mulet, X., Finet, S., Winter, R., Seddon, J. M., & Templer, R. H. (2006). Dynamics of structural transformations between lamellar and inverse bicontinuous cubic lyotropic phases. *Physical Review Letters*, 96(10), Article #108102.
- Cooper, A. (2000). Heat capacity of hydrogen-bonded networks: An alternative view of protein folding thermodynamics. *Biophysical Chemistry*, 85(1), 25–39.
- Cooper, A. (2004). *Biophysical chemistry*. London: Royal Society of Chemistry.
- Cooper A., Johnson, C. M., Lakey, J. H. & Nollmann, M. (2001). Heat does not come in different colours: entropy, enthalpy compensation, free energy windows, quantum confinement, pressure perturbation calorimetry, solvation and the multiple causes of heat capacity effects in biomolecular interactions. *Biophysical Chemistry*, 93(2–3), 215–230.
- Corti, M., Cantù, L., Brocca, P., & del Favero, E. (2007). Self-assembly in glycolipids. *Current Opinion in Colloid & Interface Science*, 12(3), 148–154.
- Costantino, V., Fattorusso, E., Mangoni, A., Di Rosa, M., & Ianaro, A. (1999). Glycolipids from sponges. VII. Simplexides, novel immunosuppressive glycolipids from the Caribbean sponge *Plakortis simplex*. *Bioorganic & Medicinal Chemistry Letters*, 9(2), 271–276.
- Costigan S. C., Booth P. J., & Templer, R. H. (2000). Estimations of lipid bilayer geometry in fluid lamellar phases. *Biochimica et Biophysica Acta*, 1468(1–2), 41–54.
- Dembitsky, V. M. (2004a). Chemistry and biodiversity of the biologically active natural glycosides. *Chemistry & Biodiversity*, 1(5), 673–781.
- Dembitsky, V. M. (2004b). Astonishing diversity of natural surfactants: 1. Glycosides of fatty acids and alcohols. *Lipids*, 39(10), 933–953.

- Dembitsky, V. M. (2005a). Astonishing diversity of natural surfactants: 6. Biologically active marine and terrestrial alkaloid glycoside. *Lipids*, 40(11), 1081–1105.
- Dembitsky, V. M. (2005b). Astonishing diversity of natural surfactants: 2. Polyether glycosidic ionophores and macrocyclic glycosides. *Lipids*, 40(3), 219–248.
- Dembitsky, V. M. (2005c). Astonishing diversity of natural surfactants: 3. Carotenoid glycosides and isoprenoid glycolipids. *Lipids*, 40(6), 535–557.
- Dembitsky, V. M. (2005d). Astonishing diversity of natural surfactants: 4. Fatty acid amide glycosides, their analogs and derivatives. *Lipids*, 40(7), 641–660.
- Dembitsky, V. M. (2005e). Astonishing diversity of natural surfactants: 5. Biologically active glycosides of aromatic metabolites. *Lipids*, 40(9), 869–900.
- Dierking, I. (2003). *Textures of liquid crystals*. Weinheim: Wiley-VCH.
- Duesing, P. M., Seddon, J. M., Templer, R. H., & Mannock, D. A. (1997). Pressure effects on lamellar and inverse curved phases of fully hydrated dialkyl phosphatidylethanolamines and β -D-xylopyranosyl-sn-glycerols. *Langmuir*, 13(10), 2655–2664.
- Efrat, R., Aserin, A., & Garti, N. (2008). On structural transitions in a discontinuous micellar cubic phase loaded with sodium diclofenoc. *Journal of Colloid and Interface Science*, 321(1), 166–176.
- Ehsan, M., Du, Y., Scull, N. J., Tikhonova, E., Tarrasch, J., Mortensen, J. S., Loland, C. J., Skiniotis, G., Guan, L., Byrne, B., Kobilka, B. K., & Chae, P. S. (2016). Highly branched pentasaccharide-bearing amphiphiles for membrane protein studies. *Journal of the American Chemical Society*, 138(11), 3789–3796.
- Eicher, B., Heberle, F. A., Marquardt, D., Rechberger, G. N., Katsaras, J., & Pabst, G. (2017). Joint small-angle X-ray and neutron scattering data analysis of asymmetric lipid vesicles. *Journal of Applied Crystallography*, 50(2), 419–429.
- Elliott S. R. (1990). *Physics of amorphous materials*. Harlow, Essex, England: Longman Scientific & Technical.
- Enquist, I. B., Nilsson, E., Ooka, A., Månsson, J. E., Olsson, K., Ehinger, M., Brady, R. O., Richter, J., & Karlsson, S. (2006). Effective cell and gene therapy in a murine model of Gaucher disease. *Proceeding of the National Academy of Sciences*, 103(37), 13819–13824.
- Enz, E., La Ferrara, V., Scalia, G. (2013). Confinement - sensitive optical response of cholesteric liquid crystals in electrospun fibers. *ACS Nano*, 7(8), 6627–6635.
- Ericsson, C. A., Ericsson, L. C., & Ulvenlund, S. (2005a). Solid-state phase behaviour of dodecylglycosides. *Carbohydrate Research*, 340, 1529–1537.

- Ericsson, C. A., Ericsson, L. C., Kocherbitov, V., Söderman, O., & Ulvenlund, S. (2005b). Thermotropic phase behaviour of long-chain alkylmaltosides. *Physical Chemistry Chemical Physics*, 7(15), 2970–2977.
- Ernst, B., Hart, G. W., & Sinay, P. (2000). *Carbohydrates in chemistry and biology*. Weinheim, Germany: Wiley-VCH.
- Fan, Z. X., & Haase, W. (1991). Determination of the translational order parameter in the liquid crystalline smectic A phase using the X-ray diffraction method. *The Journal of Chemical Physics*, 95(8), 6066–6074.
- Feehan, J., Burrows, S. P., Cornelius, L., Cook, A. M., Mikkelsen, K., Apostolopoulos, V., Husaric, M., & Kiatos, D. (2018). Therapeutic applications of polarized light: Tissue healing and immunomodulatory effects. *Maturitas*, 116, 11–17.
- Ferrier, R. J., & Furneaux, R. H. (1976). Synthesis of 1,2- trans-related 1-thioglycoside Esters. *Carbohydrate Research*, 52(1), 63–68.
- Fischer, E., & Beensch, L. (1894). Ueber einige synthetische glucoside. *Berichte der Deutschen Chemischen Gesellschaft*, 27, 2478–2486.
- Fischer, E., & Helferich, B. (1911). Ober neue synthetische glucoside. *Justus Liebigs Annalen der Chemie*, 383, 68–91.
- Fletcher, P. D. I., & Strey, R. (2002). Surfactant science "Editorial Overview". *Current Opinion in Colloid and Interface Science*, 7, 1–2.
- Fragneto, G., Delhom, R., Joly, L., & Scoppola, E. (2018). Neutrons and model membranes: Moving towards complexity. *Current Opinion in Colloid & Interface Science*, 38, 108–121.
- Freudenberg, K. (1967). Emil Fischer and his contribution to carbohydrate chemistry. *Advances in Carbohydrate Chemistry*, 21, 1–38.
- Funari, S. S., & Rapp, G. (1999). A continuous topological change during phase transitions in amphiphile/water systems. *Proceeding of the National Academy of Sciences USA*, 96(14), 7756–7759.
- Garidel, P., Howe, J., Milkereit, G., Rossle, M., Linser, S., Sven, G., Willumeit, R., Gutschmann, T., Vill, V., & Brandenburg, K. (2008). Structural polymorphism of hydrated ether-linked dimyristyl maltoside and melibioside. *Chemistry and Physics of Lipids*, 151(1), 18–29.
- Garidel, P., Kaonis, Y., Heinbockel, L., Wulf, M., Gerber, S., Munk, A., Vill, V., & Brandenburg, K. (2015). Self-organisation, thermotropic and lyotropic properties of glycolipids related to their biological implications. *The Open Biochemistry Journal*, 9, 49–72.
- Garrett, R. H., & Grisham, C. M. (2017). *Biochemistry*. Boston, MA: Cengage Learning.

- Gille, W. (2014). *Particle and particle systems characterization small-angle scattering (SAS) applications*. Florida: CRC Press.
- Glatter, V. O., & Kratky, O. (1982). *Small angle X-ray scattering*. London: London Academic press.
- Goodby, J. W. (1998). Liquid crystals and life. *Liquid Crystals*, 24(1), 25–38.
- Guo, C., Wang, J., Cao, F., Lee, R. J., & Zhai, G. (2010). Lyotropic liquid crystal systems in drug delivery. *Drug Discovery Today*, 15(23–24), 1032–1040.
- Guo, Z., Zhang, Y., DuanMu, Y., Xu, L., Xie, S., & Gu, N. (2006a). Facile synthesis of micrometer-sized gold nanoplates through an aniline-assisted route in ethylene glycol solution. *Colloids and Surfaces A: Physicochemical and Engineering Aspects*, 278(1–3), 33–38.
- Guo, Z., Zhang, Y., Mao, Y., Huang, L., & Gu, N. (2006b). Synthesis of micro-sized gold nanoplates by a self-seeding method in ethanol solution. *Materials Letters*, 60(29–30), 3522–3525.
- Haines, P. J., Reading, M., & Wilburn, F. W. (1998). *Differential thermal analysis and differential scanning calorimetry in handbook of thermal analysis and calorimetry*. Netherlands B: Elsevier Science. V.
- Hamid, H. A. A., Hashim, R., Seddon, J. M., & Brooks, N. J. (2014). Lyotropic phase behaviour and structural parameters of monosaccharide and disaccharide Guerbet branched-chain β -D-glycosides. *Advanced Materials Research*, 895, 111–115.
- Hamid, H. A. A., Hashim, R., Seddon, J. M., & Brooks, N. J. (2015). *Effects of chain length on the thermotropic and lyotropic phase behaviours of maltosides by small-angle X-ray diffraction study*. Singapore: Springer Singapore.
- Hamley, I. W. (2000). *Introduction to soft matter: Polymers, colloids, amphiphiles and liquid crystals*. England: John Wiley & Sons Ltd.
- Han, N. S., Heidelberg, T., & Salman, A. A. (2016). Spacer effect on triazole-linked sugar-based surfactants. *Journal of Dispersion Science and Technology*, 38(1), 105–109.
- Hantzel, D., Schulte, J., Enders, S., & Quitzsch, K. (1999). Thermotropic and lyotropic properties of n-alkyl- β -D-glucopyranoside surfactants. *Physical Chemistry Chemical Physics*, 1(5), 895–904.
- Hashim, R., Hashim, H. H. A., Rodzi, N. Z. M., Hussien, R. S. D., & Heidelberg, T. (2006). Branched chain glycosides: Enhanced diversity for phase behavior of easily accessible synthetic glycolipids. *Thin Solid Films*, 509(1–2), 27–35.
- Hashim, R., Sugimura, A., Minamikawa, H., & Heidelberg, T. (2012). Nature-like synthetic alkyl branched-chain glycolipids: A review on chemical structure and self-assembly properties. *Liquid Crystals*, 39(1), 1–17.

- Hashim, R., Zahid, N. I., Velayutham, T. S., Aripin, N. F. K., Ogawa, S., & Sugimura, A. (2018). Dry thermotropic glycolipid self-assembly: A Review, *Journal of Oleo Science*, 67(6), 651–668.
- Hato, M., & Minamikawa, H. (1996). The effects of oligosaccharide stereochemistry on the physical properties of aqueous synthetic glycolipids. *Langmuir*, 12(6), 1658–1665.
- Hato, M., Minamikawa, H., Tamada, K., Baba, T., & Tanabe, Y. (1999). Self-assembly of synthetic glycolipid/water systems. *Advances in Colloid and Interface Science*, 80(3), 233–270.
- Hato, M., Yamashita, I., Kato, T., & Abe, Y. (2004). Aqueous phase behavior of a 1-O-phytanyl- β -D-xyloside/water system. Glycolipid-based bicontinuous cubic phases of crystallographic space groups $Pn3m$ and $Ia3d$. *Langmuir*, 20(26), 11366–11373.
- Holmberg, K., (2001). Natural surfactants. *Current Opinion in Colloid & Interface Science*, 6, 148–159.
- Howe, J., von Minden, M., Gutschmann, T., Koch, M. H., Wulf, M., Gerber, S., Milkereit, G., Vill, V., & Brandenburg, K. (2007). Structural preferences of dioleoyl glycolipids with mono- and disaccharide head groups. *Chemistry and Physics of Lipids*, 149(1–2), 52–58.
- Huang, Z., Seddon, J. M., & Templer, R. H. (1996). An inverse micellar $Fd3m$ cubic phase formed by hydrated phosphatidylcholine/fatty alcohol mixtures. *Chemistry and Physics of Lipids*, 82(1), 53–61.
- Hui, S. K., & Sen, A. (1989). Effects of lipid packing on polymorphic phase behavior and membrane properties. *Proceeding of the National Academy of Sciences USA*, 86(15), 5825–5829.
- Hussen, R. S. D. (2006). Synthesis and liquid crystalline properties of secondary and branched chain of cellobiosides and lactosides. M.Sc. Dissertation, University of Malaya, Kuala Lumpur.
- Hyde, S. T. (2001). *Identification of lyotropic liquid crystalline mesophases in handbook of applied surface and colloid chemistry*. England: John Wiley & Sons Inc.
- Hynie, D. T. (2008). *Biological thermodynamics*. Cambridge: Cambridge University Press.
- Israelachvili, J. N., Mitchell, D. J., & Ninham, B. W. (1976). Theory of self-assembly of hydrocarbon amphiphiles into micelles and bilayers. *Journal of the Chemical Society, Faraday Transactions 2*, 72, 1525–1568.
- Israelachvili, J. N., Marcelja, S., & Horn, R. G. (1980). Physical principles of membrane organization. *Quarterly Reviews of Biophysics*, 13(2), 121–200.

- Israelachvili, J. N. (1994). The science and applications of emulsions-an overview. *Colloids and Surfaces A: Physicochemical and Engineering Aspects*, 91, 1–8.
- Israelachvili, J. N. (2011). *Intermolecular and surface forces*. Cambridge, MA: Academic Press.
- Jeffrey, G. A. (1986). Carbohydrate liquid crystals. *Accounts of Chemical Research*, 19(6), 168–173.
- Jeffrey, G. A., & Wingert, L. M. (1992). Carbohydrate liquid crystals. *Liquid Crystals*, 12(2), 179–202.
- Jewell, S. A. (2011). Living systems and liquid crystals. *Liquid Crystals*, 38(11–12), 1699–1714.
- Ji, S., Shen, W., Chen, L., Zhang, Y., Wu, X., Fan, Y., Fu, F., & Chen, G. (2019). Synthesis and properties of sugar-based surfactants alkoxyethyl β -D-glucopyranoside. *Colloids and Surfaces A: Physicochemical and Engineering Aspects*, 564, 59–68.
- John, K., Schreiber, S., Kubelt, J., Herrmann, A., & Muller, P. (2002). Transbilayer movement of phospholipids at the main phase transition of lipid membranes: Implications for rapid flip-flop in biological membranes. *Biophysical Journal*, 83(6), 3315–3323.
- Kaafarani, B. R. (2011). Discotic liquid crystals for opto-electronic applications. *Chemistry of Materials*, 23(3), 378–396.
- Kanduc, M., & Netz, R. R. (2015). From hydration repulsion to dry adhesion between asymmetric hydrophilic and hydrophobic surfaces. *Proceeding of the National Academy of Sciences USA*, 112(40), 12338–12343.
- Karp, G. (2010). *Cell biology (6th Ed.)*. Singapore: John Wiley & Sons.
- Kasch, N. (2013). Liquid crystals: applications and industry. *Liquid Crystals Today*, 22(3), 70–71.
- Kates, M. (1990). *Glycolipids, phosphoglycolipids and sulfoglycolipids*. New York, USA: Plenum Press.
- Khalil, R. A., & Zarari, A. A. (2014). Theoretical estimation of the critical packing parameter of amphiphilic self-assembled aggregates. *Applied Surface Science*, 318, 85–89.
- Kim, H. J., & Jang, C. (2016). Micro-capillary sensor for imaging trypsin activity using confined nematic liquid crystals. *Journal of Molecular Liquids*, 222, 596–600.
- Kitamoto, D., Morita, T., Fukuoka, T., Konishi, M., & Imura, T. (2009). Self-assembling properties of glycolipid biosurfactants and their potential applications. *Current Opinion in Colloid & Interface Science*, 14(5), 315–328.

- Klacsova, M., Bota, A., & Balgavy, P. (2016). DOPC-DOPE composition dependent L α -HII thermotropic phase transition: SAXD study. *Chemistry and Physics of Lipids*, 198, 46–50.
- Knepper, T. P., & Berna, J. L. (2003). Surfactants: properties, production, and environmental aspects. *Comprehensive Analytical Chemistry*, 40, 1–49.
- Kobayashi, Y., & Fukada, K. (1998). Characterization of swollen lamellar phase of dimyristoylphosphatidylcholine-gramicidin A mixed membrane by DSC, SAXS, and densimetry. *Biochimica et Biophysica Acta*, 1371(2), 363–370.
- Kocherbitov, V., Söderman, O., & Wadso, L. (2002). Phase diagram and thermodynamics of the n-octyl β -D-glucoside/water system. *Journal of Physical Chemistry B*, 106(11), 2910–2917.
- Kocherbitov, V., & Söderman, O. (2003). Phase diagram and physicochemical properties of the n-octyl α -D-glucoside/water system. *Physical Chemistry Chemical Physics*, 5(23), 5262–5270.
- Kocherbitov, V., & Söderman, O. (2004). Glassy Crystalline State and Water Sorption of Alkyl Maltosides. *Langmuir*, 20(8), 3056–3061.
- Kocherbitov, V., & Söderman, O. (2006). Hydration of dimethyldodecylamine-N-oxide: Enthalpy and entropy driven processes. *Journal of Physical Chemistry B*, 110(27), 13649–13655.
- Koynova, R., & Tenchov, B. (2013). Transitions between lamellar and non-lamellar phases in membrane lipids and their physiological roles. *OA Biochemistry*, 1(1), 1–9.
- Kracun, I., Rosner, H., Cosovic, C., & Stavljenic, A. (1984). Topographical atlas of the gangliosides of the adult human brain. *Journal of Neurochemistry*, 43(4), 979–989.
- Kren, V., & Martínková, L. (2001). Glycosides in medicine: "The role of glycosidic residue in biological activity". *Current Medicinal Chemistry*, 8(11), 1303–1328.
- Kubota, M., Narita, K., Nakagomi, T., Tamura, A., Shimasaki, H., Ueta, N., & Yoshida, S. (2016). Sphingomyelin changes in rat cerebral cortex during focal ischemia. *Neurological Research*, 18(4), 337–341.
- Kučerka, N., Gallová, J., & Uhríková, D. (2019). The membrane structure and function affected by water. *Chemistry and Physics of Lipids*, 221, 140–144.
- Kučerka, N., Liu, Y., Chu, N., Petrache, H. I., Tristram-Nagle, S., & Nagle, J. F. (2005). Structure of fully hydrated fluid phase DMPC and DLPC lipid bilayers using X-ray scattering from oriented multilamellar arrays and from unilamellar vesicles. *Biophysical Journal*, 88(4), 2626–2637.

- Kučerka, N., Nieh, M. P., & Katsaras, J. (2011). Fluid phase lipid areas and bilayer thicknesses of commonly used phosphatidylcholines as a function of temperature. *Biochimica et Biophysica Acta*, 1808(11), 2761–2771.
- Kwong, W. L., Gan, W. C., Abd Majid, W. H., Hashim, R., & Heidelberg, T. (2010). Pyroelectric detection in glycolipid thin film. *Thin Solid Films*, 518(15), 4412–4416.
- Ladd, M., & Palmer, R. (2013). *Structure determination by X-ray crystallography analysis by X-rays and neutrons*. New York: Springer.
- Lalitha, K., Gayathri, K., Prasad, Y. S., Saritha, R., Thamizhanban, A., Maheswari, C. U., Sridharan, V., & Nagarajan, S. (2018). Supramolecular gel formation based on glycolipids derived from renewable resources. *Gels*, 4(1), Article #1.
- Laurent, N., Lafont, D., Dumoulin, F., Boullanger, P., Mackenzie, G., Kouwer, P. H. J., & Goodby, J. W. (2003). Synthesis of amphiphilic phenylazophenyl glycosides and a study of their liquid crystal properties. *Journal of American Chemical Society*, 125(50), 15499–15506.
- Li, N. Y. D., Perutková, S., Iglič, A., & Rappolt, M. (2017). My first electron density map: A beginner's guide to small angle X-ray diffraction. *Elektrotehniski Vestnik*, 84(3), 69–75.
- Liao, G., Zewe, S. K., Hagerty, J., Hashim, R., Abeygunaratne, S., Vill, V., & Jákli, A. (2006). Thermotropic liquid crystalline properties of amphiphilic branched chain glycolipids. *Liquid Crystals*, 33(3), 361–366.
- Liew, C. Y., Salim, M., Zahid, N. I., & Hashim, R. (2015). Biomass derived xylose Guerbet surfactants: thermotropic and lyotropic properties from small-angle X-ray scattering. *RSC Advances*, 5(120), 99125–99132.
- Liu, J., & Conboy, J. C. (2005). 1,2-diacyl-phosphatidylcholine flip-flop measured directly by sum-frequency vibrational spectroscopy. *Biophysical Journal*, 89(4), 2522–2532.
- Liu, K., Chen, D., Marcozzi, A., Zheng, L., Su, J., Pesce, D., Zajaczkowski, W., Kolbe, A., Pisula, W., Mullen, K., Clark, N. A., & Herrmann, A. (2014). Thermotropic liquid crystals from biomacromolecules. *Proceedings of the National Academy of Sciences USA*, 111(52), 18596–18600.
- Loewenstein, A., & Igner, D. (1993). Deuterium NMR studies of n-octyl-,n-nonyl-,n-decyl-D-glucopyranoside liquid crystalline systems. *Liquid Crystals*, 13(4), 531–539.
- Lombardo, D., Kiselev, M. A., Magazu, S., & Calandra, P. (2015). Amphiphiles self-assembly: Basic concepts and future perspectives of supramolecular approaches. *Advances in Condensed Matter Physics*, 151683, 1–22.

- Love, S. (2006). Demyelinating diseases. *Journal of Clinical Pathology*, 59(11), 1151–1159.
- Luzzati, V. (1968). *Biological membranes*. London: Academic Press.
- Lynch, D. V., & Dunn, T. M. (2004). An introduction to plant sphingolipids and a review of recent advances in understanding their metabolism and function. *New Phytologist*, 161(3), 677–702.
- Malhotra, R. (2012). Membrane glycolipids: Functional heterogeneity: A review. *Biochemistry & Analytical Biochemistry*, 1(2), Article #1000108.
- Mannock, D. A., Lewis, R. N., Sen, A., & McElhaney, R. N. (1988). The physical properties of glycosyldiacylglycerols. Calorimetric studies of a homologous series of 1,2-Di-O-acyl-3-O-(beta-D-glucopyranosyl)-sn-glycerols. *Biochemistry*, 27(18), 6852–6859.
- Mannock, D. A., Akiyama, M., Lewis, R. N., & McElhaney, R. N. (2000). Synthesis and thermotropic characterization of a homologous series of racemic L-D-glucosyl dialkylglycerols. *Biochimica et Biophysica Acta*, 1509(1–2), 203–215.
- Mannock, D. A., Harper, P. E., Gruner, S. M., & McElhaney, R. N. (2001). The physical properties of glycosyl diacylglycerols. Calorimetric, X-ray diffraction and Fourier transform spectroscopic studies of a homologous series of 1,2-di-O-acyl-3-O-(beta-D-galactopyranosyl)-sn-glycerols. *Chemistry and Physics of Lipids*, 111(2), 139–161.
- Mannock, D. A., Collins, M. D., Kreichbaum, M., Harper, P. E., Gruner, S. M., & McElhaney, R. N. (2007). The thermotropic phase behaviour and phase structure of a homologous series of racemic beta-D-galactosyl dialkylglycerols studied by differential scanning calorimetry and X-ray diffraction. *Chemistry and Physics of Lipids*, 148(1), 26–50.
- Markova, N., Sparr, E., Wadso, L., & Wennerstrom, H. (2000). A calorimetric study of phospholipid hydration. Simultaneous monitoring of enthalpy and free energy. *Journal of Physical Chemistry B*, 104(33), 8053–8060.
- Marquardt, D., Geier, B., & Pabst, G. (2015). Asymmetric lipid membranes: Towards more realistic model systems. *Membranes*, 5(2), 180–196.
- McIntosh, T. J., & Simon, S. A. (1986). Area per molecule and distribution of water in fully hydrated dilauroylphosphatidylethanolamine bilayers. *Biochemistry*, 25(17), 4948–4952.
- McIntosh, T. J., & Simon, S. A. (1993). Contributions of hydration and steric (entropic) pressures to the interactions between phosphatidylcholine bilayers: Experiments with the subgel phase. *Biochemistry*, 32(32), 8374–8384.

- McIntosh, T. J. (1996). Hydration properties of lamellar and non-lamellar phases of phosphatidylcholine and phosphatidylethanolamine. *Chemistry and Physics of Lipids*, 81(2), 117–131.
- Milkereit, G., Garamus, V. M., Veermans, K., Willumeit, R., & Vill, V. (2004). Synthesis and mesogenic properties of a Y-shaped glyco-glycero-lipid. *Chemistry and Physics of Lipids*, 131(1), 51–61.
- Minamikawa, H., Murakami, T., & Hato, M. (1994). Synthesis of 1,3-di-O-alkyl-2-O-(3-glycosyl)glycerols bearing oligosaccharides as hydrophilic groups. *Chemistry and Physics of Lipids*, 72(2), 111–118.
- Minamikawa, H., & Hato, M. (1997). Phase behavior of synthetic phytanyl-chained glycolipid/water systems. *Langmuir*, 13(9), 2564–2571.
- Minamikawa, H., & Hato, M. (1998). Reverse micellar cubic phase in a phytanyl-chained glucolipid/water system. *Langmuir* 14(16), 4503–4509.
- Mislan, A. A., Foong, J. L. N., Saharin, S. M., & Zahid, N. I. (2019). Rheological behaviour of thermotropic and lyotropic liquid crystalline phases of Guerbet branched chain glycolipids. *Fluid Phase Equilibria*, 502, Article #112305.
- Naik, P. V. (2010). *Principles of physics (4th Ed)*. New Delhi: PHI Learning Pte. Ltd.
- Nagarajan, R. (2002). Molecular packing parameter and surfactant self-assembly: The neglected role of the surfactant tail. *Langmuir*, 18(1), 31–38.
- Nguan, H. S., Heidelberg, T., Hashim, R., & Tiddy, G. J. T. (2010). Quantitative analysis of the packing of alkyl glycosides: A comparison of linear and branched alkyl chains. *Liquid Crystals*, 37(9), 1205–1213.
- Nguyen, T. H., Zhang, C., Weichselbaum, E., Knyazev, D. G., Pohl, P., & Carloni, P. (2018). Interfacial water molecules at biological membranes: Structural features and role for lateral proton diffusion. *PLoS One*, 13(2), Article #e0193454.
- Nilsson, F., Söderman, O., & Johansson, I. (1997). Physical-chemical properties of some branched alkyl glucosides. *Langmuir*, 13(13), 3349–3354.
- Nilsson, F., Söderman, O., & Johansson, I. (1998). Four different C8G1 alkylglucosides. Anomeric effects and the influence of straight vs branched hydrocarbon chains. *Journal of Colloid and Interface Science*, 203(1), 131–139.
- Noh, J., Reguengo De Sousa, K., & Lagerwall, J. P. F. (2016). Influence of interface stabilisers and surrounding aqueous phases on nematic liquid crystal shells. *Soft Matter*, 12(2), 367–372.
- O'Lenick, A. J. (2001). Guerbet chemistry. *Journal of Surfactants and Detergents*, 4(3), 311–315.

- Ojha, D. P., Yurtseven H., Prajapati A. K., & Madhu Mohan M. L. N. (2013). Liquid crystal research: Current trends and future perspectives. *Advances in Condensed Matter Physics*, 2013, 1–2.
- Ogawa, S., Asakura, K., & Osanai, S. (2013). Thermotropic and glass transition behaviors of n-alkyl β -D-glucosides. *RSC Advances*, 3(44), 21439–21446.
- Pan, J., Tristram-Nagle, S., Kučerka, N., & Nagle, J. F. (2008). Temperature Dependence of Structure, Bending Rigidity, and Bilayer Interactions of Dioleoylphosphatidylcholine Bilayers. *Biophysical Journal*, 94(1), 117–124.
- Patrick, M., Zahid, N. I., Kriechbaum, M., & Hashim, R. (2018). Guerbet glycolipids from mannose: Liquid crystals properties. *Liquid Crystals*, 45(13–15), 1970–1986.
- Perera, L., Essmann, U., & Berkowitz, M. L. (1996). Role of water in the hydration force acting between lipid bilayers. *Langmuir*, 12(11), 2625–2629.
- Popov, N., Honaker, L. W., Popova, M., Usol'tseva, N., Mann, E. K., Jakli, A., & Popov, P. (2018). Thermotropic liquid crystal-assisted chemical and biological sensors. *Materials*, 11(1), 1–28.
- Pouzot, M., Mezzenga, R., Leser, M., Sagalowicz, L., Guillot, S., & Glatter, O. (2007). Structural and rheological investigation of $Fd3m$ inverse micellar cubic phases. *Langmuir*, 23(19), 9618–9628.
- Radi, H. A. & Rasmusen, J. O. (2013). *Principle of physics. For scientists and engineers*. Berlin Heidelberg: Springer-Verlag.
- Rand, R. P. (1992). Raising water to new heights. *Science*, 256(5057), 618–618.
- Rappolt, M., & Pabst, G. (2008). *Chapter 3 Flexibility and structure of fluid bilayer interfaces In: Kaushik, N. ed. Structure and dynamics of membranous interfaces*. Hoboken, New Jersey: John Wiley & Sons.
- Rau, D. C., & Parsegian, V. A. (1992). Direct measurement of the intermolecular forces between counterion-condensed DNA double helices Evidence for long range attractive hydration forces. *Biophysical Journal*, 61(1), 246–259.
- Reese, C. W., Strango, Z. I., Dell, Z. R., Tristram-Nagle, S., & Harper, P. E. (2015). Structural insights into the cubic-hexagonal phase transition kinetics of monoolein modulated by sucrose solutions. *Physical Chemistry Chemical Physics*, 17(14), 9194–9204.
- Rodzi, N. B. M., (2006), Branched chain galactosides and melibiosides: Synthesis and mesomorphic properties. M.Sc Dissertation, University of Malaya, Kuala Lumpur.
- Ruocco, M. J., Atkinson, D., Small, D. M., Skarjune, R. P., Oldfield, E., & Shipley, G. G. (1981). X-ray diffraction and calorimetric study of anhydrous and hydrated N-

- palmitoylgalactosylsphingosine (cerebroside). *Biochemistry & Analytical Biochemistry*, 20(21), 5957–5966.
- Saari, N. A. N., Mislan, A. A., Hashim, R., & Zahid, N. I. (2018). Self-assembly, thermotropic, and lyotropic phase behavior of Guerbet branched-chain maltosides. *Langmuir*, 34(30), 8962–8974.
- Sadoc, J. F., & Charvolin, J. (1986). Frustration in bilayers and topologies of liquid crystals of amphiphilic molecules. *Journal de Physique*, 47(4), 683–691.
- Sagnella, S. M., Conn, C. E., Krodkiewska, I., Mulet, X., & Drummond, C. J. (2011). Anandamide and analogous endocannabinoids: A lipid self-assembly study. *Soft Matter*, 7(11), 5319–5328.
- Salim, M., Zahid, N. I., Liew, C. Y., & Hashim, R. (2015). Cubosome particles of a novel Guerbet branched chain glycolipid. *Liquid Crystals*, 43(2), 168–174.
- Sands, D. E. (1969). *Introduction to crystallography*. New York: Dover publications.
- Sasaki, D. (2008). *Glycolipids: New research*. New York: Nova Science Publisher.
- Schadt, M. (1997). Liquid crystal materials and liquid crystal displays. *Annual Review of Materials Research*, 27(1), 305–379.
- Schnablegger, H., & Singh, Y. (2011). *The SAXS guide*. Graz: Anton Paar GmbH.
- Scholefield, J. H., Gerber, M. A., & Dwyer, P. (1982). Liquid crystal forehead temperature strips. *American Journal of Diseases of Children*, 136(3), 198–201.
- Schulze, H., & Sandhoff, K. (2011). Lysosomal lipid storage diseases. *Cold Spring Harbor Perspective in Biology*, 3(6), Article #a004804.
- Seddon, J. M., Cevc, G., Kaye, R. D., & Marsh, D. (1984). X-ray diffraction study of the polymorphism of hydrated diacyl- and dialkylphosphatidylethanolamines. *Biochemistry*, 23(12), 2634–2644.
- Seddon, J. M. (1990). Structure of the inverted hexagonal (H_{II}) phase, and non-lamellar phase transitions of lipids. *Biochimica et Biophysica Acta*, 1031(1), 1–69.
- Seddon, J. M., & Templer, R. H. (1993). Cubic phases of self-assembled amphiphilic aggregates. *Philosophical Transactions of the Royal Society A: Mathematical, Physical and Engineering Sciences*, 344(1672), 377–401.
- Seddon, J. M., & Templer, R. H. (1995). *Polymorphism of lipid-water systems in handbook of biological physics (structure and dynamics of membranes from cells to vesicles)*. North Holland: Elsevier Science B. V.
- Seddon, J. M., Templer, R. H., Warrender, N. A., Huang, Z., Cevc, G., & Marsh, D. (1997). Phosphatidylcholine–fatty acid membranes: Effects of headgroup

hydration on the phase behaviour and structural parameters of the gel and inverse hexagonal H_{II} phases. *Biochimica et Biophysica Acta*, 1327(1), 131–147.

Seddon, J. M., Robins, J., Gulik-Krzywicki, T., & Delacroix, H. (2000). Inverse micellar phases of phospholipids and glycolipids. *Physical Chemistry Chemical Physics*, 2(20), 4485–4493.

Seddon, J. M., Squires, A. M., Conn, C. E., Ces, O., Heron, A. J., Mulet, X., Shearman, G. C., & Templer, R. H. (2006). Pressure-jump X-ray studies of liquid crystal transitions in lipids. *Philosophical Transactions of the Royal Society A: Mathematical, Physical and Engineering Sciences*, 364(1847), 2635–2655.

Sekhon, B. S. (2013). Surfactants: Pharmaceutical and medicinal aspects. *Journal of Pharmaceutical Technology, Research and Management*, 1(1), 43–68.

Shearman, G. C., Ces, O., Templer, R. H., & Seddon, J. M. (2006). Inverse lyotropic phases of lipids and membrane curvature. *Journal of Physics: Condensed Matter*, 18(28), S1105–1124.

Sun, R. G., & Zhang, J. (2004). The cubic phase of phosphatidylethanolamine film by small angle X-ray scattering. *Journal of Physics D: Applied Physics*, 37(3), 463–467.

Takada, A., Fukuda, T., Miyamoto, T., Yakoh, Y., & Watanabe, J. (1992). Columnar liquid crystals in oligosaccharide derivatives. II. Two types of discotic columnar liquid-crystalline phase of cellobiose alkanoates. *Liquid Crystals*, 12(2), 337–345.

Tenchov, B., & Koynova, R. (2017). Cubic phases in phosphatidylethanolamine dispersions: Formation, stability and phase transitions. *Chemistry and Physics of Lipids*, 208, 65–74.

Thiesen, P. H., Rosenfeld, H., Konidala, P., Garamus, V. M., He, L., Prange, A., & Niemeyer, B. (2006). Glycolipids from a colloid chemical point of view. *Journal of Biotechnology*, 124(1), 284–301.

Tristram-Nagle, S., Petrache, H. I., & Nagle, J. F. (1998). Structure and interactions of fully hydrated dioleoylphosphatidylcholine bilayer. *Biophysical Journal*, 75(2), 917–925.

Tschierske, C. (2007). Liquid crystal engineering--new complex mesophase structures and their relations to polymer morphologies, nanoscale patterning and crystal engineering. *Chemical Society Reviews*, 36(12), 1930–1970.

Tyman, J. H. P. (1992). *Surfactants in lipid chemistry: Recent synthetic, physical and biodegradative studies*. Cambridge: Royal Society of Chemistry.

van Boeckel, C. A. A., & van Boom, J. H. (1980). Synthesis of phosphatidyl- α -glucosyl-diacylglycerol containing palmitic and oleic acid esters. *Tetrahedron Letters*, 21(38), 3705–3708.

- van Boeckel, C. A. A., Westerduin, P., & van Boom, J. H. (1981). Synthesis of 2,3-di-O-phytanyl-1-O- α -glucosyl(galactosyl)- β (1 \rightarrow 6)-mannosyl- α (1 \rightarrow 2)-glucosyl- α (1 \rightarrow 1)-sn-glycerol. Purple membrane glycolipid. *Tetrahedron Letters*, 22(29), 2819–2822.
- Vaskan, I. S., Solovyeva, D. O., Chistyakov, A. A., Efremov, R. G., Volynsky, P. E., Shtykova, E. V., Korchagina, E. Yu, Mochalov, K. E., Bovin, N. V. & Oleinikov, V. A. (2018). Neoglycolipids micelle-like structures as a basis for drug delivery systems. *KnE Energy*, 3(2), 519–527.
- van't Hag, L., Gras, S. L., Conn, C. E., & Drummond, C. J. (2017). Lyotropic liquid crystal engineering, moving beyond binary compositioned space-ordered nanostructural amphiphile self-assembly materials by design. *Chemical Society Reviews*, 46(10), 2705–2731.
- Vertogen, G. & de Jeu, W. H. (2012). *Thermotropic liquid crystals, fundamentals*. Berlin Heidelberg: Springer-Verlag.
- Vill, V., Böcker, T., Thiem, J., & Fischer, F. (1989). Studies on liquid-crystalline glycosides. *Liquid Crystals*, 6(3), 349–356.
- Vill, V., & Hashim, R. (2002). Carbohydrate liquid crystals: Structure–property relationship of thermotropic and lyotropic glycolipids. *Current Opinion in Colloid and Interface Science*, 7(5–6), 395–409.
- von Minden, H. M., Morr, M., Milkereit, G., Heinz, E., & Vill, V. (2002). Synthesis and mesogenic properties of glycosyl diacylglycerols. *Chemistry and Physics of Lipids*, 114(1), 55–80.
- von Rybinski, W., & Hill, K. (1998). Alkyl polyglycosides properties and applications of a new class of surfactants. *Angewandte Chemie International Edition*, 37(10), 1328–1345.
- Wess, T. J., Drakopoulos, M., Snigirev, A., Wouters, J., Paris, O., Fratzl, P., Collins, M., Hiller, J. & Nielsen, K. (2001). The use of small-angle X-ray diffraction studies for the analysis of structural features in archaeological samples. *Archaeometry*, 43 (1), 117–129.
- Yaghmur, A., & Rappolt, M. (2013). The Micellar Cubic $Fd3m$ Phase. *Advances in Planar Lipid Bilayers and Liposomes*, 18, 111–145.
- Yamakawa, T., & Nagai, Y. (1978). Glycolipids at the cell surface and their biological functions. *Trends in Biochemical Sciences*, 3(2), 128–131.
- Yang, Z., Xu, R., Ali-Rachedi, F., Chambert, S., Xavier, N. M., Soulère, L., Ahmar, M., Mackenzie, G., Davis, E. J., Goodby, J. W., Cowling, S. J. & Queneau, Y. (2017). Liquid crystalline glyco steroids and acyl steroid glycosides (ASG). *Liquid Crystals*, 44(12–13), 2089–2107.

- Yilmaz, S., & Yildirim, A. (2009). Numerical determination of thermal-diffusivity coefficients of some nematic liquid crystals in situ. *International Journal of Thermophysics*, 30(6), Article #2015.
- Yu, R. K., Tsai, Y., Ariga, T., & Yanagisawa, M. (2011). Structures, biosynthesis, and functions of gangliosides—An overview. *Journal of Oleo Science*, 60(10), 537–544.
- Zahid, N. I., Abou-Zied, O. K., Hashim, R., & Heidelberg, T. (2012). Fluorescence probing of the temperature-induced phase transition in a glycolipid self-assembly: hexagonal \leftrightarrow micellar and cubic \leftrightarrow lamellar. *Langmuir*, 28(11), 4989–4995.
- Zahid, N. I., Conn, C. E., Brooks, N. J., Ahmad, N., Seddon, J. M., & Hashim, R. (2013). Investigation of the effect of sugar stereochemistry on biologically relevant lyotropic phases from branched-chain synthetic glycolipids by small-angle X-ray scattering. *Langmuir*, 29(51), 15794–15804.
- Zhang, R., Zhang, L., & Somasundaran, P. (2004). Study of mixtures of n-dodecyl-beta-D-maltoside with anionic, cationic, and nonionic surfactant in aqueous solutions using surface tension and fluorescence techniques. *Journal of Colloid and Interface Science*, 278(2), 453–460.
- Zhou, Y., Wang, S. Z., Lv, M., Niu, J., & Xu, B. (2017). Analysis of the effects of hydrocarbon chain on foam properties of alkyl polyglycosides. *Journal of Surfactants and Detergents*, 20(3), 623–630.

LIST OF PUBLICATIONS AND PAPER PRESENTED

PUBLICATIONS

Academic Journal

1. **Hamid, H. A. A.**, Hashim, R., Seddon, J. M., & Brooks, N. J. (2014). Lyotropic phase behaviour and structural parameters of monosaccharide and disaccharide Guerbet branched-chain β -D-glycosides. *Advanced Materials Research*, 895, 111-115.
2. Brooks, N. J., **Hamid, H. A. A.**, Hashim, R., Heidelberg, T., Seddon, J. M., Conn, C. E., Hussein, S. M. M., Zahid, N. I., & Hussien. R. S. D. (2011). Thermotropic and lyotropic liquid crystalline phases of Guerbet branched-chain β -D-glucosides. *Liquid Crystal*, 38(11-12), 1725 – 1734.

Presentations:

Oral

1. Phase Behaviour and Structural Parameters of Guerbet Branched-Chain 2-octyldodecyl β -D-glycosides/Water Systems: Effects of Headgroup, 4th International Conference on Solid State Science & Technology, 18th - 20th December 2014, Holiday Inn, Malacca, Malaysia.
2. Effect of Chain Length on the Thermotropic and Lyotropic Phase Behaviours of Maltosides, Proceedings of International Conference on Global Sustainability and Chemical Engineering, 20th – 22nd August 2014, Cititel Mid Valley, Kuala Lumpur, Malaysia.

Poster

1. Small-Angle X-Ray Diffraction Study of the Chain Length Effect on the Thermotropic and Lyotropic Behaviours of β -D-Maltosides, International Conference on Nano Materials: Science, Technology and Applications (ICNM' 13), 5th -7th December 2013, B. S. Abdur Rahman University, Chennai, India.
2. Small-Angle X-Ray Diffraction Study of the Thermotropic and Lyotropic Behaviour of 2-decyltetradecyl β -D-maltoside, International on Nanoscience and Nanotechnology 2013 (NANO – SciTech 2013), 1st - 4th March 2013, Grand Bluewave Hotel Shah Alam, Selangor, Malaysia.
3. Limiting Hydration of Guerbet Branched-Chain 2-octyldodecyl β -D-glycosides/Water System, Lipids and Membrane Biophysics: Faraday Discussion 161 2012, 11th – 13th September 2012, Burlington House, London, United Kingdom.